Restriction/Classification Cancelled

BNWL-394
NASA-CR-54840

AEC RESEARCH and DEVELOPMENT REPORT

FINAL REPORT

BASIC BEHAVIOR AND PROPERTIES OF W-UO_2 CERMETS

JULY 1964 - NOVEMBER 1965



R. J. BAKER, J. L. DANIEL, W. J. LACKEY,
R. J. LOBSINGER, F. A. SCOTT, E. A. SNAJDR, and W. E. ROAKE

(NASA-CR-54840) BASIC BEHAVIOR AND PROPERTIES OF W-UO2 CERMETS Final Report, Jul. 1964 - Nov. 1965 (Battelle-Northwest) 145 p

N73-71335

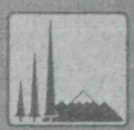
Unclas
00/99 54526

(CATEGORY)

Restriction/Classification Cancelled

DATA

Restriction/Classification Cancelled



BATTELLE-NORTHWEST
BATTELLE MEMORIAL INSTITUTE / PACIFIC NORTHWEST LABORATORY

Restriction/Classification Cancelled

CLASSIFICATION CHANGE
TO UNCLASSIFIED
By authority of T.D. No. 73-221
Changed by O. L. Merritt Date 1/30/73

LEGAL NOTICE

This report was prepared as an account of Government sponsored work. Neither the United States, nor the Commission, nor any person acting on behalf of the Commission:

A. Makes any warranty or representation, expressed or implied, with respect to the accuracy, completeness, or usefulness of the information contained in this report, or that the use of any information, apparatus, method, or process disclosed in this report may not infringe privately owned rights; or

B. Assumes any liabilities with respect to the use of, or for damages resulting from the use of any information, apparatus, method, or process disclosed in this report.

As used in the above, "person acting on behalf of the Commission" includes any employee or contractor of the Commission, or employee of such contractor, to the extent that such employee or contractor of the Commission, or employee of such contractor prepares, disseminates, or provides access to, any information pursuant to his employment or contract with the Commission, or his employment with such contractor.

PACIFIC NORTHWEST LABORATORY
RICHLAND, WASHINGTON
operated by
BATTELLE MEMORIAL INSTITUTE
for the
UNITED STATES ATOMIC ENERGY COMMISSION UNDER CONTRACT AT(45-1)-1830

PRINTED BY/FOR THE U. S. ATOMIC ENERGY COMMISSION

AEC-RLDO RICHLAND, WASH.

C67-3117

CONFIDENTIAL

NOTICE - THIS DOCUMENT CONTAINS INFORMATION AFFECTING THE NATIONAL DEFENSE OF THE UNITED STATES WITHIN THE MEANING OF THE ESPIONAGE LAWS, TITLE 18 U.S.C., SECTION 793 AND 794. ITS TRANSMISSION OR REVELATION OF ITS CONTENTS IN ANY MANNER TO AN UNAUTHORIZED PERSON IS PROHIBITED BY LAW.

BNWL-394
NASA-CR-54840

C-91 Nuclear Reactors
for Rocket Propulsion
M-3679 (48th Ed.)

FINAL REPORT

BASIC BEHAVIOR AND PROPERTIES OF W-UO_2 CERMETS

JULY 1964 - NOVEMBER 1965

By

R. J. Baker, J. L. Daniel, W. J. Lackey,
R. J. Lobsinger, F. A. Scott, E. A. Snajdr, and W. E. Roake

Materials Development Section
Materials Department

This program was funded by the National Aeronautics and Space Administration under an interagency agreement with the Atomic Energy Commission

(Project No. C-17079-A)

October 12, 1966

Technical Management
NASA Lewis Research Center
Cleveland, Ohio
Materials and Structures Division
Neal T. Saunders
Richard E. Gluyas

RESTRICTED DATA

This document contains Restricted Data as defined in the Atomic Energy Act of 1954. Its transmittal or the disclosure of its contents in any manner to an unauthorized person is prohibited.

PACIFIC NORTHWEST LABORATORY
RICHLAND, WASHINGTON

Group 1
Excluded from Automatic Downgrading and Declassification

CONFIDENTIAL

Restriction/Classification Cancelled

BNWL-394
NASA-CR-54840

Printed in the USA. Charge $3.45. Available from the U.S Atomic Energy Commission, Division of Technical Information Extension, P.O. Box 62, Oak Ridge, Tennessee. Please direct to the same address inquiries covering the procurement of other classified AEC reports.

FINAL REPORT
BASIC BEHAVIOR AND PROPERTIES OF W-UO_2 CERMETS
JULY 1964 - NOVEMBER 1965

By

R. J. Baker, J. L. Daniel, W. J. Lackey,
R. J. Lobsinger, F. A. Scott, E. A. Snajdr, and W. E. Roake

ABSTRACT

Thermal cycling studies on cermets prepared from tungsten and UO_2 powder mixtures and cermets prepared using tungsten coated UO_2 particles are discussed. The cermets were tested in hydrogen at high temperatures to determine the effects of temperature, thermal cycling, and hydrogen pressure. Basic mechanism studies of tungsten-UO_2 interactions in thermally cycled cermets are also described.

TABLE OF CONTENTS

INTRODUCTION 1

SUMMARY 2

PART I - THERMAL CYCLING STUDIES ON TUNGSTEN UO_2 POWDER CERMETS 5

Cermet Fabrication 5

Thermal Cycling Test Procedure 11

Results and Discussion 13

Effect of Materials and Fabrication Variables on Cermet Behavior 13

Effect of Thermal Cycling Conditions on Cermet Behavior 20

Effect of Cermet Composition on Thermal Cycling Behavior 25

Conclusions 25

PART II - THERMAL CYCLING STUDIES ON W-UO_2 COATED PARTICLE CERMETS 28

Cermet Fabrication 28

Thermal Cycling Test Procedure 34

Effect of Fabrication Variables on Cermet Behavior . . . 34

Effect of Thermal Cycling Conditions on Cermet Behavior 47

Effect of Cermet Composition on Thermal Cycling Behavior 69

PART III - BASIC MECHANISM STUDIES 77

W-UO_2 Cermet Interactions 77

Analysis of Gas Content of Cycled Cermet Specimens . . . 77

Grain Boundary Phenomena in W-UO_2 Cermets 79

Grain Boundary Experiments 85

Bicrystal Cube Experiments 89

TABLE OF CONTENTS (contd)

Proposed Mechanism of Fuel Loss and Degeneration of W-UO_2 Cermets During Thermal Cycling 93
Stage 1 - Hydrogen Penetration 95
Stage 2 - Limited Fuel Migration and Vaporization . . . 98
Stage 3 - Mechanical Failure and Gross Fuel Migration . 100
Concluding Remarks and Recommendations 101

APPENDIX A - HIGH CAPACITY, HIGH TEMPERATURE, HIGH PRESSURE HYDROGEN FURNACE 103

APPENDIX B - THERMAL EXPANSION CHARACTERISTICS OF PNEUMATICALLY IMPACTED W-UO_2 CERMETS 114

APPENDIX C - PROGRESS TOWARD CONSTITUENT ANALYSIS OF W-UO_2 CERMETS 117

REFERENCES 128

LIST OF FIGURES

1	Fabrication of Tungsten-UO_2 Cermet Specimens	6
2	Results of Nitric Acid Dissolution of UO_2 from a W-20 vol% UO_2 Cermet Fabricated by Pneumatic Impaction of Noncoated UO_2 and 1μ Tungsten	9
3	Resistance Heated, High Pressure, Tungsten-Filament Furnace Used for Thermal Cycling W-UO_2 Cermets	12
4	Fuel Loss from Nonclad W-UO_2 Cermets During 10 Thermal Cycles to 2600 °C in 68 atm Static Hydrogen	14
5	Microstructure of a W-20 vol% UO_2 Cermet Fabricated by Pneumatic Impaction of Micronized UO_2 (< 4μ) and 1μ Tungsten	17
6	Influence of Postimpaction Annealing of Micronized UO_2-W (20 vol% UO_2) Cermets on Thermal Cycling Behavior Under Standard Test Conditions in Static Hydrogen	18
7	Static Hydrogen Pressure Effects on the Thermal Cycling Behavior of W-Micronized UO_2 Cermets	21
8	Static Hydrogen Pressure Effects on Cracking During Thermal Cycling of Micronized UO_2-W (20 vol% UO_2) Cermets	22
9	Effect of Hydrogen Pressure and Flow Rate on Fuel Loss During Thermal Cycling of a W-20 vol% Micronized UO_2 Cermet	23
10	Effect of Cycle Duration on the Fuel Loss from W-Micronized UO_2 Cermets	24
11	Fuel Loss from W-UO_2 Cermets During Thermal Cycling to 2500 °C in 40.8 atm Dry Hydrogen	26
12	Fabrication of W-UO_2 Coated Particle Cermet Specimens	29
13	Cermet Fabrication Effects: Dissolution of Molybdenum Hardware Used in Assemblies for 1600 °C Impactions	31

14 Nitric Acid Dissolution of Exposed UO_2 from a Nonannealed W–24 vol% UO_2 Cermet Fabricated by Pneumatic Impaction of Tungsten-Coated UO_2 and 5μ Tungsten 32

15 Electron Micrographs of Pneumatically Impacted W–13.3 vol% UO_2 Coated Particle-Powder Cermets 37

16 Influence of Hydrogen Pretreatment and Postimpaction Annealing of Tungsten-Coated UO_2-W (13.3 vol% UO_2) Cermets on Thermal Cycling to 2500 °C in 40.8 atm Static Hydrogen 38

17 Electron Micrographs of Pneumatically Impacted W–13.3 vol% UO_2 Cermets 39

18 Effect of Pneumatic Impaction Temperature on Fuel Loss During Thermal Cycling W–41.3 vol% UO_2 Coated Particle Cermets 41

19 Effects of Dissolution of Molybdenum Impaction Hardware on the Thermal Cycling Behavior of W–29.8 vol% (UO_2 + mole% Y_2O_3 Solid Solution) Coated Particle Cermets 42

20 Test Specimen Edge Effects on Tungsten-Coated UO_2-W (13.3 vol% UO_2) Cermets 44

21 Electron Micrographs of Pneumatically Impacted W–13.3 vol% UO_2 Coated Particle-W Powder Cermets 45

22 Microstructures of Nonannealed and Annealed Tungsten-Coated UO_2–W 13.3 vol% Cermets (No pretreatment) After Standard Thermal Cycle Tests in 40.8 atm Static Hydrogen 46

23 Thermal Cycling Behavior of Tungsten-Coated UO_2-W (13.3 vol% UO_2) Cermets Under Accelerated Test Conditions in 68 atm Static Hydrogen 48

24 Thermal Cycling Behavior of Tungsten-Coated UO_2-W (13.3 vol% UO_2) Cermets Under Standard Test Conditions in 40.8 atm Static Hydrogen 49

25 Microstructures of Noncycled and Cycled Tungsten-Coated UO_2-W Cermets (13.3 vol% UO_2) 50

26 Thermal Cycling Temperature Effects on the Microstructure of a Tungsten-Coated UO_2-W (13.3 vol%) Cermet 51

27 Variation in UO_2 Migration in a Thermally Cycled Tungsten-Coated UO_2-W (13.3 vol% UO_2) Cermet (No Acid Pretreatment) No Etchant 52

28 Effect of Pressure and Flow Rate on the Thermal Cycling Behavior of a Tungsten-Coated UO_2-W Cermet Containing 13.3 vol% UO_2 54

29 Microstructure of a Tungsten-Coated 13.3 vol% UO_2-W Cermet After Thermal Cycling to 2500 °C in 40.8 atm Static Hydrogen 55

30 Microstructure of a Tungsten-Coated 13.3 vol% UO_2-W Cermet After Thermal Cycling to 2500 °C in 1 atm Flowing Hydrogen 56

31 Microstructure of a Tungsten-Coated 13.3 vol% UO_2-W Cermet After Thermal Cycling to 2500 °C in 1 atm Flowing Hydrogen 57

32 Microstructure of a Tungsten-Coated 13.3 vol% UO_2-W Cermet After Thermal Cycling to 2500 °C in 40.8 atm Flowing Hydrogen 58

33 Microstructure of a Tungsten-Coated 13.3 vol% UO_2-W Cermet After Thermal Cycling to 2500 °C in 40.8 atm Flowing Hydrogen 59

34 Microstructure of a Tungsten-Coated Particle 13.3 vol% UO_2-W Cermet After Thermal Cycling to 2500 °C in 40.8 atm Flowing Hydrogen 60

35 Effect of Hydrogen Flow Rate on Fuel Loss During Thermal Cycling of a Tungsten-Coated UO_2-W Cermet Containing 13.3 vol% UO_2 61

36 Effect of Hydrogen Pressure on Fuel Loss for W-UO_2 Coated Particle Cermets Containing 9.4 and 13.3 vol% UO_2 62

37 Thermal Cycling Behavior of W-UO_2 Coated Particle Cermets Containing 10 mole% Y_2O_3 in UO_2 Solid Solution 63

38 Thermal Cycling Behavior of Coated Particle W-UO_2 Cermets 65

39 Thermal Cycling Behavior of BSA Specimens 66

40	Microstructure of a Thermally Cycled W–29. 8 vol% Fuel Coated Particle Cermet Containing 10 mole% Y_2O_3 in Solid Solution in the UO_2	67
41	Microstructure of a Thermally Cycled W–29. 8 vol% Fuel Coated Particle Cermet Containing 10 mole% Y_2O_3 in Solid Solution in the UO_2	68
42	Fuel Loss of W-UO_2 Coated Particle Cermets During Thermal Cycling to 2500 °C (10 min/cycle) in 40. 8 atm, 16. 5 liters/min Flowing Dry Hydrogen	70
43	Effect of UO_2 Content on Fuel Loss During Thermal Cycling W-UO_2 Cermets	73
44	Thermal Cycling Behavior of Coated Particle W-UO_2 Cermets Under 40. 8 atm Flowing Dry Hydrogen	74
45	Thermal Cycling Behavior of W-UO_2 Coated Particle Cermets Under 1 atm Flowing Dry Hydrogen	75
46	Electron Micrographs of Pneumatically Impacted W–13. 3 vol% UO_2 Coated Particle-W Powder Cermets	78
47	Outgassing Characteristics of Cycled Cermets	80
48	Effect of Thermal Cycling on the Hydrogen Content of a W–20 vol% Micronized UO_2 Cermet	81
49	GB-Type Experiments	83
50	BC-Type Experiments	84
51	Results of Tungsten-UO_2 Vapor Diffusion Experiment	87
52	Hydrogen and Helium Penetration of Electron Beam Refined Tungsten Bicrystals	88
53	Tungsten Bicrystal with Uranium in Cavity	92
54	Proposed Mechanism of the Thermal Cycling Behavior of W-UO_2 Cermets	94
55	High Capacity, High Temperature, High Pressure Hydrogen Furnace - Front View	104
56	High Capacity, High Temperature, High Pressure Hydrogen Furnace - Top View	105

57	Gas Flow and Regulation System Schematic	106
58	Cooling Water Flow System Schematic Large Capacity, High Temperature, High Pressure, Hydrogen Furnace	107
59	Design Details of the High Capacity, High Temperature, High Pressure Furnace	108
60	Safety and Control Systems for the High Capacity, High Temperature, High Pressure Furnace	110
61	Details of Building Exhaust	111
62	Specimen Holder and Perforated Pedestal	112
63	Thermal Expansion of Sintered and Unannealed Impacted 80 vol% W–20 vol% UO_2 Cermets (One thermal cycle)	115
64	Gas Handling System	122
65	Uptake of Oxygen by Powdered Cermet	124
66	Rate of Oxygen Removal from Mixed Oxide Ceramics	126

LIST OF TABLES

I	Nitric Acid (9.7 molal) Dissolution of Exposed UO_2 from W-Micronized UO_2 Cermets	8
II	Composition, Raw Materials, and Fabrication Description of W-UO_2 Cermets	10
III	Hydrogen Pretreatment and Annealing Effects on Impacted Tungsten Powder	15
IV	Oxygen Content Associated with Tungsten in 20 vol% Micronized UO_2-W Cermets	16
V	Composition, Raw Materials and Fabrication Description of W-UO_2 Cermets	33
VI	Fabrication Pretreatment Effects on the Thermal Cycling Behavior of W–41.3 vol% UO_2 Coated Particle Cermets	36
VII	Composition and Raw Materials for W-UO_2 Coated Particle-W Powder Cermets	71
VIII	Tungsten Grain Boundary Experiments (GB-Type Experiments)	85
IX	Tungsten Bicrystal Cube Experiments (BC-Type Experiments)	90

FINAL REPORT
BASIC BEHAVIOR AND PROPERTIES OF W-UO_2 CERMETS
JULY 1964 - NOVEMBER 1965

R. J. Baker, J. L. Daniel, W. J. Lackey,
R. J. Lobsinger, F. A. Scott, E. A. Snajdr, and W. E. Roake

INTRODUCTION

This report summarizes the work conducted under National Aeronautics and Space Administration contract C-17079-A through an interagency agreement with the United States Atomic Energy Commission for the period July 1, 1964, through November 15, 1965. The work herein described is the first phase of the program in which much of the understanding tested in the second phase was developed. Phase two is included in a report published jointly by Battelle-Northwest and NASA-Lewis Research Center personnel.[1] These two reports and a third report[2] should be read and evaluated together.

Battelle-Northwest has conducted research and development in several areas of technology concerned with the development of a W-UO_2 cermet fuel for a water moderated, space nuclear propulsion reactor.[3] The reactor concept requires that W-UO_2 fuel elements containing 10 to 35 vol% UO_2 operate intermittently, on demand, in a high velocity flowing hydrogen atmosphere at temperatures to 2500 °C for periods totaling up to 10 hr.

The purpose of the studies described in this report was to investigate the effects of fabrication, composition, and thermal cycling conditions on the fuel loss from W-UO_2 cermets to develop an understanding of the basic mechanism of that fuel loss. It was expected that the results of these studies would aid in cermet development in order to obtain fuel elements capable of withstanding at least 25 thermal cycles to 2500 °C in 40.8 atmospheres of flowing dry hydrogen without more than 1 wt% fuel loss.

The three major topics treated in this report include:

- Thermal cycling studies on W-UO_2 powder cermets without surface cladding. The specific objective of this study area was to investigate the effects of reactor operation parameters (hydrogen pressure and flow when thermal cycling to 2500 °C) on the powder-type cermets and to survey possible problems inherent to powder cermet processing.
- Thermal cycling studies on W-UO_2 coated particle cermets without surface cladding. The specific objective of this study area was to investigate the effect of reactor operation conditions on coated particle type cermets including the effects of cermet fuel loading, fuel additive, and process parameters on fuel loss.
- Basic mechanism studies. The specific objective of this study area was to investigate fundamental W-UO_2 interactions under the conditions of reactor operation using tungsten bicrystals of various orientations; to perform special analyses on cycled cermets; and to correlate fundamental experiments with actual cermet experience.

Since the primary goal of this program was to develop a cermet capable of performing in the nuclear rocket environment and since it was necessary to apply research results immediately to cermet development, only a very limited number of specimens were tested at each experimental condition. Therefore, the results described exhibit trends in cermet behavior and are not statistically quantitative.

SUMMARY

Fabrication, thermal cycling conditions, and composition variables were related to fuel loss during thermal cycling of W-UO_2 cermets prototypic of those which might be required for a water moderated space nuclear propulsion reactor. The studies were performed on first generation fuels fabricated from W and UO_2 powders and on second generation W-UO_2 cermets prepared from coated particles by pneumatic impaction. Basic studies of the mechanism of fuel loss during thermal cycling led to a detailed hypothesis describing that mechanism.

Thermal cycling studies on unclad W-UO_2 powder cermets showed:

1. A marked increase in fuel loss with increased hydrogen pressure;
2. A marked increase in fuel loss when thermal cycled in flowing hydrogen;
3. The beneficial effects of a pre-cleaning treatment of W and UO_2 powder mixtures, of loading the impaction can assembly in an inert atmosphere, of pre-heating of the impaction can assembly in flowing hydrogen prior to evacuating for pneumatic impaction, and of annealing the impacted cermets;
4. The insensitivity of fuel loss behavior to the initial O/U ratio of the starting material; and
5. Increased fuel loss with increased carbon impurity content.

Thermal cycling studies on unclad W-UO_2 coated particle cermets showed that:

1. Special hydrogen pre-cleaning treatments, inert gas handling, and pre-impaction heating in flowing hydrogen are not required when the entire cermet composition consists of coated particles (when fine grain W powder is added to the cermet, it is still recommended that the W powder be pre-cleaned and protected from an oxidizing environment throughout pneumatic impaction);
2. Annealing of coated particle cermets is beneficial in reducing fuel loss during thermal cycling;
3. Chemical attack of nonclad coated particle cermet surfaces during the dissolution of molybdenum mandrels from the impaction assemblies resulted in premature fuel loss during thermal cycling;
4. Increased hydrogen pressure during thermal cycling has a deleterious effect on the fuel loss from 10 vol% UO_2–W

nonclad cermets; data scatter due to fabrication and surface effects prevented a firm conclusion on the hydrogen pressure effects on nonclad 35 vol% UO_2–W cermets;

5. Cycling in flowing hydrogen greatly increases fuel loss; and
6. The addition of 10 mole% Y_2O_3 to the UO_2 (in solid solution) is effective in reducing the fuel loss during thermal cycling.

Basic mechanism studies showed that fuel loss during thermal cycling occurs in three stages which are sequential for a specific grain boundary but are probably concurrent throughout the nonclad cermet. The first stage is described as a hydrogen penetration mechanism by which hydrogen permeates the cermet via the tungsten grain boundaries which are widened by the expansions and contraction of the gas during thermal cycling. Important factors affecting this first stage include the degree of tungsten grain boundary mismatch, hydrogen pressure, and heating and cooling rates.

Stage two comprises migration of oxygen (water) and, to a limited extent, fuel through widened grain W boundaries to the exposed surfaces, and vaporization of the fuel from the surfaces of the cermet. This stage is significantly long (in terms of thermal cycles) only for cermets containing stabilized fuel. The rate controlling step is thought to be the removal of oxygen (water) from the cermet after formation by hydrogen reduction of excess oxygen in hyperstoichiometric fuel (rare earth stabilized UO_2 has been shown to be hyperstoichiometric).

The third stage represents ultimate mechanical failure and catastrophic fuel loss from the cermet brought on by extensive fuel migration and/or by hydriding of free uranium precipitated in the fuel particle. In nonstabilized UO_2-W cermets, the latter causes complete failure of the cermet. UO_2 partially dissociates above 2000 °C to form a substoichiometric, equilibrium phase irrespective of the hydrogen environment. Free uranium precipitated during cooling of the substoichiometric fuel forms uranium hydride in the hydrogen environment and the associated volume change disrupts the cermet. The final fuel loss is via free vaporization from the shattered cermet.

CONFIDENTIAL

BNWL-394
NASA-CR-54840

PART I

THERMAL CYCLING STUDIES ON TUNGSTEN-UO_2 POWDER CERMETS

CONFIDENTIAL

PART I. THERMAL CYCLING STUDIES ON TUNGSTEN-UO_2 POWDER CERMETS

CERMET FABRICATION

All of the tungsten-UO_2 cermets studied in this portion of the program were prepared by pneumatic impaction of tungsten and UO_2 powder mixtures.[4] The final process (Figure 1) developed during the study of the effect of fabrication variables on thermal cycling behavior consisted of the following:

- Manually blending tungsten and UO_2 powder compositions in air in a vial or by using a vibratory mixer
- Control impurities by heating the mixtures for 1 hr at 1000 °C in flowing hydrogen
- Load the impaction can assembly in 8% hydrogen–92% argon
- Preheat the can assembly for 1/2 hr in a 1200 °C furnace while maintaining a flowing hydrogen atmosphere within the can and evacuate immediately prior to impaction
- Pneumatically impact at greater than 17,600 kg/cm^2, at 1200 °C in vacuum
- Remove cermet specimens from the impacted can assembly by machining
- Anneal 12 hr at 1750 °C in tank hydrogen
- Dissolve exposed UO_2 from cut specimen surfaces.

Variations of this process (Figure 1) studied during the program included: (1) no hydrogen treatment of the mixed powders, (2) loading of the impaction can in air, (3) pre-impaction heat treatment in vacuum instead of in hydrogen, (4) no dissolution of exposed UO_2 in final specimens, and (5) no final annealing treatment.

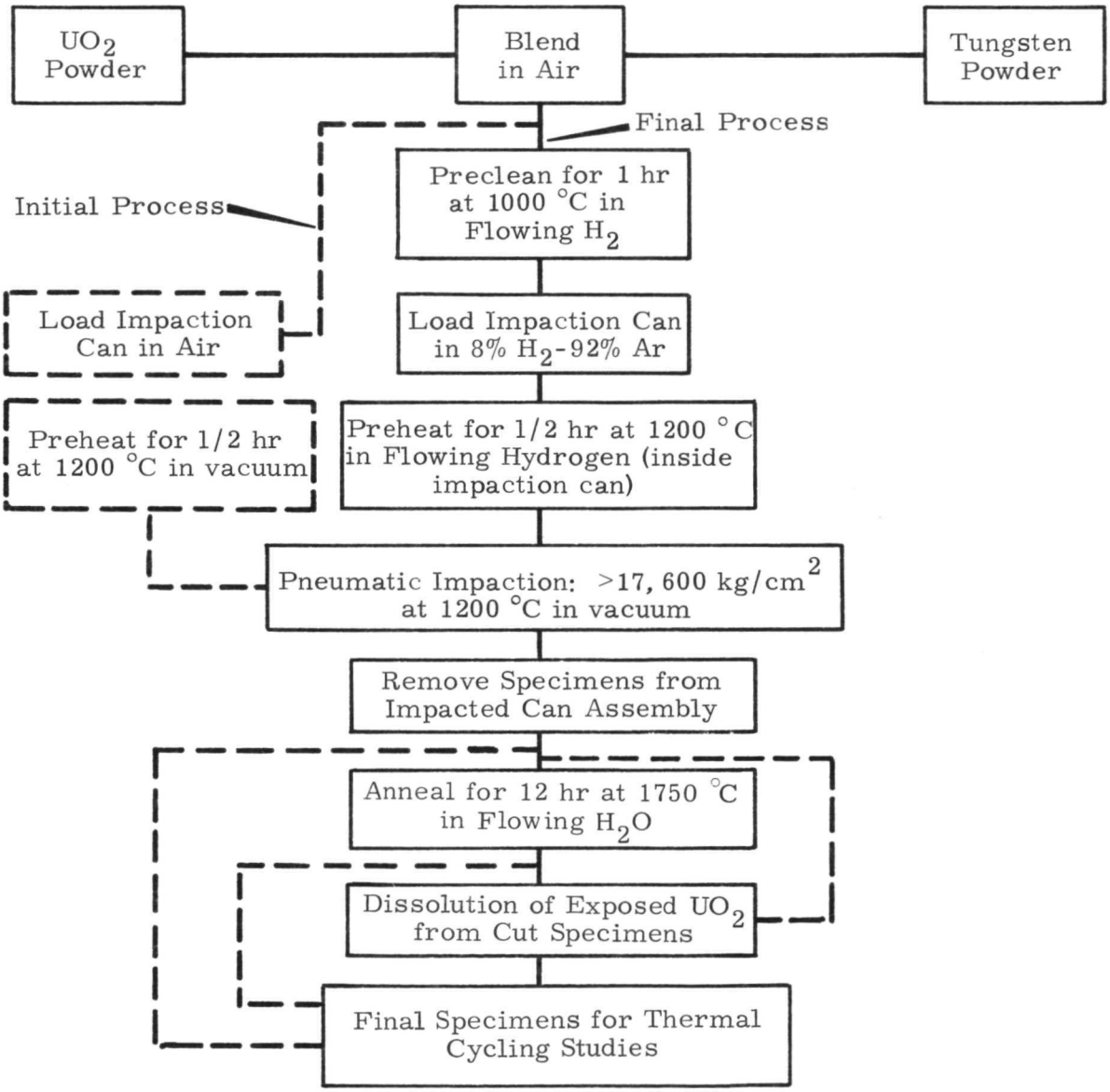


FIGURE 1. Fabrication of Tungsten-UO_2 Cermet Specimens

The assembly of the pneumatic impaction can consisted of loading layers of mixed powders into a stainless steel can using stainless steel separators between powder layers, and TIG welding the final closure and outgassing stem to the can. After pneumatic impaction, the can assembly was opened by machining and the cermet plates were manually separated from the spacers. The cermet plates obtained in this process were approximately 6 cm in diameter and 0.050 to 0.076 cm thick. Specimens 0.48 cm square to be used in thermal cycling studies were cut from these cermet plates. Consequently, UO_2 is exposed at the cut and at all surfaces of W-micronized UO_2 cermet specimens. Exposed UO_2 is lost rapidly by vaporization during the thermal cycling and there are indications (see Part II of this report) that such edge losses can lead to a loss rate of interior UO_2 somewhat greater than if the exposed fuel were removed prior to cycling.

To remove exposed UO_2, nonclad W-UO_2 cermets fabricated by pneumatic impaction of tungsten and UO_2 powders were immersed in a 9.7 molal nitric acid solution at room temperature for times up to 23 hr. Some specimens were annealed 12 hr at 1750 °C in tank hydrogen prior to the acid treatment. These studies (Table I; Figure 2) indicated that annealing specimens prior to the acid treatment significantly reduced the loss of fuel during the acid treatment. Although the increase in density during the annealing treatment was usually approximately 1%, these results suggest that interconnected porosity is reduced, a factor thought to contribute to the improved fuel retention properties of the annealed cermet as is shown later in this report. These studies also show that relatively short acid treatment times are required in order to prevent dissolution of the interior fuel from W-micronized UO_2 cermets.

Fabrication data for the tungsten-UO_2 cermet specimens produced for this portion of the program are compiled in Table II.

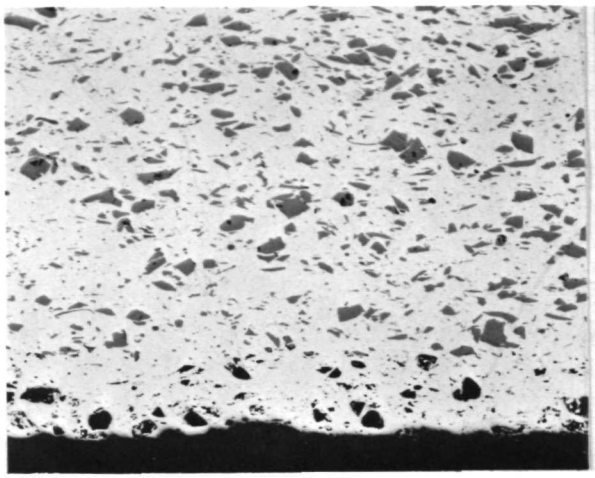
TABLE I. Nitric Acid (9.7 molal) Dissolution of Exposed UO_2 from W-Micronized UO_2 Cermets

Specimen	Time in Acid, hr	UO_2 Removed
20 vol%, 37μ UO_2 (10 mole% CaO) in 1μ W, non-annealed; cermet AR	4	25% (Figure 2)
20 vol%, 37μ UO_2 (10 mole% CaO) in 1μ W, non-annealed; cermet AR	23	90% (Figure 2)
20 vol%, 37μ UO_2 (10 mole% CaO) in 1μ W, annealed before acid treatment	23	Surface Exposed Only[(a)] (Figure 2)
20 vol% micronized (<4μ) UO_2 - 1μ W, non-annealed	23	100%
20 vol% micronized (<4μ) UO_2 - 1μ W, annealed before acid treatment	23	50%

[(a)] Surface exposed UO_2 is approximately 6%.

BNWL-394
NASA-CR-54840

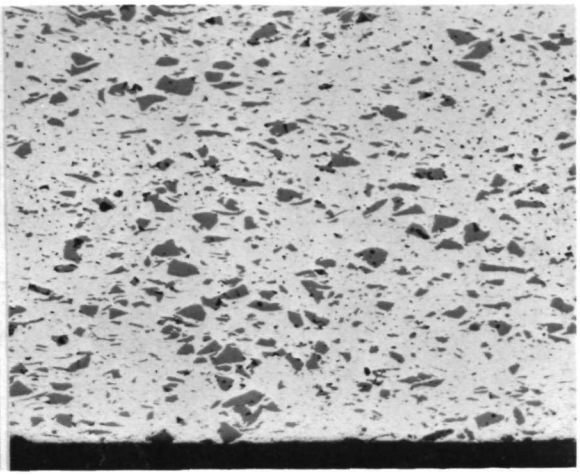
Cermet AR



Neg 46585 100X

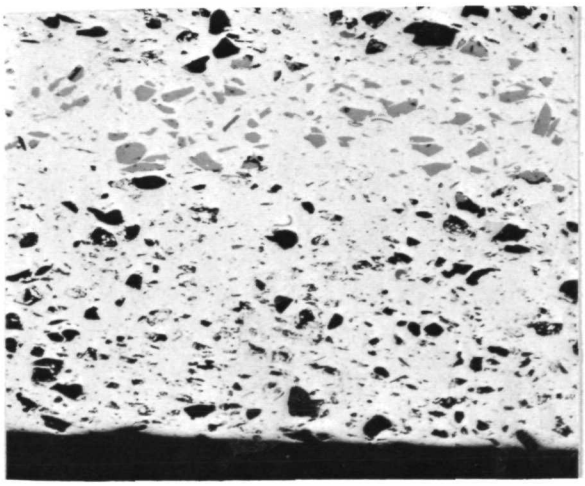
Not Annealed,
4 hr Acid Treatment

Cermet ARA



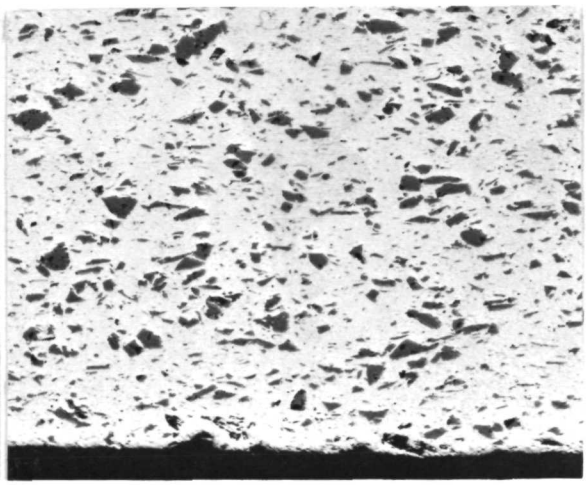
Neg 465194A Nonetched

Annealed,
No Acid Treatment



Neg 465494 100X

Not Annealed,
23 hr Acid Treatment



Neg 465493 Nonetched

Annealed,
23 hr Acid Treatment

FIGURE 2. Results of Nitric Acid Dissolution of UO_2 from a W-20 vol% UO_2 Cermet Fabricated by Pneumatic Impaction of Noncoated UO_2 and 1μ Tungsten

TABLE II. Composition, Raw Materials, and Fabrication Description of W-UO_2 Cermets

Cermet[a]	Composition, wt% UO_2	W	Raw Materials	Fabrication Process[b]	Impaction Temp °C	Bulk Density[c] (100μ)% TD
KK & KKA	12.5 (20.0 vol%)	87.5	Micronized UO_2 (<4μ), 1μ W	Initial process	1200	
QQ & QQA	12.5 (20.0 vol%)	87.5	Micronized UO_2 (<4μ), 1μ W	Final process except UO_2 not pretreated in H_2 and heated for impaction in vacuum	1200	91.6
3Q & 3QA	12.5 (20.0 vol%)	87.5	Micronized UO_2 (<4μ), 1μ W	Final process except heated for impaction in vacuum	1200	3Q = 87
UU & UUA	12.5 (20.0 vol%)	87.5	Micronized UO_2 (<4μ), 1μ W	Final process except UO_2 not pretreated in H_2	1200	
3U & 3UA	12.5 (20.0 vol%)	87.5	Micronized UO_2 (<4μ), 1μ W	Final process	1200	3UA = 86
VA	12.5 (20.0 vol%)	87.5	<44μ arc fused UO_2 (O/U = 1.93), 1μ W	Final process except UO_2 not pretreated in H_2	1200	91
VB	12.5 (20.0 vol%)	87.5	<44μ arc fused UO_2 (O/U = 1.93), 1μ W	Final process except UO_2 not pretreated in H_2	1200	86
VC	12.5 (20.0 vol%)	87.5	<44μ arc fused UO_2 (O/U = 2.01), 1μ W	Final process except UO_2 not pretreated in H_2	1200	89
VD	12.5 (20.0 vol%)	87.5	<44μ arc fused UO_2 (O/U = 2.05), 1μ W	Final process except: (1) UO_2 not pretreated in H_2 and (2) heated for impaction in vacuum	1200	92
WA	12.5 (20.0 vol%)	87.5	44-62μ arc fused UO_2, 5-62μ W	Initial process except heated for impaction 1 hr with nontrapped vacuum pump	1200	
WB	12.5 (20.0 vol%)	87.5	44-62μ arc fused UO_2, 5-62μ W	Initial process except with nontrapped vacuum pump	1200	
WC	12.5 (20.0 vol%)	87.5	44-62μ arc fused UO_2, 5-62μ W	Initial process except heated for impaction 1 hr	1200	
WD	12.5 (20.0 vol%)	87.5	44-62μ arc fused UO_2, 5-62μ W	Initial process except heated for impaction 1 hr	1200	
PP	19.6 (30.0 vol%)	80.4	Coprecipitated W + UO_2	Initial process except heated for impaction 1 hr	1200	89
OO	19.6 (30.0 vol%)	80.4	Coprecipitated W + UO_2	Initial process except heated 12 hr at 1750 °C in wet H_2 prior to loading impaction can	1200	90
ARA	12.5 (20 vol%) plus 2.15 wt% CaO in UO_2 solid solution[d]	86 plus 1.05 wt% ThO_2	<37μ UO_2-CaO solid solution, 1μ W, 0.06μ ThO_2	Final process	1200	AR = 93.2
ASA	23.4 (35 vol%) plus 2.15 wt% CaO in UO_2 solid solution[d]	75.0 plus 1.05 wt% ThO_2	<37μ UO_2-CaO solid solution, 1μ W, 0.06μ ThO_2	Final process	1200	AS = 93.2

[a] Cermet designations ending with the letter "A" indicate that the specimens cut from these plates were annealed 12 hr at 1750 °C in hydrogen.

[b] See Figure 1.

[c] Mercury porosimeter technique--all open porosity greater than 100μ in diameter is filled with mercury giving the bulk density value; theoretical density based on W = 19.3 gm/cc; UO_2 = 10.97 gm/cc.

[d] 10 mole% CaO in UO_2 solid solution.

THERMAL CYCLING TEST PROCEDURE

Thermal cycling experiments were performed in pressurized hydrogen in a resistance heated tungsten-filament furnace (Figure 3). The cermet specimens were both supported and heated by the tungsten filament.

Two thermal cycling test procedures were used in this study. These were:

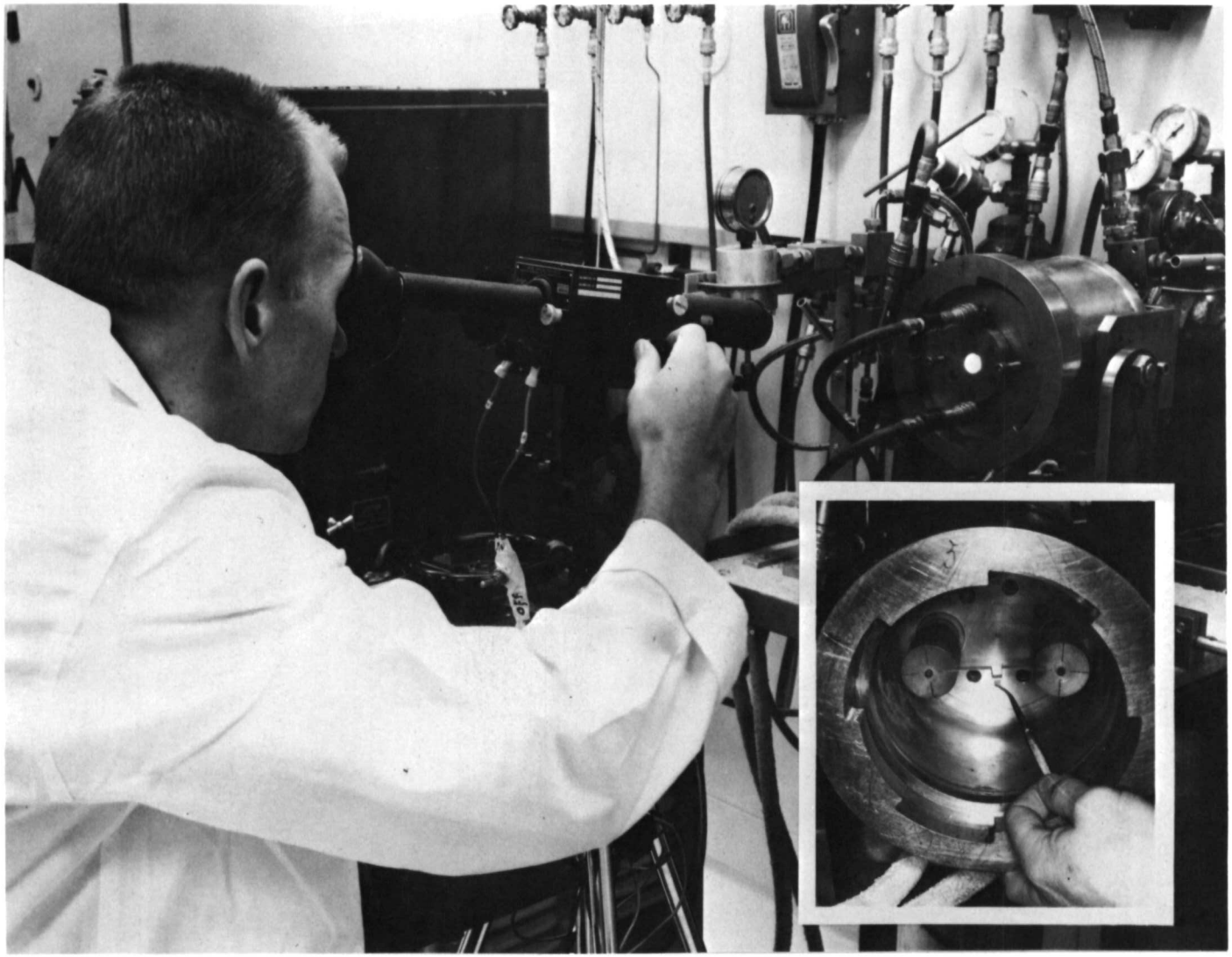
1. The standard test, consisting of a 1 min temperature rise to 2500 °C, a 10 min* (8 in some early work) hold at temperature, a 1 min cooling by interrupting furnace power, and at least 15 sec hold between cycles. The pressure was maintained at either 40.8 atm or 1 atm of dry hydrogen, either static or flowing as specified. These standard conditions comprise the basis for comparison and evaluation of all cermet fuels studied at Battelle-Northwest.
2. The accelerated test, consisting of "instantaneous" (approximately 2 sec) heating to 2600 °C, 2 min holding at temperature, cooling to below visual thermal radiation temperature (about 400 °C) in approximately 2 sec, and at least 15 sec hold between cycles. The pressure was maintained at 68 atm of hydrogen.

A flow rate of 16.5 liters pressurized hydrogen per min** was normally used in flow tests. Hydrogen referred to as "dry hydrogen" in this report contained an average of 7 ppm water by volume. Vendor specifications for the sum of all other impurities were less than 10 ppm.

---

*Referred to as 10 min cycles throughout this report.

**Actual gas velocity past the specimen depends on furnace shape, size, and specimen position and temperatures. The filament furnace used for these tests is a cylinder approximately 15 cm inside diameter and 10 cm deep with the specimen located near the geometric center. Hydrogen enters the end of the furnace at room temperature.



Neg 0650628

FIGURE 3. Resistance Heated, High Pressure, Tungsten-Filament Furnace Used for Thermal Cycling W-UO_2 Cermets

BNWL-394
NASA-CR-54840

CONFIDENTIAL

When tests were conducted in static hydrogen, the furnace was purged, filled with dry hydrogen to the desired pressure, and then isolated from the hydrogen supply and room atmosphere.

Fuel loss data were calculated from periodic weight measurements. Calculations were performed by dividing the cumulative total weight loss of the specimen by the original weight of fuel (UO_2 or UO_2 plus any additive present in the UO_2) and multiplying by 100.

RESULTS AND DISCUSSION

Effect of Materials and Fabrication Variables on Cermet Behavior

Numerous W and UO_2 powder cermets were fabricated for the purpose of correlating fabrication and materials variables with fuel loss occurring during thermal cycling. The following process and materials parameters were of particular interest:

- Hydrogen pretreatment of the tungsten-UO_2 powder mixtures prior to compaction
- Annealing of fabricated cermets 12 hr at 1750 °C in tank hydrogen
- Oxygen-to-uranium ratio of the fuel
- Carbon content of the fabricated cermet
- Coprecipitation of the cermets versus mixing of powders.

The cermet specimens used in studying these variables were cycled under the accelerated test conditions. Analysis of the thermal cycling data (Figure 4) led to the following observations.

Hydrogen Pretreatment

Cermets KK, QQ, and 3Q were respectively prepared with no hydrogen pretreatment, hydrogen pretreatment of the tungsten only, and hydrogen pretreatment of the tungsten and UO_2 powder mixtures. The thermal cycling data for these nonannealed specimens (Figure 4) indicate that the hydrogen pretreatment is partially effective in reducing fuel losses. The largest effect was noted when both the

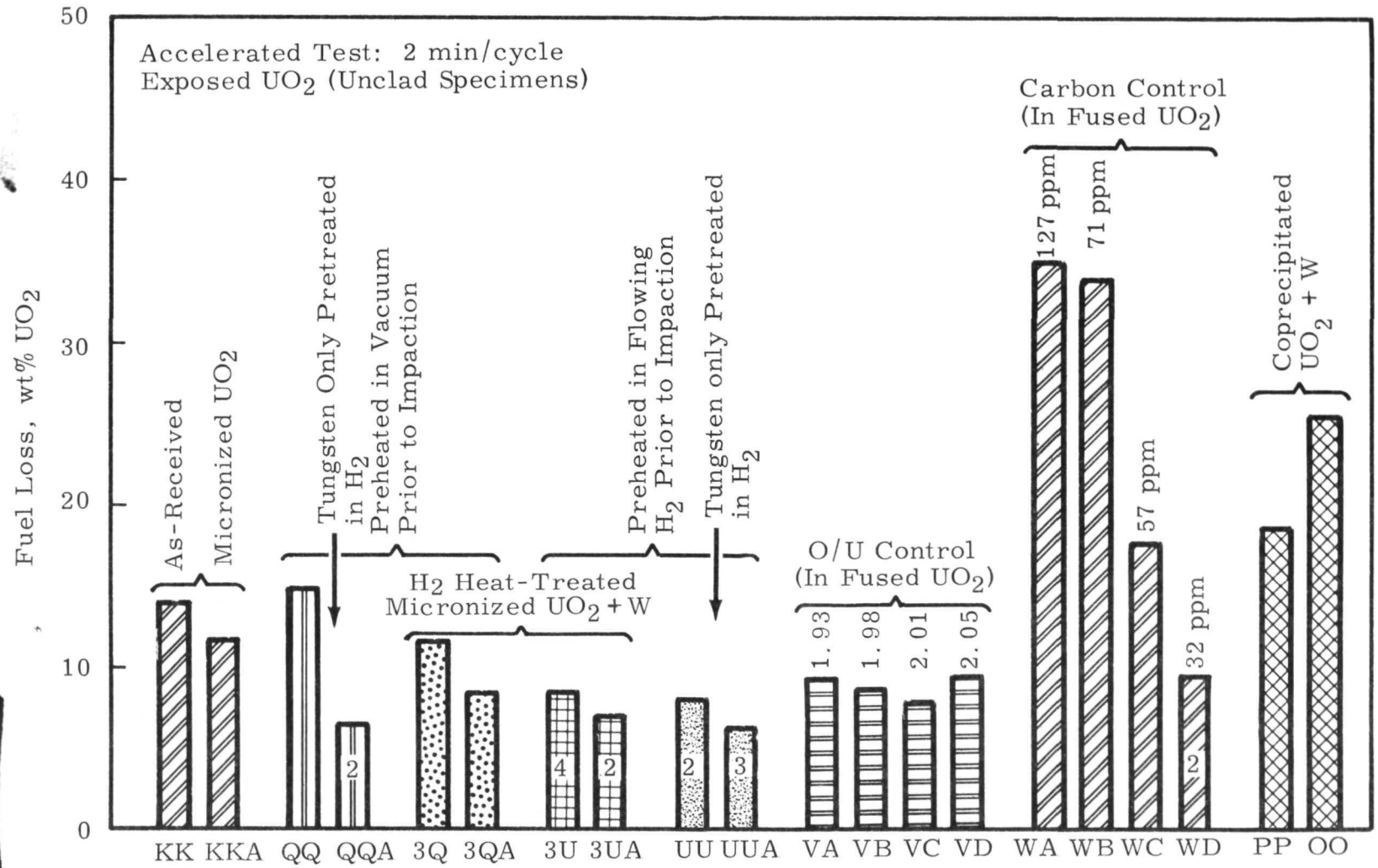


FIGURE 4. Fuel Loss from Nonclad W-UO_2 Cermets During 10 Thermal Cycles to 2600 °C in 68 atm Static Hydrogen (One Specimen Unless Otherwise Noted Within the Bars)

BNWL-394
NASA-CR-54840

tungsten and UO_2 powders underwent hydrogen pretreatment. Heating in hydrogen prior to impaction may further reduce fuel loss during thermal cycling (compare cermets UU and 3U with QQ and 3Q, respectively). Reduction of fuel loss by the various hydrogen pretreatments is more significant for annealed specimens (compare KKA, QQA, and UUA; 3QA and 3UA).

Hydrogen pretreatment studies on the pneumatically impacted 1μ W (no fuel; Table III) indicated that the combined hydrogen pretreatments of the powder and the impaction can assembly reduced the oxygen in the tungsten by a factor of three (compare XX with YY).

Analysis of cermets 3Q and 3U for the oxygen content of the tungsten shows that the hydrogen pretreatment in the presence of the micronized UO_2 removes about half of the oxygen in the tungsten and that the use of a flowing hydrogen atmosphere during pre-impaction heating reduces the oxygen content further but does not completely remove it (Table IV).

TABLE III. Hydrogen Pretreatment and Annealing Effects on Impacted Tungsten Powder

Specimen	Bulk Density (100μ)%	Material	Fabrication Process	Oxygen[(a)] ppm	Carbon, ppm
XX	90	1μ W powder	No H_2 pretreatment, impacted under vacuum at 1200 °C	2300	38
XXA	91	1μ W powder	Same as XX plus 12 hr heat treatment at 1750 °C in tank H_2 after impaction	74	9
YY	85	1μ W powder	Same as XX except heated in purified H_2 for 1 hr at 1000 °C and 1/2 hr to 1200 °C before impaction (Final process: Figure 1)	850	42
YYA	89	1μ W powder	Same as YY plus 12 hr heat treatment at 1750 °C in tank H_2 after impaction	41	13

[(a)] Oxygen analyses provided by NASA Lewis Research Center.

TABLE IV. Oxygen Content Associated with Tungsten in 20 vol% Micronized UO_2-W Cermets

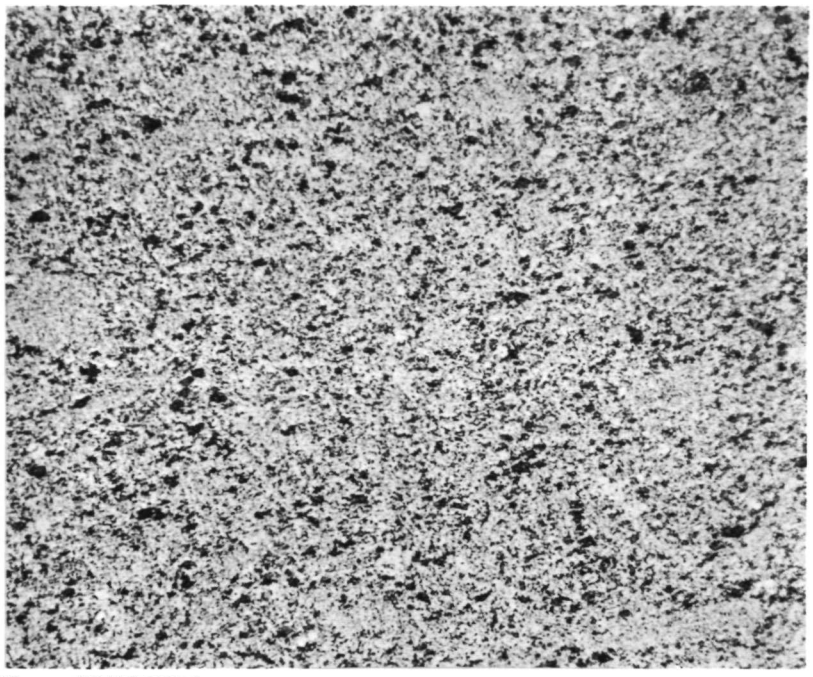
Specimen	Condition	Oxygen Content, ppm [a]
1μ W Powder	As received	3065
3Q	Hydrogen precleaned; heated in vacuum prior to impaction	1450
3U	Hydrogen precleaned; heated in hydrogen prior to impaction	725
3QA	3Q plus annealed after impaction	37

[a] See Appendix C

Annealing Studies

Fuel losses from W-micronized UO_2 cermets cycled 10 times under the accelerated test conditions were reduced significantly by post-pneumatic impaction annealing of the cermets 12 hr at 1750 °C in hydrogen (compare KK, QQ, 3Q, UU and 3U with KKA, QQA, 3QA, UUA and 3UA, respectively, Figure 4). In addition, comparison of cermets 3U (non-annealed) and 3UA (nonannealed and annealed respectively; Figure 5) shows the postimpaction annealing treatment to be quite significant at 25 thermal cycles under standard test conditions (Figure 6). In each cermet studied, the annealing treatment was effective in reducing fuel losses during thermal cycling.

The beneficial effect of annealing on the fuel loss experienced during thermal cycling of the cermets is probably due to the reduction in size or number of channels available for fuel migration and perhaps due to the purification of the cermet during the annealing treatment. The acid treatment studies previously discussed showed that the annealing treatment limited acid leaching of the fuel which is probably the result of fewer channels available for acid permeation and reaction product escape. Studies on pneumatically impacted, 1μ tungsten (Table III) showed that



Neg 465200D

Etchant: Murakami
500X

Cermet 3U - Nonannealed



Neg 465201D

Etchant: Murakami
500X

Cermet 3UA - Annealed

FIGURE 5. Microstructure of a W-20 vol% UO_2 Cermet Fabricated by Pneumatic Impaction of Micronized UO_2 ($<4\mu$) and 1μ Tungsten (No Acid Treatment)

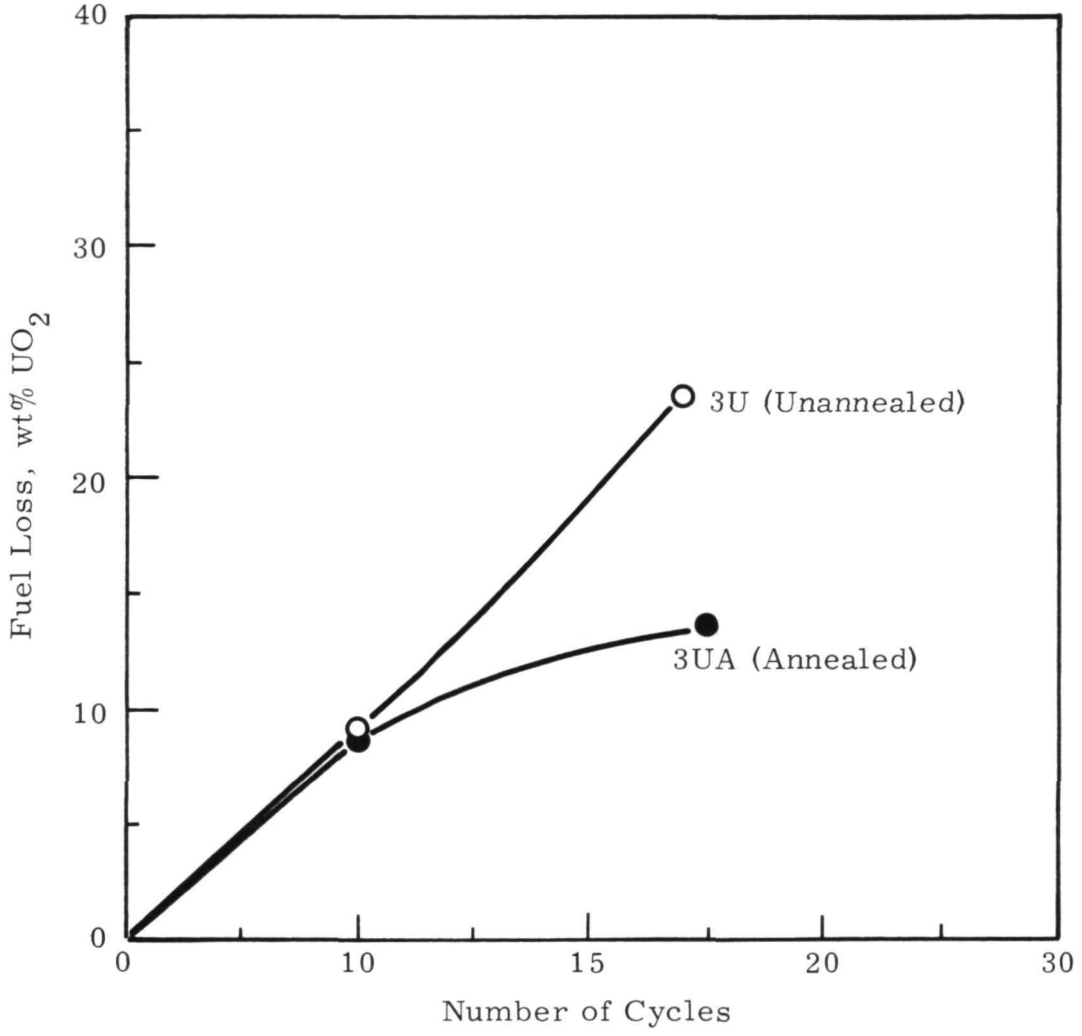


FIGURE 6. Influence of Postimpaction Annealing of Micronized UO_2-W (20 vol% UO_2) Cermets on Thermal Cycling Behavior Under Standard Test Conditions in Static Hydrogen

the annealing treatment also reduced the oxygen content of the tungsten by factors of 20 to 30 and the carbon content by a factor of 4. The annealing treatment also reduces the oxygen content of the W in the presence of the UO_2 to a similar level (cermet 3QA; Table IV).

Fuel Stoichiometry

The O/U ratio of the source UO_2 powder appears to have only a minor effect on the fuel loss behavior of the fabricated cermet. Cermets VA, VB, VC, and VD (Table II), containing fused UO_2 (<44μ particle size) with initial O/U ratios of 1.93, 1.98, 2.01 and 2.05, respectively, behaved essentially the same on thermal cycling (Figure 4). It is likely that a change toward O/U = 2.00 occurred in the cermet during the fabrication procedure.

Carbon Impurities

Organic material (such as introduced by backstreaming from mechanical vacuum pumps) has a significant influence on thermal cycling behavior of the W-micronized UO_2 cermets. Carbon content of four cermets (WA, WB, WC, and WD; Table II) was controlled to 127, 71, 57, and 32 parts per million respectively by using cold traps and various forepumping times during heating to 1200 °C prior to pneumatic impaction. A significant decrease in fuel losses during thermal cycling occurred at carbon contents below 70 ppm. Elimination of carbon impurities introduced in starting materials and from fabrication procedures is very important to the behavior of these cermets.

Material Sources

Cermets fabricated from as-received, coprecipitated UO_2/W (cermet PP) and from hydrogen heat treated, coprecipitated UO_2/W (12 hr, 1750 °C flowing H_2; cermet DO) experienced higher thermal cycling losses than did cermets fabricated from the dry mixed UO_2 and tungsten powders. The appearance of the coprecipitated powders, however, indicated probable impurity contamination.

Effect of Thermal Cycling Conditions on Cermet Behavior

Cermets 3UA and UUA (Table II) were studied to evaluate the effects of pressure, hydrogen flow and of temperature on fuel loss resulting from thermal cycling.

Hydrogen Pressure

Specimens of cermet 3UA were cycled to 2500 °C under 1, 13.6, 40.8, and 68 atm of static hydrogen to determine hydrogen pressure effect on thermal cycling behavior. These experiments (Figure 7) indicated that increases in static hydrogen pressure between 13.6 and 68 atm increased the fuel losses after 25 standard thermal cycles. Thermal cycling fuel losses under 1 atm static hydrogen is markedly lower. Qualitative observations (steromicroscope at 40X) of surface microcracks after 25 thermal cycles showed that the incidence of microcracks increased with increasing hydrogen pressure, ranging from no cracking after testing in 1 atm hydrogen to extensive cracking after testing in 68 atm hydrogen (Figure 8).

Hydrogen Flow

The effect of flowing hydrogen (16.5 liters/min) on the thermal cycling behavior of cermet 3UA was determined at both 1 and 40.8 atm of hydrogen. The fuel loss data (Figure 9) shows a markedly deleterious effect of the hydrogen flow rate on thermal cycling behavior. The effect of the hydrogen flow is probably caused by the sweeping of reaction products from the surface of the cermet.

Time at Temperature

Thermal cycling of cermet UUA in 40.8 atm of static dry hydrogen to 2500 °C for 2 and 10 min/cycle showed a significant increase in fuel loss as a function of the time at temperature (Figure 10). This result is to be expected for the nonclad W-micronized UO_2 cermets because the cermet should behave essentially as a W filter (the matrix) with UO_2 in the interstices. The W matrix only prevents the fuel from having a large surface exposed.

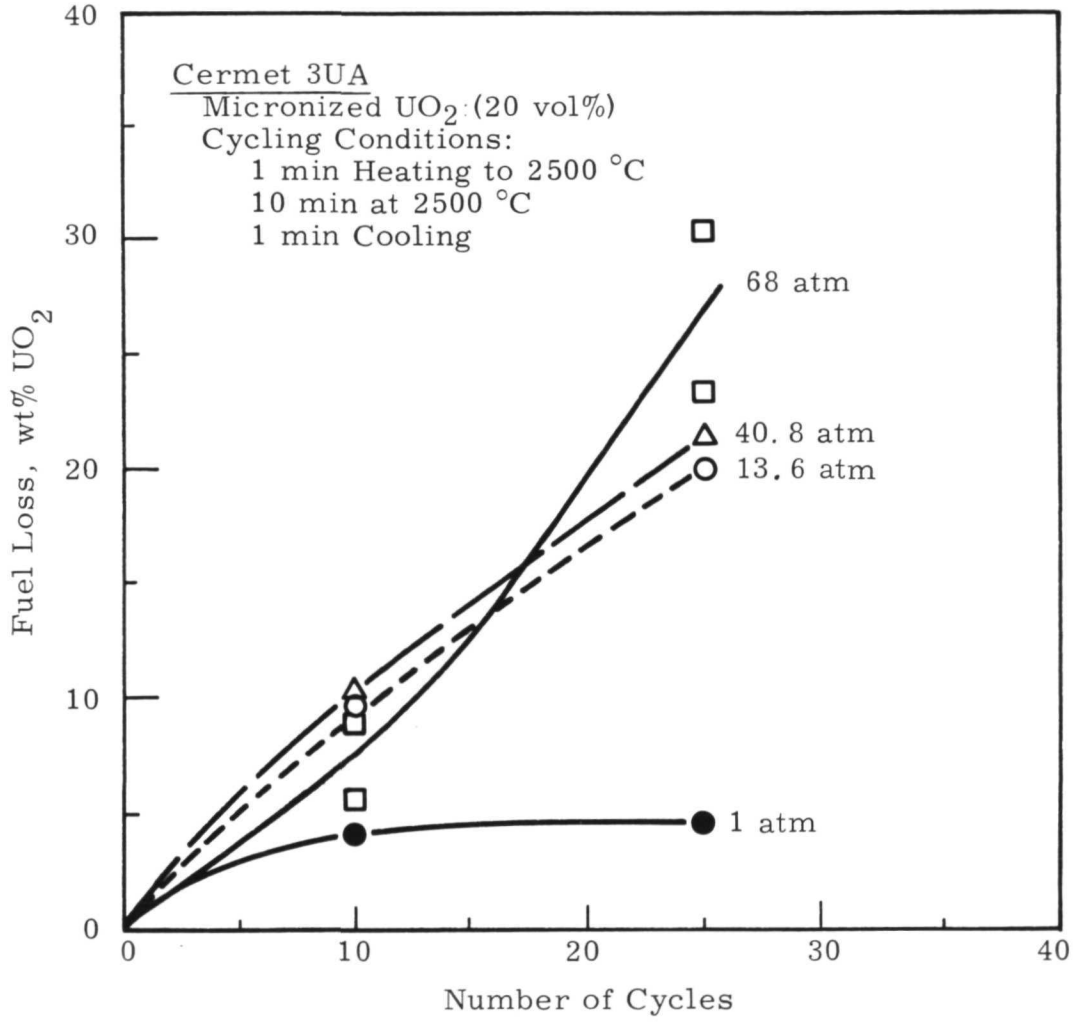
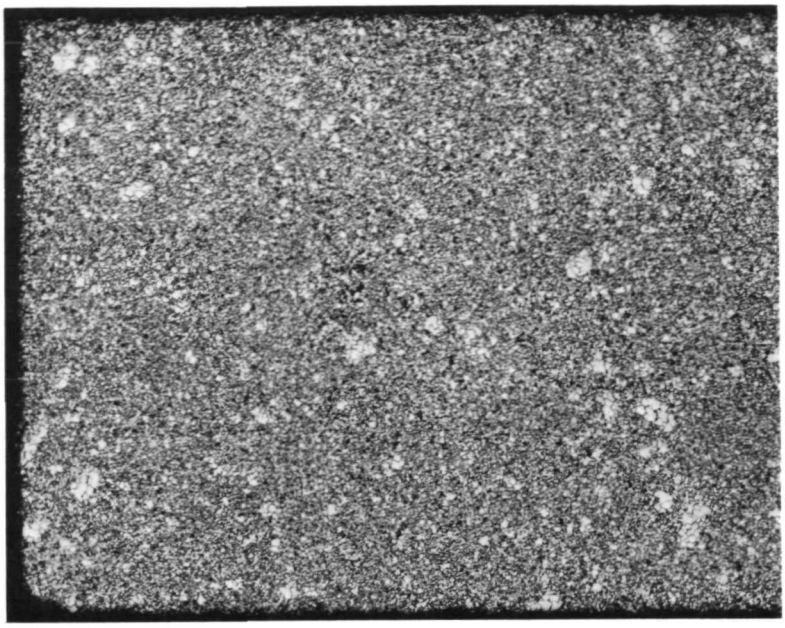


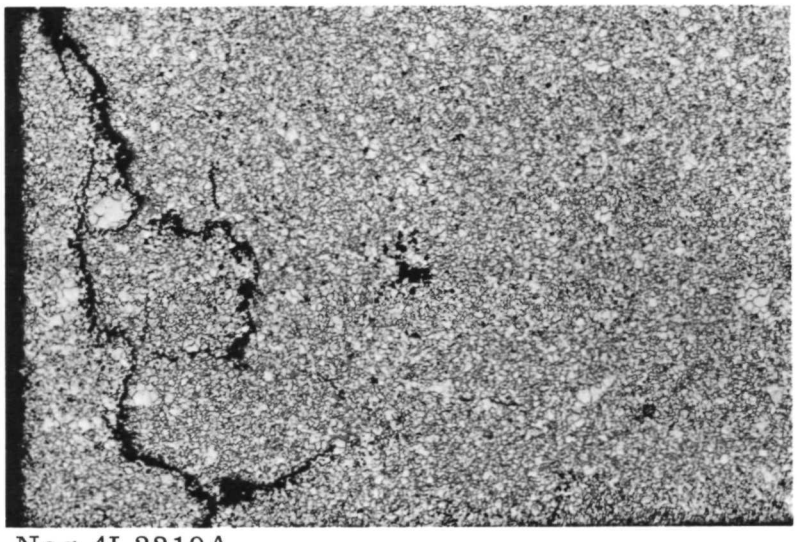
FIGURE 7. Static Hydrogen Pressure Effects on the Thermal Cycling Behavior of W-Micronized UO_2 Cermets



Neg 4L2218A

Etchant: Murakami
100X

a. Cermet 3UA-10
(Cycled 25 times under Standard test conditions
1 atm static H_2 pressure; Fuel loss = 4.7 wt%)



Neg 4L2219A

Etchant: Murakami
100X

b. Cermet 3UA-11
(Cycled 25 times under Standard test conditions
68 atm static H_2 pressure; Fuel loss = 30.4 wt%)

FIGURE 8. Static Hydrogen Pressure Effects on Cracking During Thermal Cycling of Micronized UO_2-W (20 vol% UO_2) Cermets

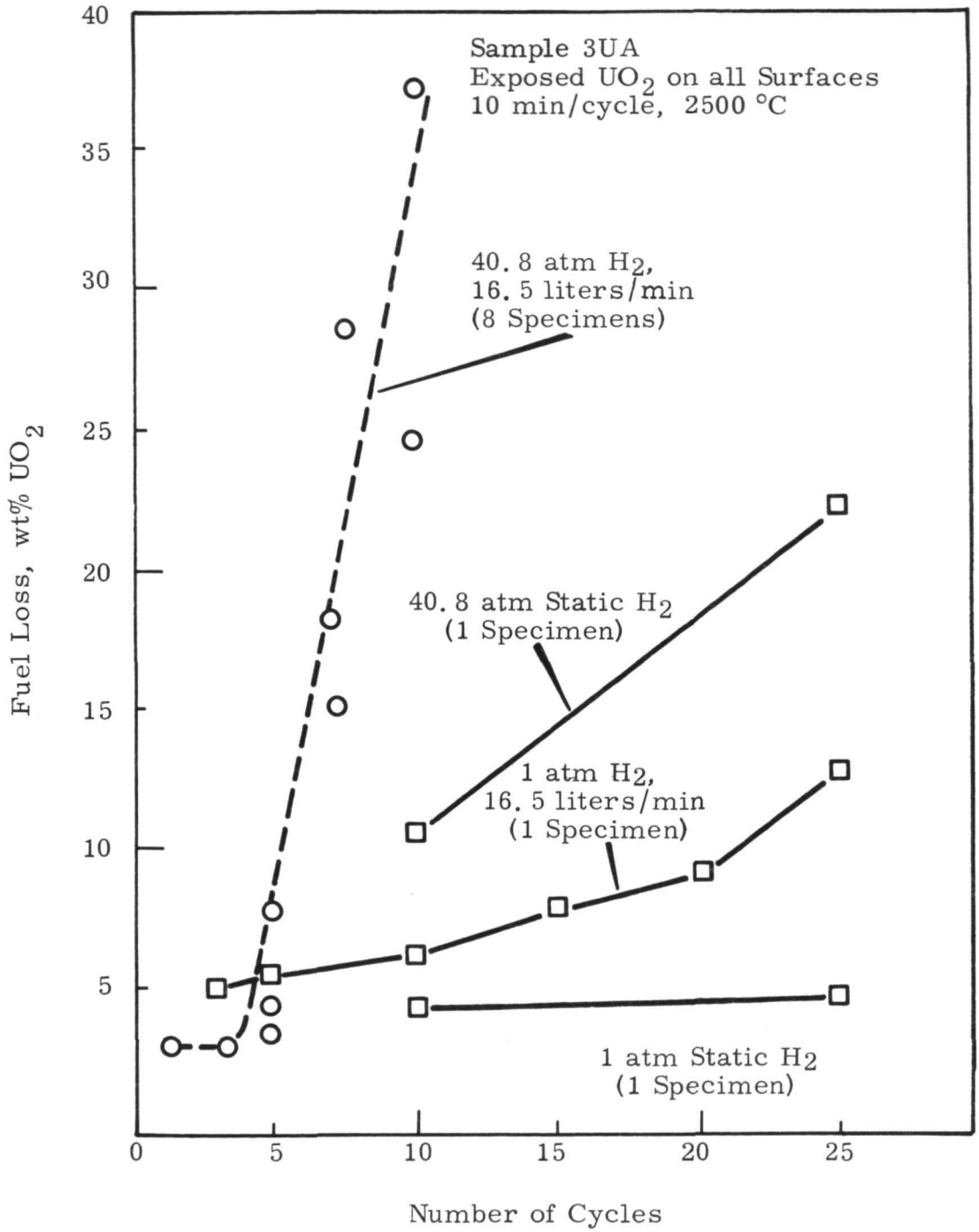


FIGURE 9. Effect of Hydrogen Pressure and Flow Rate on Fuel Loss During Thermal Cycling of a W-20 vol% Micronized UO_2 Cermet

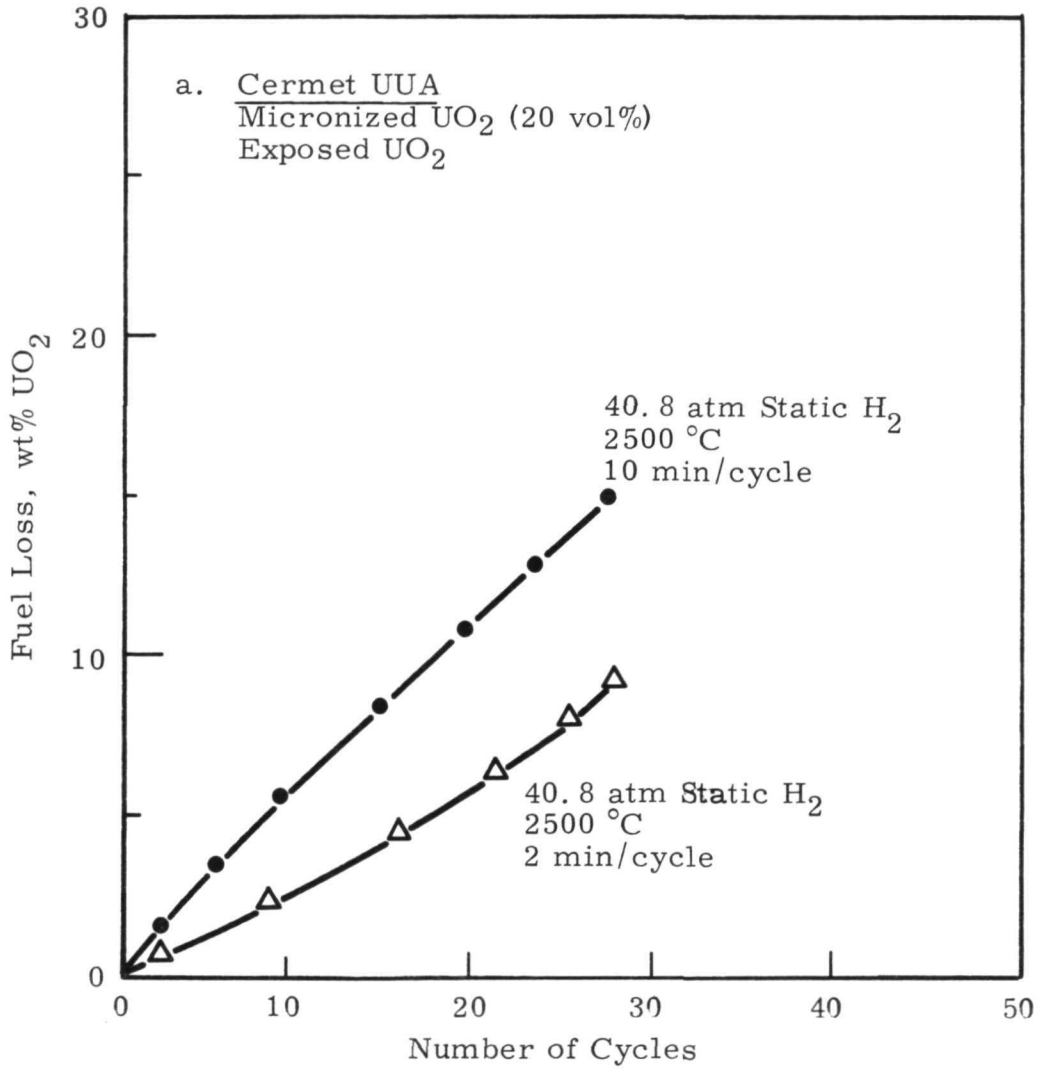


FIGURE 10. Effect of Cycle Duration on the Fuel Loss from W-Micronized UO_2 Cermets

Effect of Cermet Composition on Thermal Cycling Behavior

Cermets 3UA (20 vol% UO_2 with no additives) ARA (20 vol% UO_2 with 10 mole% CaO in solid solution--see Reference 5 for discussion of the effects of CaO--and finely dispersed ThO_2 in the tungsten matrix--see Reference 6 for a discussion of methods for controlling fuel loss under thermal cycling conditions), and ASA (35 vol% UO_2 with 10 mole% CaO in solid solution and finely dispersed ThO_2 in the tungsten matrix) (Table II) were thermally cycled in static and 16.5 liters/min flowing H_2.

Fuel loss data from nonclad cermets (3UA, ARA and ASA) cycled under 40.8 atm in either static or flowing H_2 are shown in Figure 11. CaO and ThO_2 additives (cermets ARA and ASA) improved cermet integrity from that of specimens (3UA) not having the additives. The latter cermet reverted to powder after 10 thermal cycles in the flowing H_2. Cermets ARA and ASA did not revert to powder even after 25 thermal cycles and catastropic fuel loss.

Increasing the fuel content (CaO stabilized) from 20 to 35 vol% reduced the percent of fuel loss but the mass of fuel lost was approximately the same from both cermets (compare ARA with ASA; Figure 11). This result suggests that a reaction or vaporization product removal step may be controlling the rate of fuel loss.

CONCLUSIONS

Thermal cycling studies on W-UO_2 powder cermets have shown:

1. The beneficial effects of a precleaning treatment of W and UO_2 powder mixtures, the loading of the impaction can assembly in inert atmosphere, the preheating of the impaction can assembly in flowing hydrogen prior to drawing a vacuum for pneumatic impaction, and annealing the cermets on fuel loss behavior during thermal cycling
2. The insensitivity of fuel loss behavior to the O/U ratio of the starting material

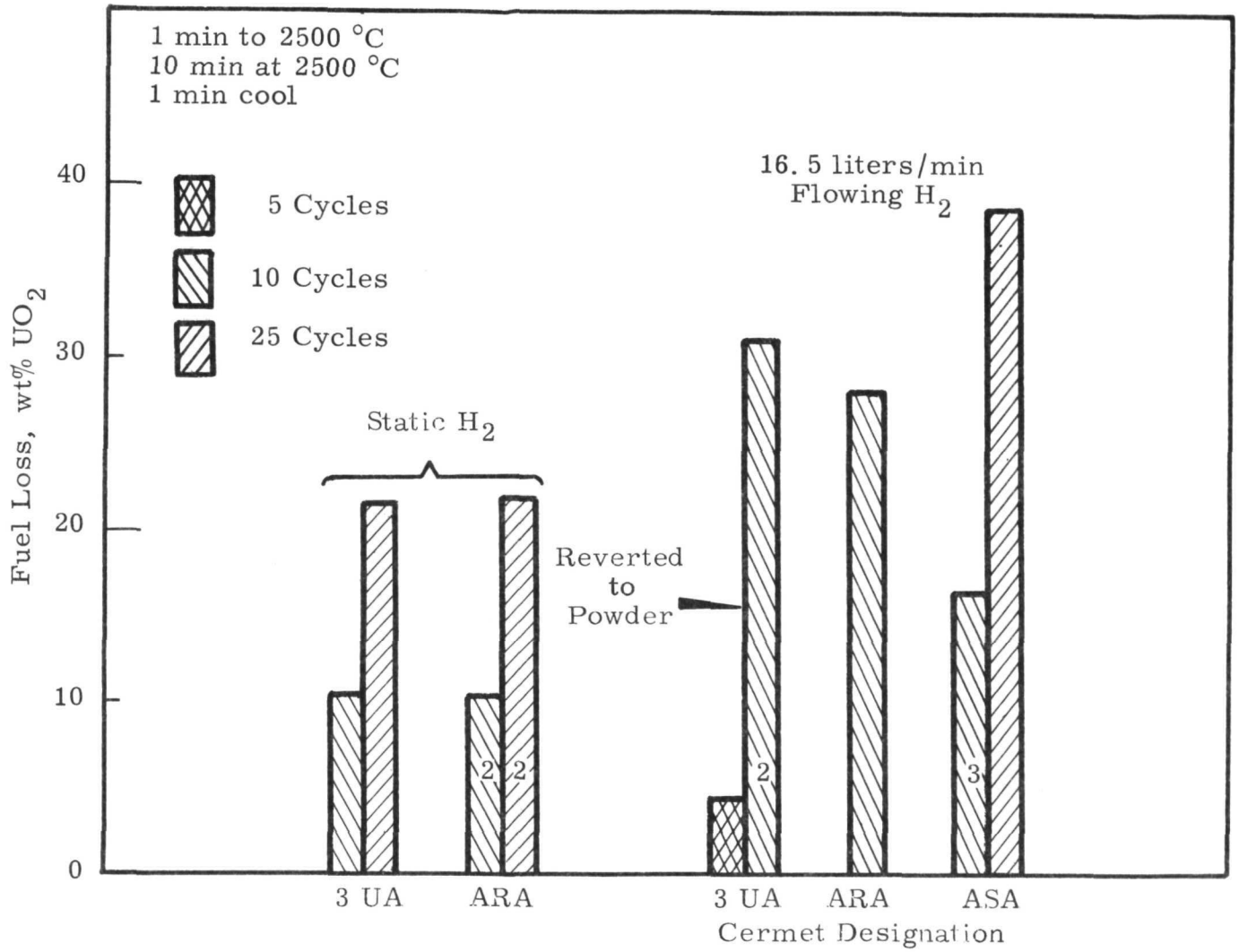


FIGURE 11. Fuel Loss from W-UO_2 Cermets During Thermal Cycling to 2500 °C in 40.8 atm Dry Hydrogen (One Specimen Tested Unless Otherwise Noted Within the Bars)

BNWL-394
NASA-CR-54840

3. Increased fuel loss with increased carbon impurity content
4. A marked increase in fuel loss with increased hydrogen pressure from 1 atm to 13.6 to 68 atm
5. A marked increase in fuel loss characteristics when thermal cycling in flowing hydrogen versus static hydrogen.

BNWL-394
NASA-CR-54840

PART II

THERMAL CYCLING STUDIES ON W-UO_2 COATED PARTICLE CERMETS

PART II. THERMAL CYCLING STUDIES ON W-UO_2 COATED PARTICLE CERMETS

CERMET FABRICATION

The W-UO_2 coated particle* cermets studied in this portion of the program were prepared by: (a) pneumatic impaction of 100% tungsten coated (vapor deposited) UO_2 particles, and (b) pneumatic impaction of mixtures of tungsten-coated UO_2 and fine grain tungsten powder. The final process (Figure 12) developed during the study of the effect of fabrication variables on thermal cycling behavior consisted of the following:

1. Loading the tungsten-coated fuel particles into the impaction can assembly in air
2. Preheating the impaction can assembly for 40 min, including 10 to 15 min at 1600 °C
3. Pneumatic impaction at greater than 17, 600 kg/cm^2 at 1600 °C in vacuum
4. Furnace cooling of the impacted can assembly from 800 °C
5. Removal of cermet specimens from the impaction can assembly by machining and chemical dissolution
6. Dissolution of exposed fuel from cut specimens
7. Twelve hour annealing at 1750 °C in hydrogen. **

Variations (Figure 12) of this process during the program included: (1.) blending tungsten powder with the coated particles in air; (2) preheating the cermet mixture for 1 hr at 1000 °C in flowing hydrogen; (3) loading the impaction can assembly in 8% hydrogen–92% argon; (4) preimpaction heat treatment in vacuum or in flowing hydrogen at 1200 °C; and (5) pneumatic impaction in vacuum at 1200 °C.

*Spherical UO_2 particles coated with tungsten by reduction of WF_6

**5 ppm H_2O, 0.1% O_2 maximum at furnace inlet, gas at outlet may contain up to 1000 ppm H_2O.

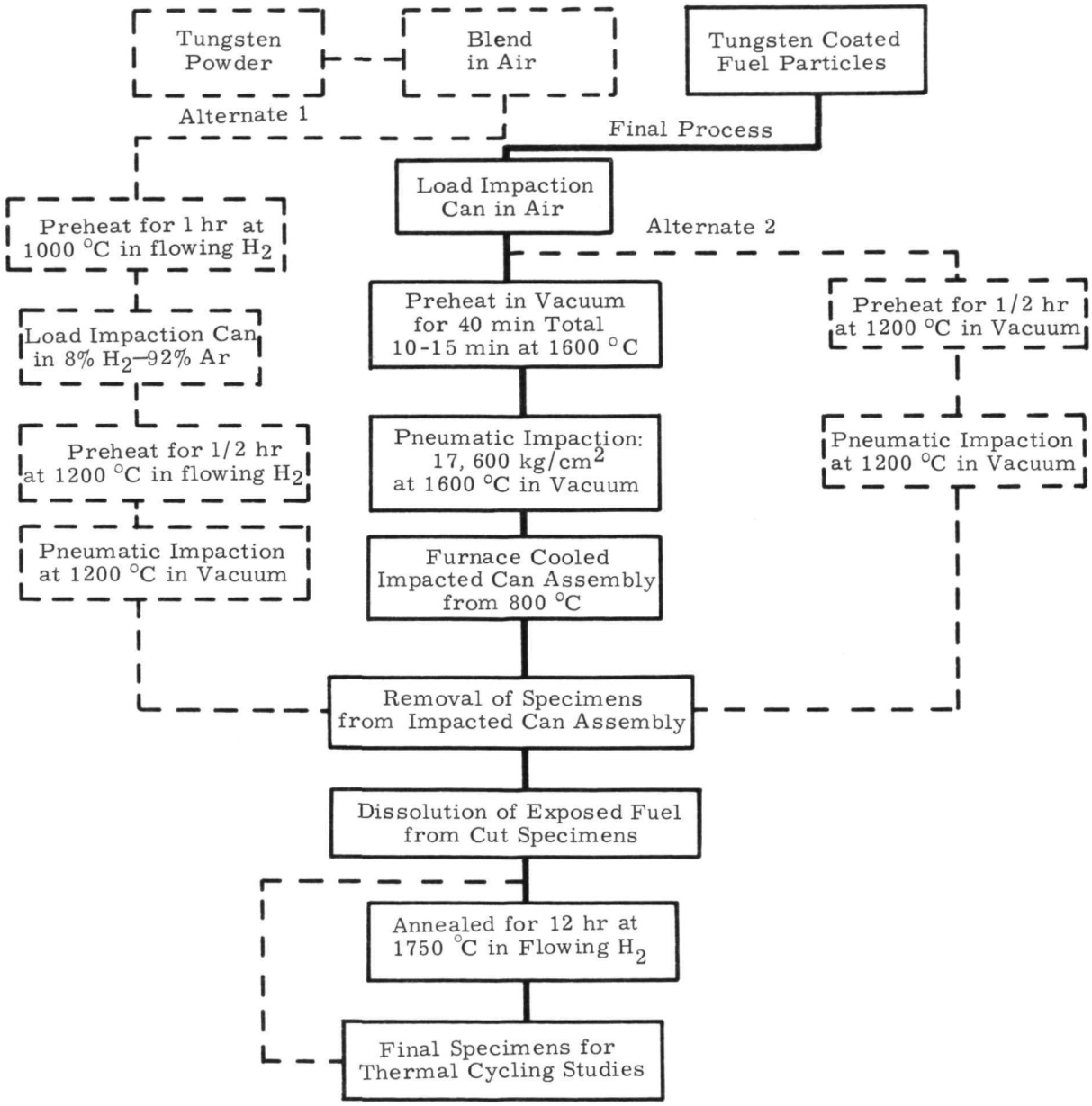


FIGURE 12. Fabrication of W-UO_2 Coated Particle Cermet Specimens

The assembly of the impaction can for impaction at 1600 °C consisted of loading a molybdenum can using molybdenum separators between the plate specimens, Al_2O_3 as a filler material and TIG welding the final closure and outgassing stem to the can assembly. After pneumatic impaction, the can assemblies were opened by machining followed by chemical dissolution of the molybdenum spacers in a recirculating acid bath (60 vol% HNO_3, 20 vol% H_2SO_4, 20 vol% H_2O).

Cermets impacted at 1200 °C were loaded into stainless steel cans. After impaction, the stainless steel separators were removed by dissolution in HCl.

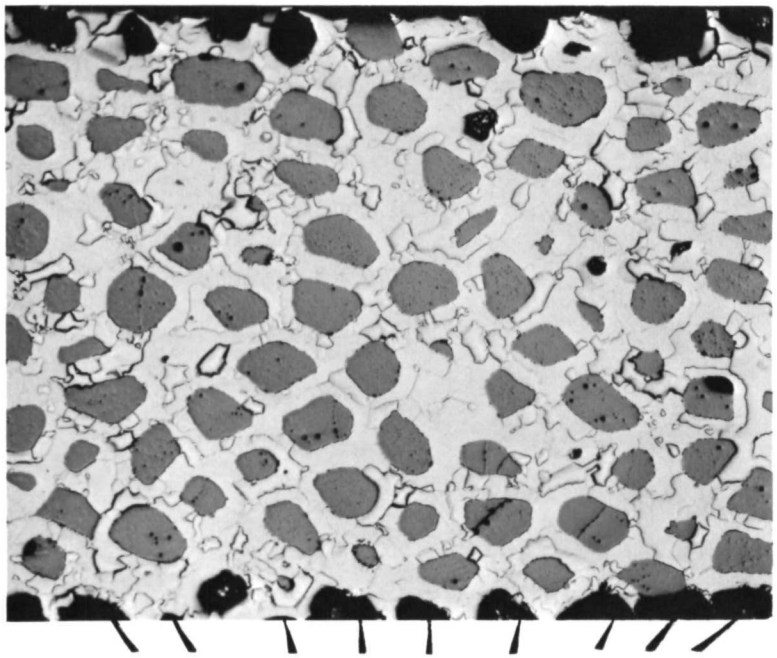
Furnace cooling of the impacted can assembly from 800 °C to room temperature was found to be especially advantageous in the fabrication of honeycomb fuel element structures.[2]

Chemical dissolution of molybdenum spacers from between cermet plates resulted in attack of the surface layer fuel particles, ranging from complete removal at the edges to moderate attack on the tungsten coatings near the center (Figure 13). This reduction of the particle coating thickness near the center of the specimens resulted in premature loss of fuel during thermal cycling. The severe attack at the edges of the cermet plate may result in a stress corrosion effect which would enhance fuel loss from these areas as will be shown later in this report.

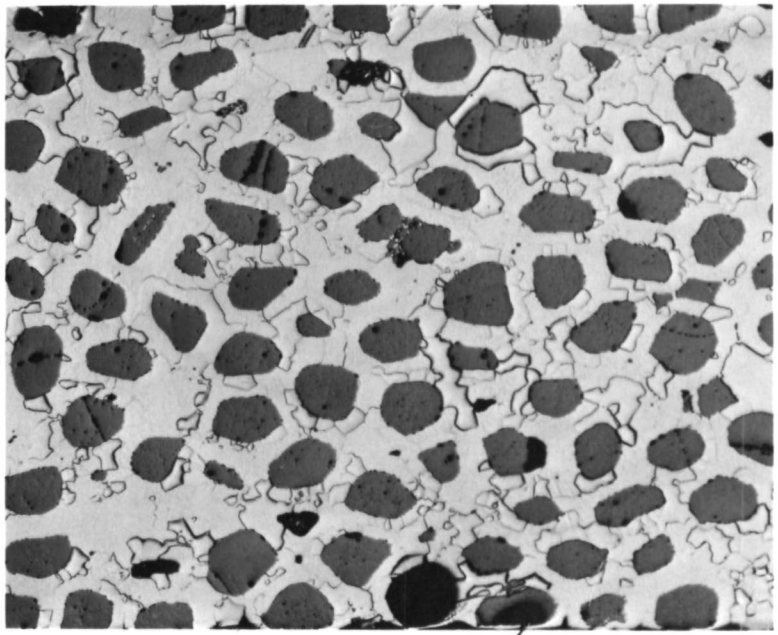
Nine different nonclad, W-UO_2 coated particle cermets were immersed in a 9.7 molal nitric acid solution at room temperature for times up to 48 hr in order to remove the edge exposed fuel. There was no apparent gross damage to the cermet during this treatment (Figure 14).

Fabrication data for the W-UO_2 cermet specimens produced for this portion of the program are compiled in Table V.

CONFIDENTIAL



Surface Layer of Particles Dissolved
a.



Partial Dissolution of Particle
b.

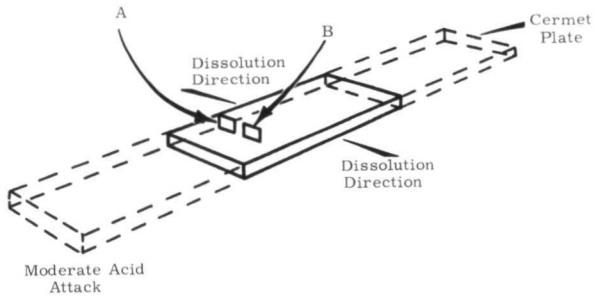
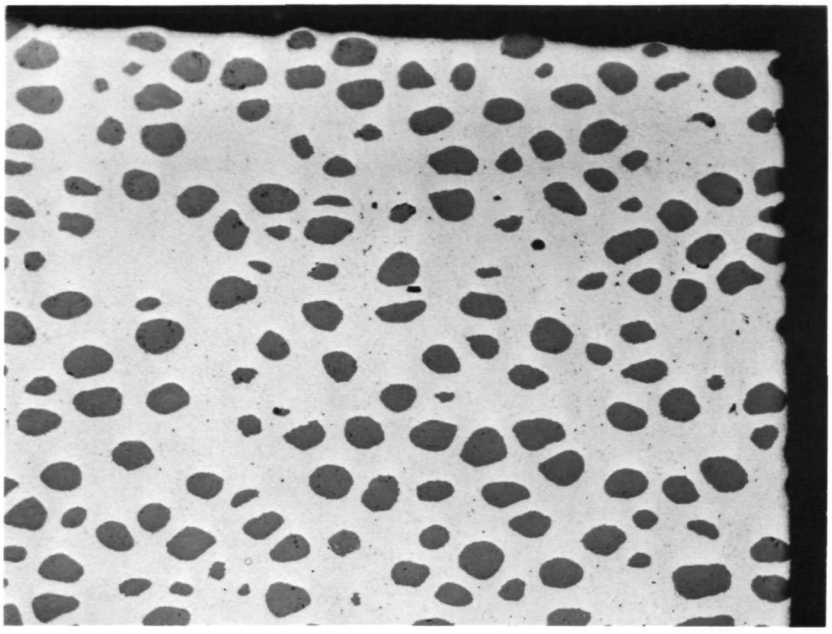


FIGURE 13. Cermet Fabrication Effects: Dissolution of Molybdenum Hardware Used in Assemblies for 1600 °C Impactions (a. Severe Acid Attack, Neg 4652038, 150X; b. Moderate Acid Attack, Neg 4652037B, 100X Nonetched)

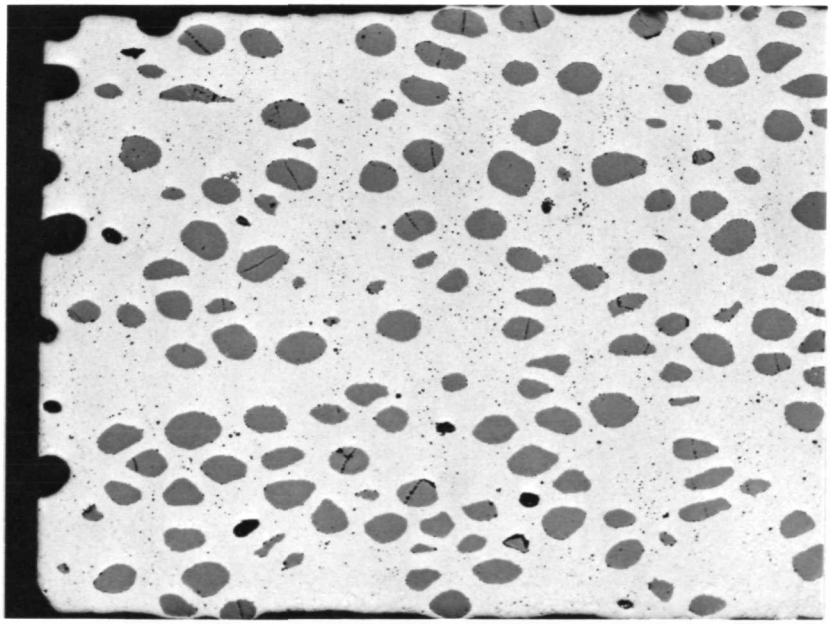
CONFIDENTIAL

BNWL-394
NASA-CR-54840



No Acid Treatment

Neg 465208A



48 hr Acid Treatment

Neg 465202A

FIGURE 14. Nitric Acid Dissolution of Exposed UO_2 from a Nonannealed W-24 vol% UO_2 Cermet Fabricated by Pneumatic Impaction of Tungsten-Coated UO_2 and 5μ Tungsten (Cermet AVA, 100X, Nonetched)

TABLE V. Composition, Raw Materials and Fabrication Description of W-UO_2 Cermets

Cermet[a]	Composition,[c] wt% Fuel[b]	Added W	Raw Materials W	Fuel	Additive	W Coating Thickness in μ	Fabrication Process[d]	Impaction Temperature	Bulk Density[e] (100μ) % TD
MM & MMA	8.0 (13.3 vol%)	32.1	1μ	40-60μ UO_2	None	16	Alternate 2	1200 °C	
AB & ABA	8.0 (13.3 vol%)	32.1	1μ	40-60μ UO_2	None	16	Alternate 1	1200 °C	AB = 87.8
AG & AGA	28.6 (41.3 vol%)	None	-	44-53μ UO_2	None	10	Alternate 1 except no H_2 pretreatment and impaction can loaded in air	1200 °C	AGA = 92.6
AL & ALA	28.6 (41.3 vol%)	None	-	44-53μ UO_2	None	10	Alternate 1 except impaction can loaded in air	1200 °C	
AH & AHA	28.6 (41.3 vol%)	None	-	44-53μ UO_2	None	10	Alternate 1	1200 °C	
AN & ANA	28.6 (41.3 vol%)	None	-	44-53μ UO_2	None	10	Alternate 2	1200 °C	ANA = 95.6
AK & AKA	28.6 (41.3 vol%)	None	-	44-53μ UO_2	None	10	Alternate 2 plus preheated in H_2 for 1 hr at 1000 °C	1200 °C	
AJ & AJA	28.6 (41.3 vol%)	None	-	44-53μ UO_2	None	10	Alternate 2 plus preheated in H_2 for 1 hr at 1000 °C and impaction can loaded in 8% H_2–92% Ar	1200 °C	
AT & ATA	15.3 (24.0 vol%)	46.7	1μ	44-53μ UO_2	None	10	Alternate 1	1200 °C	ATA = 90.1
AV & AVA	15.3 (24.0 vol%)	46.7	5μ	44-53μ UO_2	None	10	Alternate 1	1200 °C	AVA = 95.1
AU & AUA	15.3 (24.0 vol%)	46.7	5μ	44-53μ UO_2	None	10	Alternate 1 plus exposed to air for 5 sec prior to impaction in air	1200 °C	AUA = 93.1
AW & AWA	25.7 (37.8 vol%)	42.8	5μ	37-44μ UO_2	None	4.5	Alternate 1	1200 °C	AWA = 95.5
AX & AXA	13.7 (21.9 vol%)	69.5	5μ	37-44μ UO_2	None	4.5	Alternate 1	1200 °C	AXA = 92.8
AY & AYA	25.7 (37.8 vol%)	42.8 with 1.05 ThO_2 added	5μ	37-44μ UO_2	0.06 wt% ThO_2 (to W)	4.5	Alternate 1	1200 °C	AYA = 95.1
AZ & AZA	25.7 (37.8 vol%)	42.8	5μ	37-44μ UO_2	None	4.5	Alternate 2	1200 °C	AZA = 94.4
BC & BCA	5.5 (9.4 vol%)	None	-	37-44μ UO_2	None	30	Final Process	1600 °C	BCA = 100
BE & BEA	21.4 (32.3 vol%)	None	-	44-53μ UO_2	None	10	Final Process	1600 °C	BEA = 96.5
BD & BDA	12.0 (19.4 vol%)	43.8	1μ	44-53μ UO_2	None	10	Final Process	1600 °C	BDA = 95.9
BG & BGA	28.6 (41.3 vol%)	None	-	44-53μ UO_2	None	10	Final Process	1600 °C	BGA = 98.7
BN & BNA	24.6 (38.0 vol%)	None	-	-	5 mole % Y_2O_3 in UO_2 solid solution	10	Final Process	1600 °C	BNA = 90.5
BS & BSA	17.7 (29.8 vol%)	None	-	37-53μ UO_2	10 mole % Y_2O_3 in UO_2 solid solution	10	Final Process	1600 °C	
BU & BUA	5.4 (10.1 vol%)	None	-	37-53μ UO_2	10 mole % Y_2O_3 in UO_2 solid solution	10	Final Process	1600 °C	
BV & BVA[f]	17.7 (29.8 vol%)	None	-	37-53μ UO_2	10 mole %	10	Final Process	1600 °C	BVA = 100

[a] Cermet designations ending with the letter "A" indicate that the specimens cut from these plates were annealed for 12 hr at 1750 °C in H_2.

[b] Coated particle analysis by a fluorescence technique

[c] The remaining material is the tungsten-coating on the fuel particles

[d] See Figure 12

[e] Mercury porosimeter technique--all open porosity >100μ in diameter is filled with H_g giving the bulk density value; theoretical density based on W = 19.3 gm/cc; UO_2 = 10.97 gm/cc

[f] Identical to BS, BSA except plates impacted on end

THERMAL CYCLING TEST PROCEDURE

Thermal cycling experiments were performed in a resistance heated, high pressure, tungsten-filament furnace (Figure 3). The cermet specimens were both supported and heated by the tungsten-filament.

The standard test consisted of a 1 min temperature rise to 2500 °C, a 10 min hold at temperature, a 1 min cooling, and at least 15 sec between cycles in either 40.8 atm or 1 atm of either static or flowing hydrogen. When tests were performed in flowing hydrogen, a flow rate of 16.5 liters/min was used. The accelerated test consisted of "instantaneous" (~2 sec) heating to 2600 °C, a 2 min hold at temperature, cooling to below visible color temperature (about 400 °C) in ~2 sec, and at least 15 sec between cycles in 68 atm of static hydrogen.

The fuel loss data were calculated from inter-cycle weight measurements. Data are reported as the cumulative total weight losses of the specimen divided by the original weight of fuel (UO_2 or UO_2 plus any additive put in the UO_2), and multiplied by 100.

RESULTS AND DISCUSSIONS

Effect of Fabrication Variables on Cermet Behavior

W-UO_2 coated particle cermets were fabricated for the purpose of correlating fabrication variables with fuel loss occurring during thermal cycling. The following specific fabrication parameters were evaluated:

- Hydrogen pretreatment of the coated particle prior to fabrication
- Loading of the impaction can assembly in an inert atmosphere
- Preheating of the impaction can assembly in hydrogen before impaction
- Pneumatic impaction temperature (1200 and 1600 °C)
- Acid dissolution of molybdenum from the impacted assembly
- Dissolution of exposed fuel from cut specimens
- Annealing of fabricated cermets for 12 hr at 1750 °C in flowing hydrogen.

Materials Handling. A series of W–41.3 vol% UO_2 coated particle cermets (100% coated particles; 70 ppm O_2 associated with the W; cermets AG through AN; Table IV) were studied to determine the effects of hydrogen pretreatment, loading in an inert atmosphere and heating of the impaction assembly in flowing hydrogen prior to impaction at 1200 °C. The accelerated test procedure previously described was used. No significant benefit in reducing fuel losses under the accelerated test conditions was observed (Table VI), in contrast with the studies of the W-micronized UO_2 cermets (Part I of this report) where these materials handling procedures were found to be beneficial. The sole effect of these procedures must, therefore, be purification of the W. For 100% coated particle cermets, it is sufficient to load the impaction can assembly in air and to preheat in vacuum prior to pneumatic impaction.

In the absence of the annealing treatment, pronounced differences are seen between specimens fabricated from coated particles and from as-received, high oxide content powders (MM-2; 24.7 wt% fuel loss) and those prepared from coated particles and tungsten powders pretreated in 1000 °C hydrogen before impaction (AB-1; 6.6 wt% fuel loss). The microstructure shows a third phase surrounding the UO_2 grains and penetrating the boundaries between the columnar tungsten grains in MM (Figure 15). In contrast, even more extensive cycling of the pretreated AB specimen does not show an appreciable effect on the fuel or grain boundaries. The beneficial effect of pretreating cermet AB in a reducing atmosphere is again probably due to cleaning of the 1μ tungsten powder (extent of cleaning is demonstrated in Part I of this report). Thermal cycling studies of cermets impacted from mixture of W-UO_2 coated particles and tungsten powder (cycled to 2500 °C in 40.8 atm static hydrogen) indicate that handling in a reducing atmosphere is not necessary when the finished specimens are annealed (Figures 16 and 17), which reflects the more efficient cleaning of the tungsten during annealing (Tables III and IV).

Impact Temperature Effects. An investigation of the effect of pneumatic impaction temperature on fuel loss was carried out on cermet plates

TABLE VI. Fabrication Pretreatment Effects on the Thermal Cycling Behavior of W–41.3 vol% UO_2 Coated Particle Cermets

Fabrication Variables				
Specimen**	Purification of Powders	Handling Atmosphere After Purification	Pneumatic Impaction Preheating Atmosphere	% UO_2 Weight Loss in 10 Accelerated Test Cycles* to 2600 °C
AG	none	Air	Hydrogen and vacuum	2.9
AGA***				3.9
AH	H_2 at 1000 °C, 1 hr	8% H_2–Ar	Hydrogen and vacuum	5.9 (7 cycles)
AHA				7.1
AJ	H_2 at 1000 °C, 1 hr	8% H_2–Ar	Vacuum	6.1 (9 cycles)
AJA				
AK	H_2 at 1000 °C, 1 hr	Air	Vacuum	4.8
AKA				6.2
AL	H_2 at 1000 °C, 1 hr	Air	Hydrogen and vacuum	3.3
ALA				4.7
AN	none	Air	Vacuum	7.4
ANA				4.1

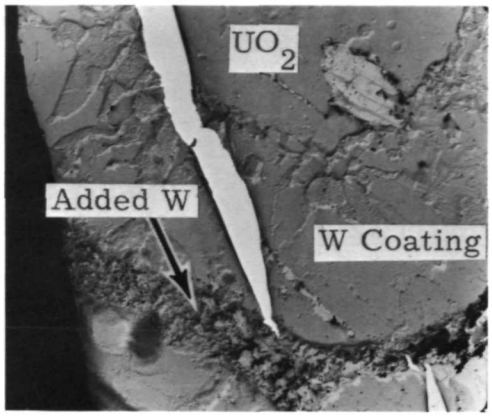
* ~2 sec heating, 2 min at temperature, and ~2 sec cooling

** 41.3 vol% UO_2, as 44 to 53μ UO_2 particles with 10μ tungsten coating; no additional tungsten powder

*** The suffix "A" refers to specimens annealed 12 hr, 1750 °C in tank hydrogen after impaction

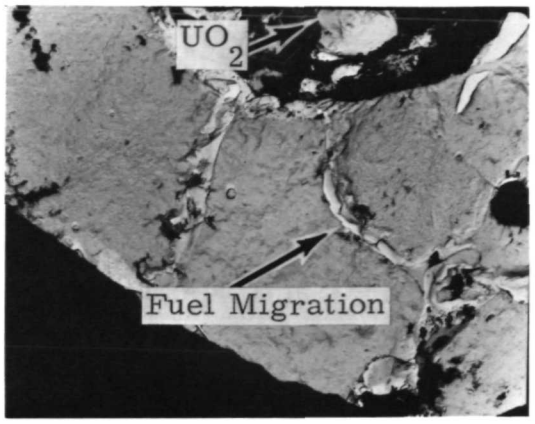
CONFIDENTIAL

PWAC-394
NASA-CR-54840



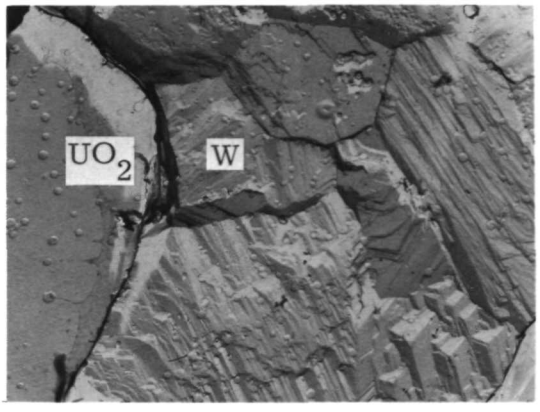
Neg J2585

Cermet MM; As-Fabricated



Neg J2592

Cermet MM; 30 Cycles
24.7 wt% UO_2 Loss



Neg J2759

Cermet AB; 50 Cycles
6.6 wt% UO_2 Loss

FIGURE 15. Electron Micrographs of Pneumatically Impacted W–13.3 vol% UO_2 Coated Particle-Powder Cermets (Carbon Replicas). Comparison of Effects of 2 min Thermal Cycles to 2450 °C in 68.2 atm Static Hydrogen. As-Fabricated Specimens; Etched 1500X

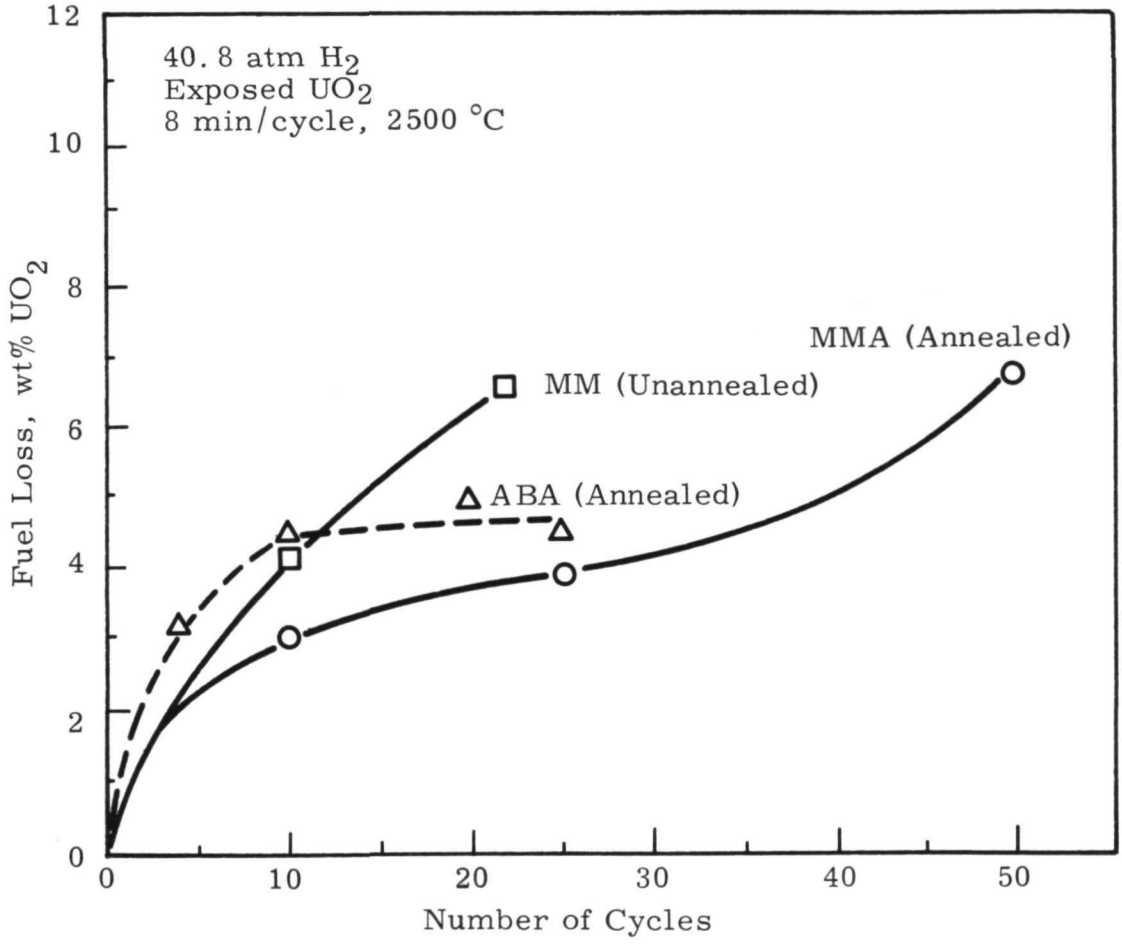
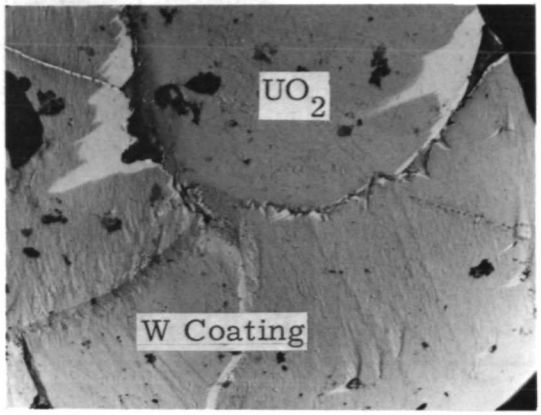
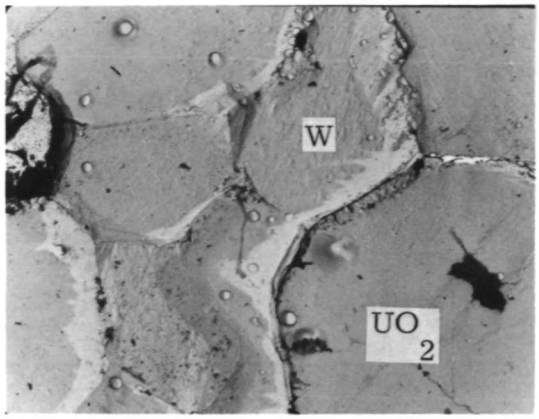


FIGURE 16. Influence of Hydrogen Pretreatment and Postimpaction Annealing of Tungsten-Coated UO_2-W (13.3 vol% UO_2) Cermets on Thermal Cycling to 2500 °C in 40.8 atm Static Hydrogen



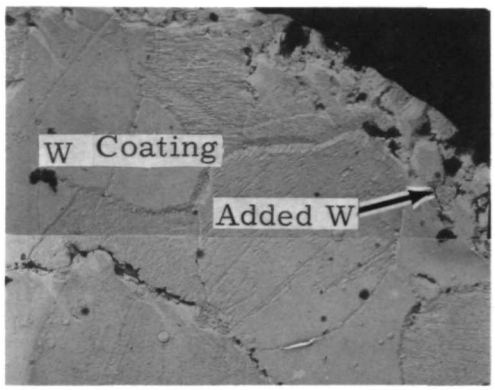
Neg J2520

Specimen MMA-O; As Annealed



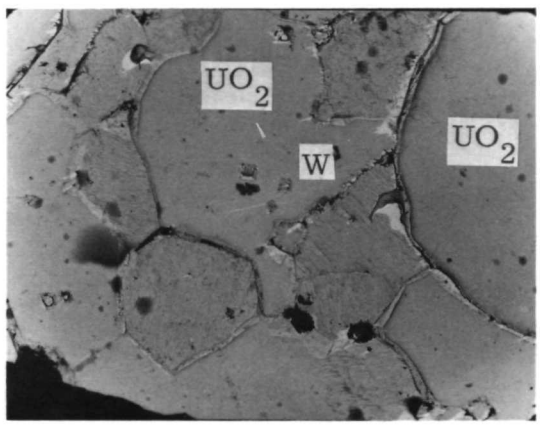
Neg J2750

Cermet MMA; 25 Cycles,
1.9 wt% UO_2 Loss



Neg J2488/2491

Specimen ABA-O; As Annealed



Neg J2465

Cermet ABA; 25 Cycles
1.7 wt% UO_2 Loss

FIGURE 17. Electron Micrographs of Pneumatically Impacted W–13.3 vol% UO_2 Cermets (carbon replicas). Comparison of Effects of 10 min Thermal Cycles to 2500 °C in 40.8 atm Static Hydrogen. Annealed Specimens. Etched; 1500X

fabricated from a common batch of coated particles (44-53μ UO_2, 10μ coating techniques, 41.3 vol% UO_2) by impaction at 1200 °C (cermet ANA) and 1600 °C (cermet BGA). Other than the impaction temperature, the only difference in fabrication processes for the two cermets was that cermet ANA was impacted between stainless steel spacers which were subsequently dissolved in hydrochloric acid and cermet BGA was impacted between molybdenum spacers which were subsequently dissolved in a mixture of nitric and sulphuric acids. The specimens were immersed in nitric acid for 48 hr to remove UO_2 exposed at the cut edges and were subsequently annealed 12 hr at 1750 °C in flowing hydrogen. Increasing the impaction temperature resulted in a density increase from 95.6% TD to 98.7% TD for annealed specimens.

The cermet specimens were evaluated using standard test conditions, cycling to 2500 °C in 40.8 atm, 16.5 liters/min flowing dry hydrogen. Fuel loss data (Figure 18) show large differences between nominally identical cermet specimens particularly for cermet ANA (impacted at 1200 °C) tending to overshadow any clear-cut effect of impaction temperature on fuel retention properties. Impaction at 1600 °C rather than 1200 °C, however, does not appear to significantly influence the fuel loss behavior, but may reduce fabrication variables in the cermet leading to more reproducible fuel element behavior.

Dissolution of Molybdenum Impaction Hardware. Pneumatic impaction at 1600 °C required that a nitric and sulphuric acid combination be used to dissolve the molybdenum impaction separators. This dissolution technique caused a "picture frame" effect, i.e., the surface particles on the outer perimeter of the cermet plates were devoid of fuel (Figure 13). The effect of the presence or absence of the fuel in the surface layer of particles was studied on a W-UO_2 coated particle cermet impacted at 1600 °C (cermet BVA; Table V). Thermal cycling on standard test conditions (Figure 19) showed: (1) significantly lower

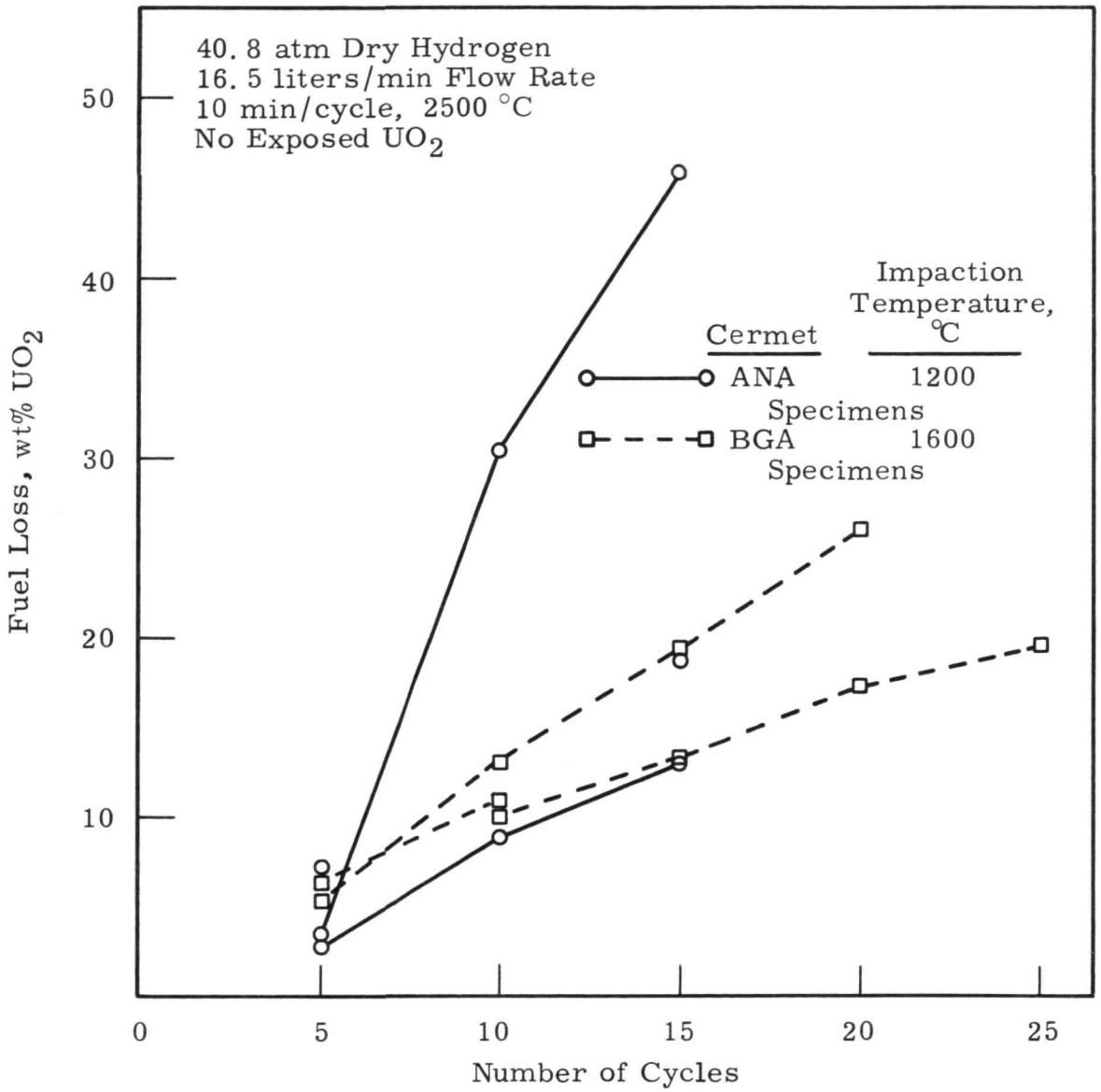


FIGURE 18. Effect of Pneumatic Impaction Temperature on Fuel Loss During Thermal Cycling W–41.3 vol% UO_2 Coated Particle Cermets

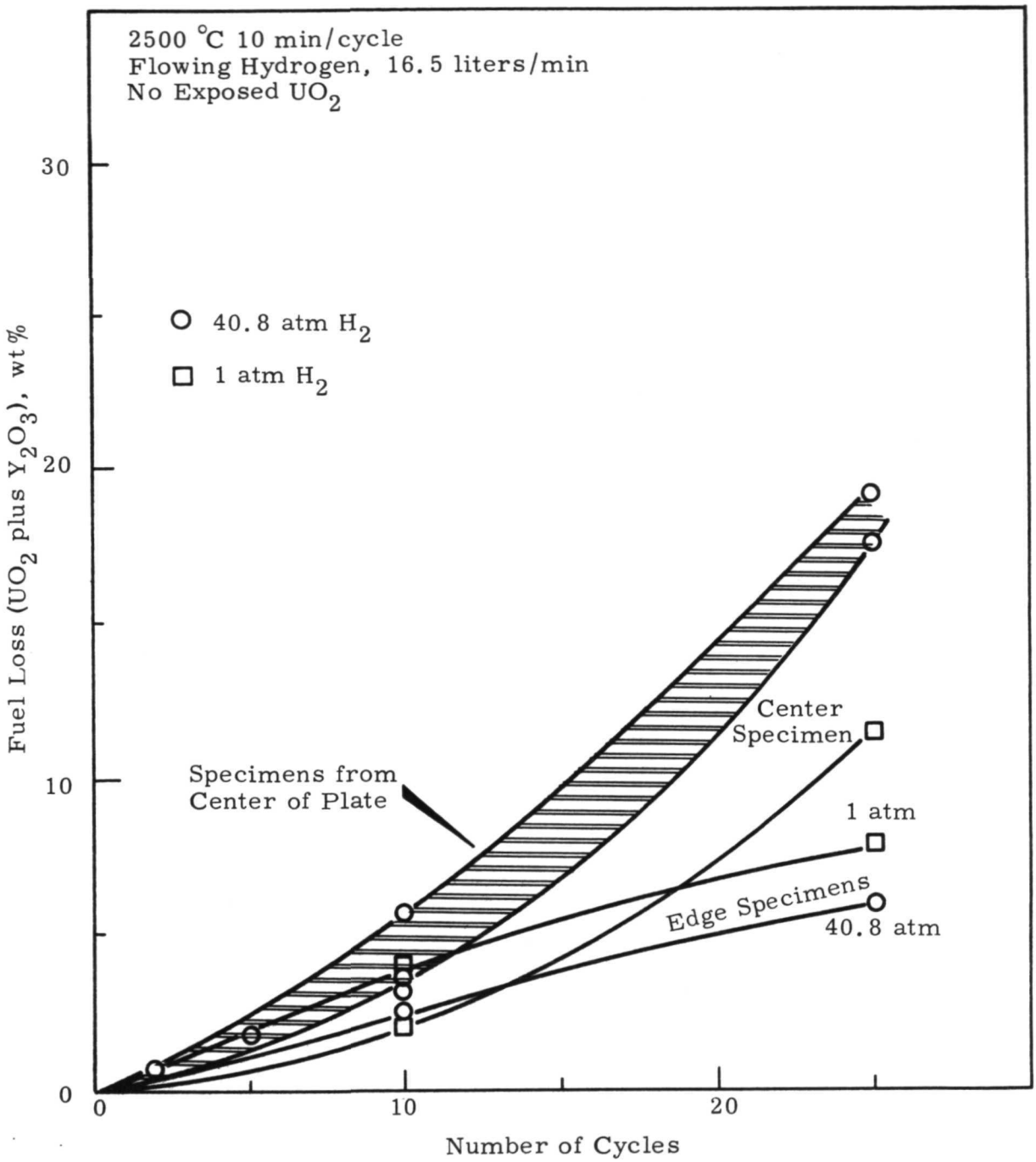


FIGURE 19. Effects of Dissolution of Molybdenum Impaction Hardware on the Thermal Cycling Behavior of W–29.8 vol% (UO_2 + mole% Y_2O_3 Solid Solution) Coated Particle Cermets (Cermet BVA)

fuel losses at 25 thermal cycles from edge specimens (surface layer devoid of fuel) and (2) reverse pressure effects for edge specimens as compared with specimens taken from the center of the cermet plates (surface layer of particles present but W coating attacked). These studies showed a need for further development of techniques for dissolution of molybdenum hardware from these cermet specimens, and that fabrication variables overshadow the effects of thermal cycling environment.

Effects of Edge Exposed Fuel. The effect of edge exposed UO_2 on the thermal cycling behavior of cermet AVA was studied using both the accelerated test (2 min/cycle, 68 atm static hydrogen) and the standard test (10 min/cycle, 40.8 atm static hydrogen). Fuel loss data (Figure 20) show that under standard test conditions the initial fuel loss is higher for as-cut specimens, but that the rate of fuel loss after the initial loss is the same as specimens having no edge exposed UO_2. Results from the accelerated test, however, indicate that the presence of the edge exposed UO_2 affects the rate of fuel loss after the initial loss of the exposed fuel.

Annealing Effects. A postforming annealing treatment for 12 hr at 1750 °C flowing hydrogen for W–13.3 vol% UO_2 coated particle-W powder cermets (cermets MM, MMA and ABA) was evaluated under standard test conditions. Microstructure observations on noncycled cermets (Figure 21) shows that the annealing treatment results in the recrystallization of the added tungsten powder and of the tungsten coating of the coated particles. Fuel loss data (Figure 16) and microstructure observations of cycled cermets (Figure 22) show improved thermal cycling behavior as a result of the annealing treatment. The beneficial effect of the annealing treatment is believed to reflect purification and stress relieving of the cermet. Earlier experiments (Part I of this report) show a marked reduction in the oxygen and carbon content in the 1μ tungsten powders used in these cermets after a postimpaction annealing treatment. Thermal expansion data (Appendix B) show that stress relief takes place upon reheating the impacted cermets.

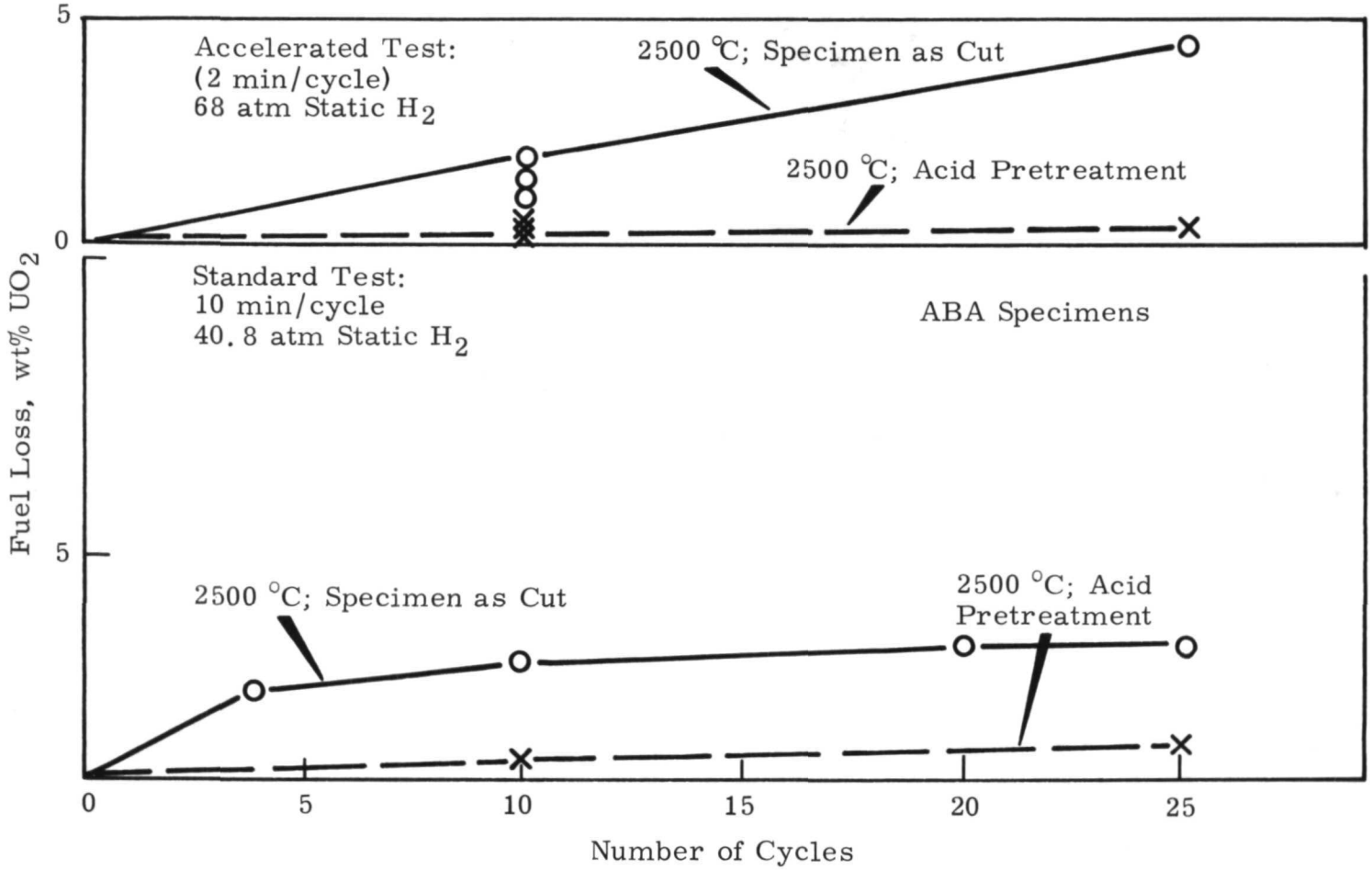


FIGURE 20. Test Specimen Edge Effects on Tungsten-Coated UO_2-W (13.3 vol% UO_2) Cermets

CONFIDENTIAL

CONFIDENTIAL

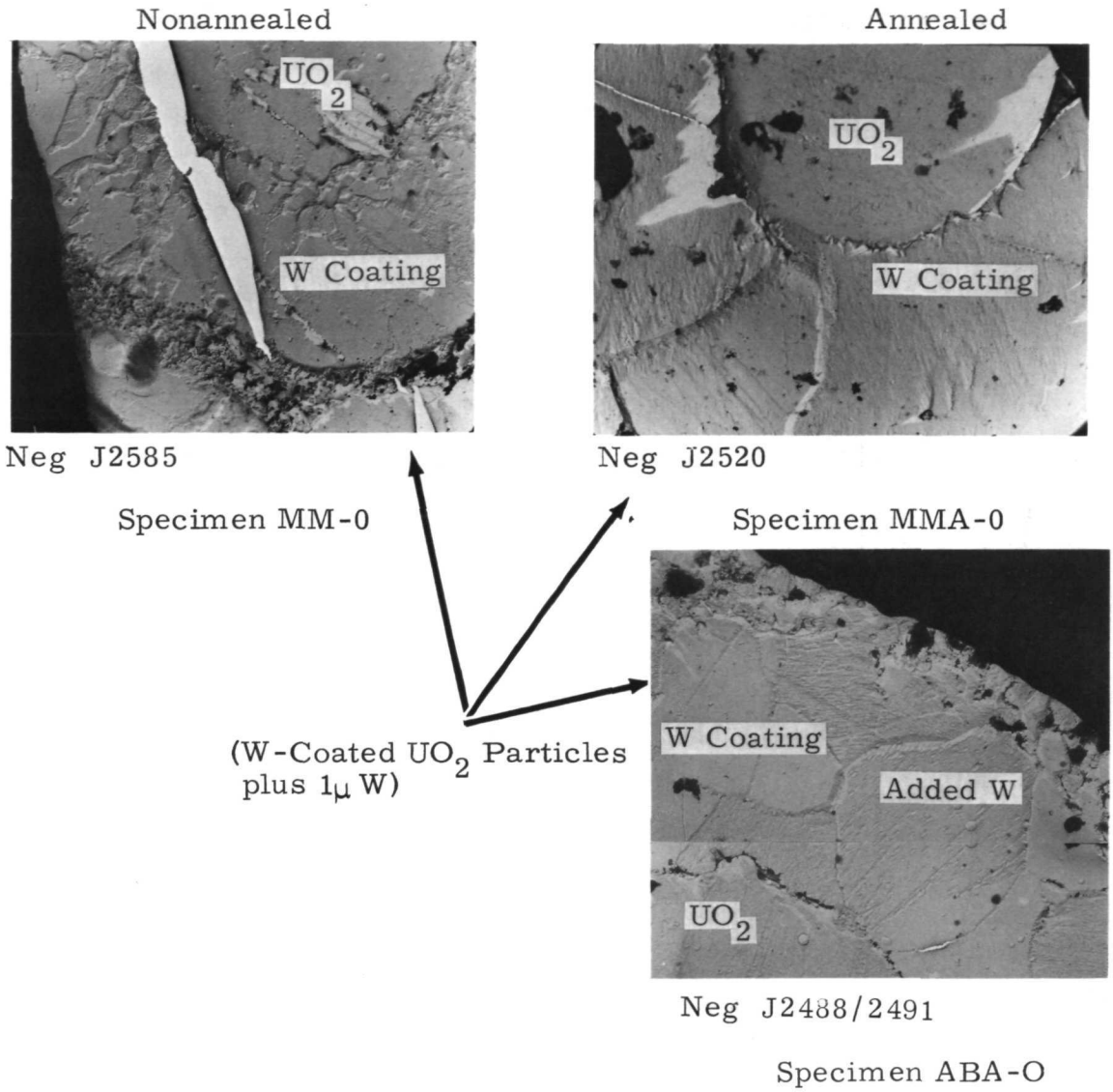
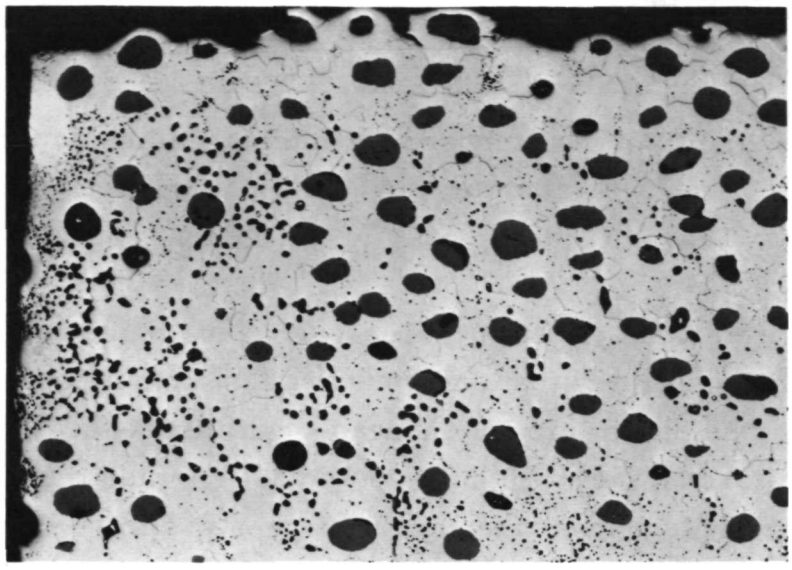


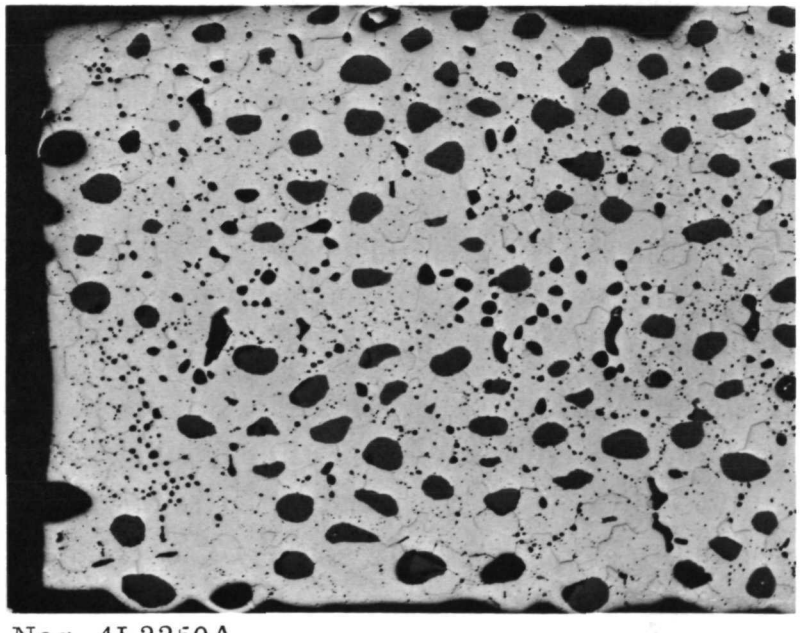
FIGURE 21. Electron Micrographs of Pneumatically Impacted W–13.3 vol% UO_2 Coated Particle-W Powder Cermets (carbon replicas). Comparison of As-Fabricated Microstructures Etched; 1500X



Neg 4L2249A

100X

a. Cermet MM
(Cycled 22 times; Fuel loss = 6.4 wt%)



Neg 4L2250A

100X
No Etchant

b. Cermet MMA
(Cycled 50 times; Fuel loss = 6.6 wt%)

FIGURE 22. Microstructures of Nonannealed and Annealed Tungsten-Coated UO_2–W 13.3 vol% Cermets (No pretreatment) After Standard Thermal Cycle Tests in 40.8 atm Static Hydrogen

Effect of Thermal Cycling Conditions on Cermet Behavior

The effects of the standard test, the accelerated test and cycling temperature were evaluated for cermet ABA (tungsten coated UO_2 plus 1μ W powder, 13.3 vol% UO_2).[6] Fuel loss data from these experiments show:

- A deleterious effect of increased cycling temperature under both accelerated test and standard test conditions. Fuel loss rate and fuel migration increased with increased cycling temperature (Figures 23, 24, 25 and 26). In addition, a wide range of fuel loss rate occurred when cycling to 2600 °C under accelerated test conditions with nominally identical specimens (Figure 23).
- Microstructures (Figure 27) show relatively little UO_2 migration in the center of the specimens, but significant fuel migration and loss near the surface of the specimens. This behavior is probably caused by the combined hydrogen penetration and removal of reaction products from the cermet.
- Fuel losses under both the accelerated and the standard cycling test conditions in static hydrogen are similar at cycling temperatures up to 2500 °C so long as identical cermet fabrication techniques are used (compare Figures 23 and 24).

The effects of hydrogen pressure (1 atm versus 40.8 atm) and hydrogen flow rate (static versus 16.5 liters/min) were determined on nominally 10 vol% UO_2–W cermets and on nominally 35 vol% UO_2–W cermets. In addition, nominally 10 vol% UO_2–W cermets were tested in 47.2 liters/min flowing hydrogen. Nonclad cermets were tested using the standard test procedure.

Nominally 10 vol% UO_2–W Cermets. Thermal cycling studies of cermet MMA (13.3 vol% UO_2) in 1 atm flowing hydrogen, 40.8 atm static hydrogen and 40.8 atm flowing hydrogen show that flowing hydrogen

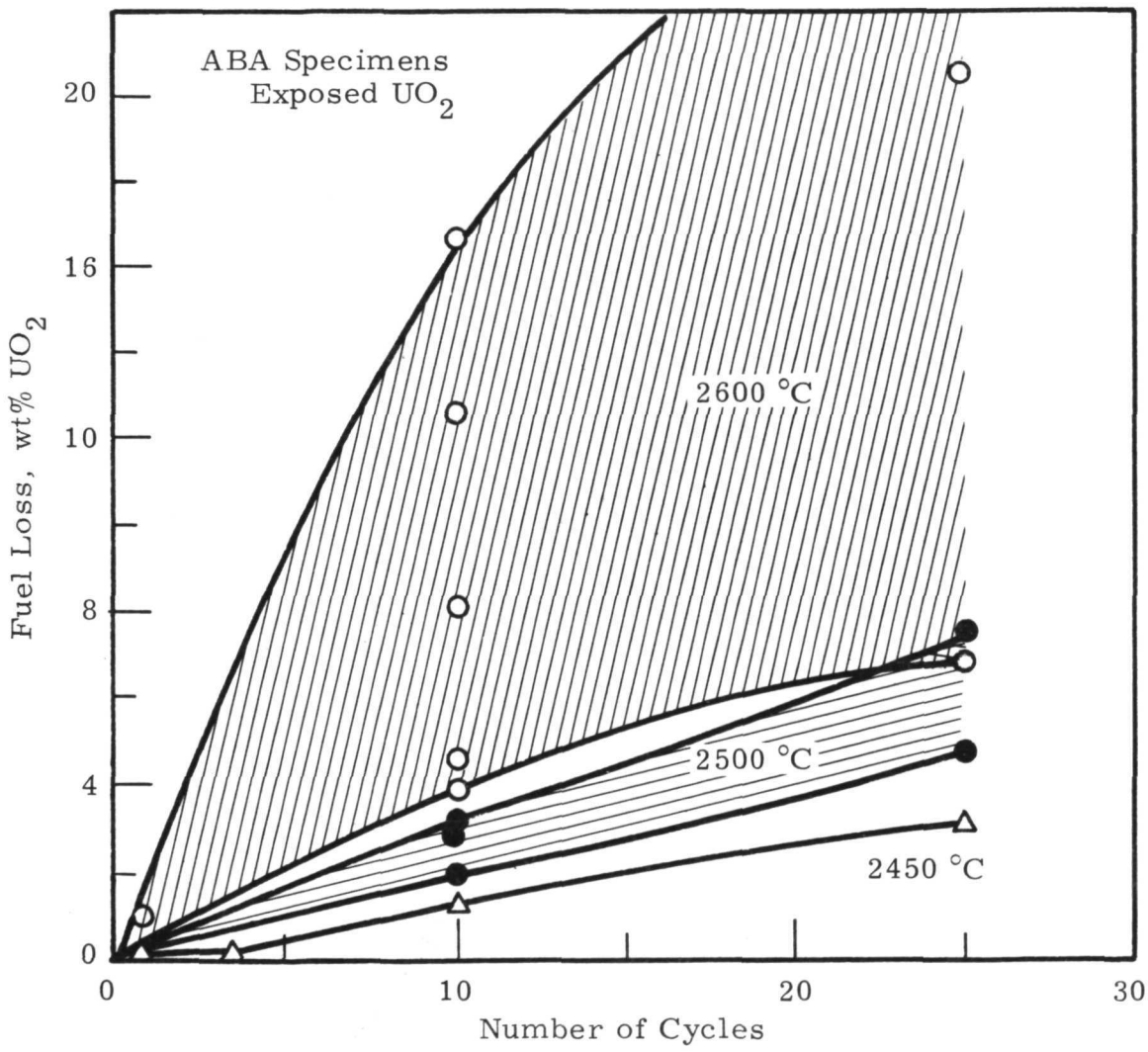


FIGURE 23. Thermal Cycling Behavior of Tungsten-Coated UO_2-W (13.3 vol% UO_2) Cermets Under Accelerated Test Conditions in 68 atm Static Hydrogen

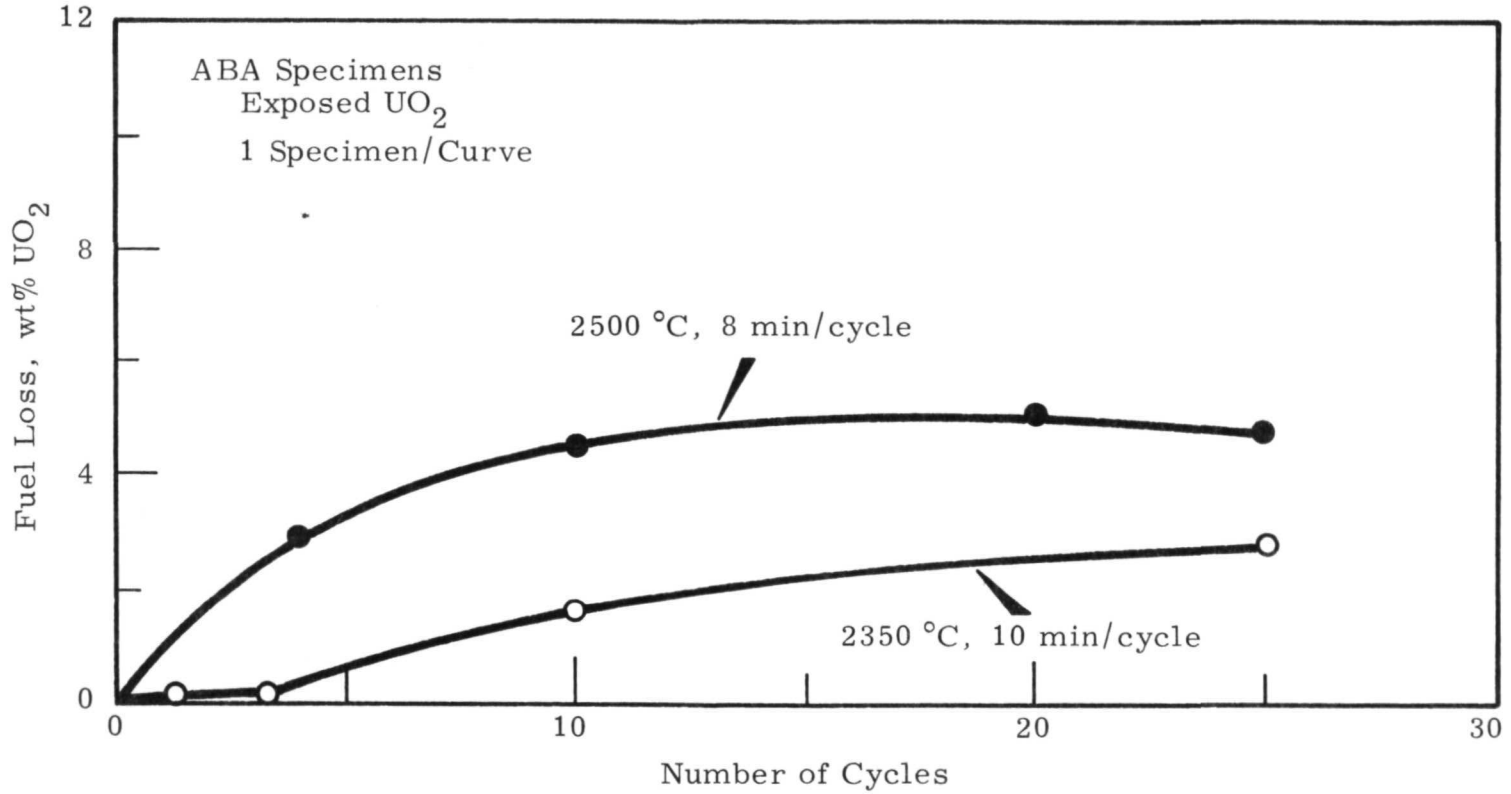
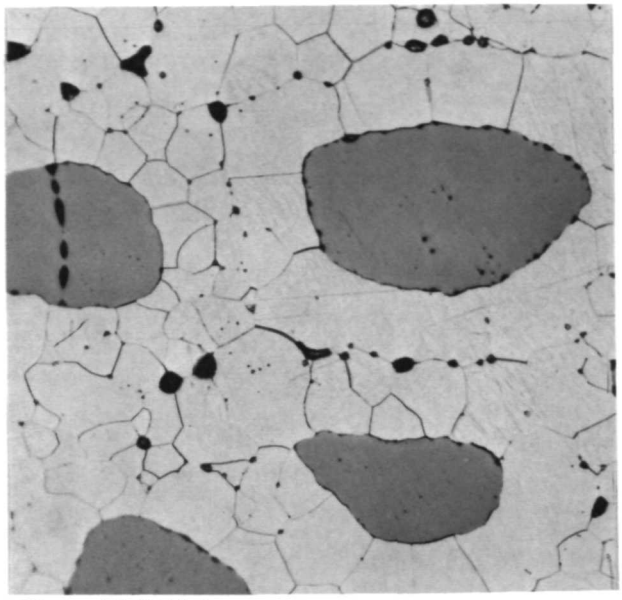


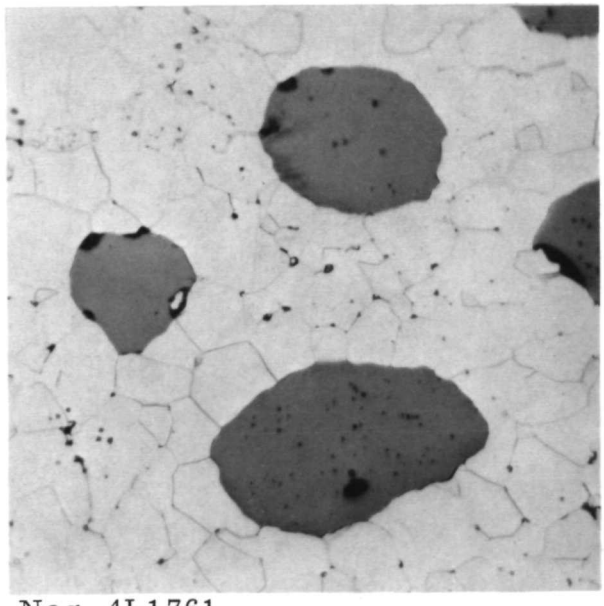
FIGURE 24. Thermal Cycling Behavior of Tungsten-Coated UO_2-W (13.3 vol% UO_2) Cermets Under Standard Test Conditions in 40.8 atm Static Hydrogen

BNWL-394
NASA-CR-54840



Neg 4L1644 500X

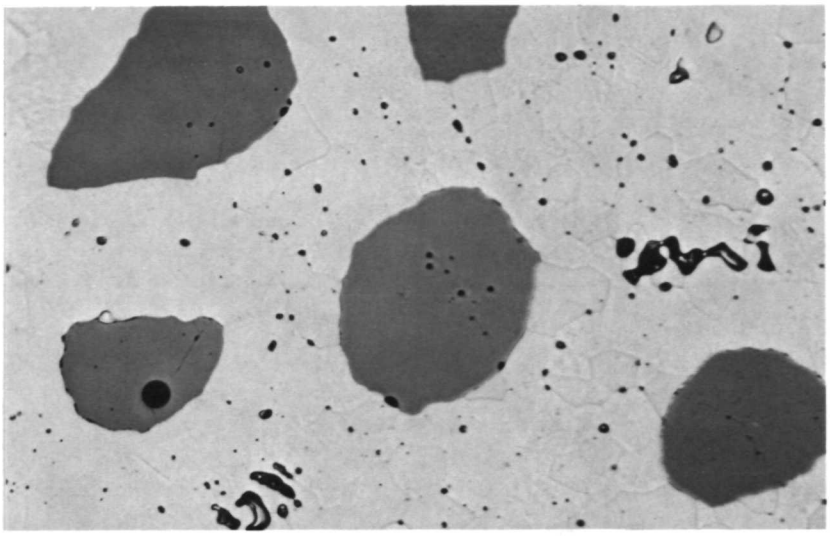
a. Cermet ABA, Noncycled



Neg 4L1761 500X

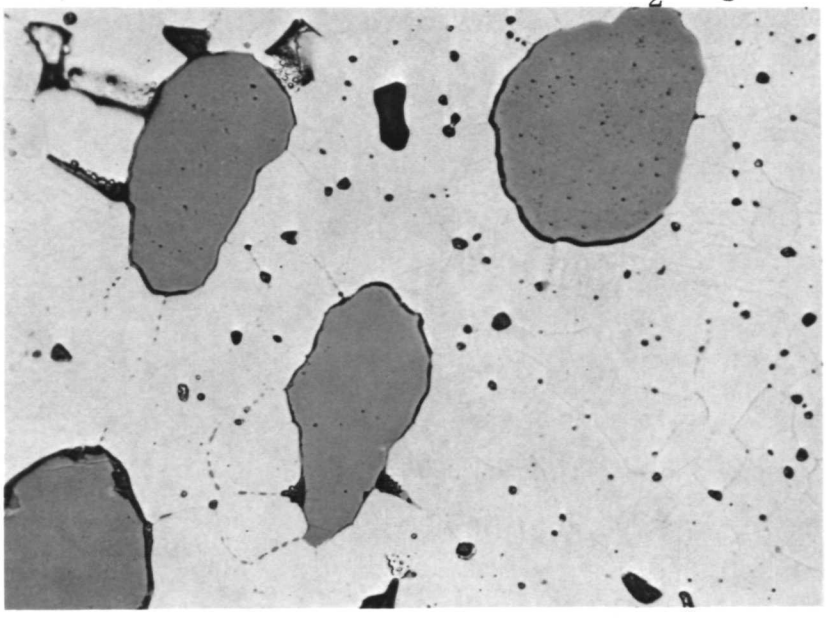
b. Cermet ABA (No Acid Pretreatment)
Cycled 50 times (10 min cycle, 1 min heating and cooling) to 2500 °C in 40.8 atm (600 psi) Static H_2. Fuel loss = 4.7 wt%. No UO_2 Migration. Etchant: Murakami

FIGURE 25. Microstructures of Noncycled and Cycled Tungsten-Coated UO_2-W Cermets (13.3 vol% UO_2)



Neg 4L1976

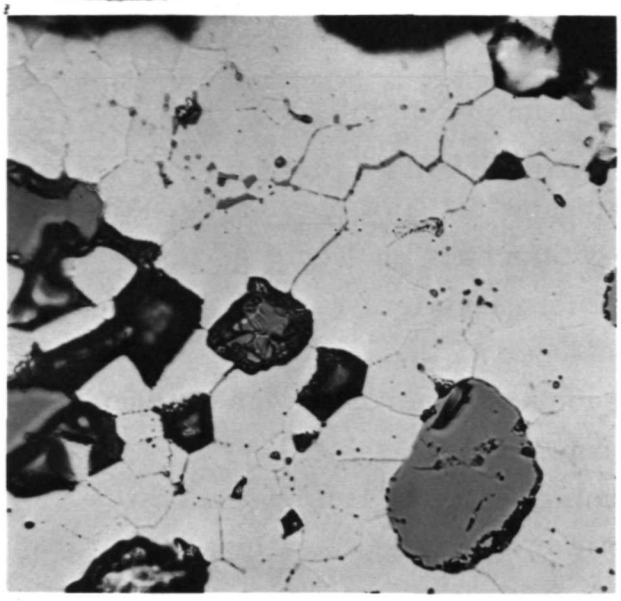
a. Cermet
(1.7 wt% fuel loss at 2500 °C. No UO_2 Migration)



Neg 4L1977

b. Cermet ABA
(4.4 wt% fuel loss at 2600 °C. UO_2 migration observed in portions of the cermet)

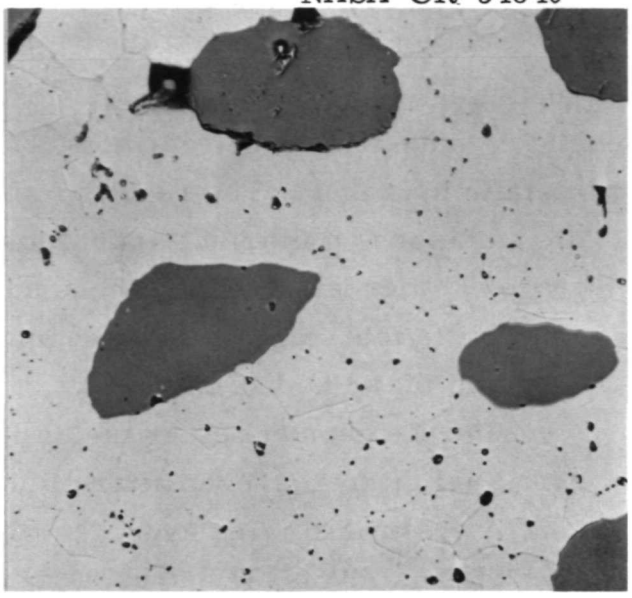
FIGURE 26. Thermal Cycling Temperature Effects on the Microstructure of a Tungsten-Coated UO_2-W (13.3 vol%) Cermet [Cycled 25 times under Standard test Conditions (10 min/cycle) in 40.8 atm Static Hydrogen]



Neg 4L1975A

500X

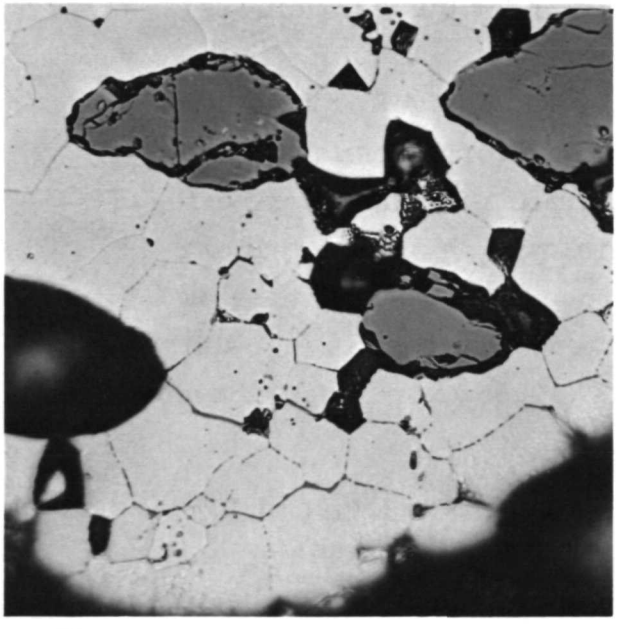
a. UO_2 Migration near Top Surface of Cermet



Neg 4L1975B

500X

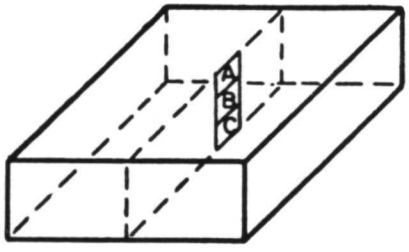
b. No UO_2 Migration in Center of Cermet



Neg 4L1975C

500X

c. UO_2 Migration near Bottom Surface of Cermet



Locations of the Micrographs in Relation to the Sample

Note: Cermet ABA (Fuel loss = 16.3 wt% after ten 2 min cycles to 2600 °C in 68 atm static H_2)

FIGURE 27. Variation in UO_2 Migration in a Thermally Cycled Tungsten-Coated UO_2-W (13.3 vol% UO_2) Cermet (No Acid Pretreatment) No Etchant

at 40.8 atm greatly increases fuel losses from nonclad W-UO_2 coated particle, tungsten powder cermets (Figure 28) over that obtained in 40.8 atm static hydrogen. The results further show that flowing hydrogen at 1 atm has more of an effect on fuel losses than does 40.8 atm static hydrogen. Microstructure of these specimens show:

- Little fuel migration in specimens after 25 thermal cycles in 40.8 atm static hydrogen (Figure 29; substantial porosity was introduced into the cermet during the 25 thermal cycles).
- Fuel migration even after 15 thermal cycles in 1 atm, 16.5 liters/min flowing hydrogen [this is more extensive after 25 thermal cycles (Figures 30 and 31)].
- Catastrophic failure of the cermet between 15 and 25 thermal cycles in 40.8 atm, 16.5 liters/min flowing hydrogen (Figure 28) [the specimen physically deteriorates under these conditions (Figures 32, 33 and 34)].
- The physical deterioration is far more extensive for specimens cycled in 40.8 atm flowing hydrogen than for specimens cycled in 1 atm flowing hydrogen. Fuel migration is much more extensive for cermets cycled in 40.8 atm flowing hydrogen than for those cycled in 40.8 atm static hydrogen. Increasing the flow rate from 16.5 liters/min to 47.2 liters/min results in a shifting of the onset of catastrophic fuel loss to a lower number of cycles (Figure 35).

Fuel loss from a 100% coated particle cermet (cermet BCA, 9.4 vol% UO_2) is nearly identical with that from a cermet comprising coated particles plus fine grain tungsten powder (cermet MMA, 13.3 vol% UO_2) (Figure 36). A 100% coated particle cermet containing 10.1 vol% fuel (cermet BUA) in which the UO_2 was stabilized with 10 mole% Y_2O_3 in solid solution exhibited fuel loss similar to that from coated particle cermets containing nonstabilized UO_2 (compare Figure 37 with Figure 36).

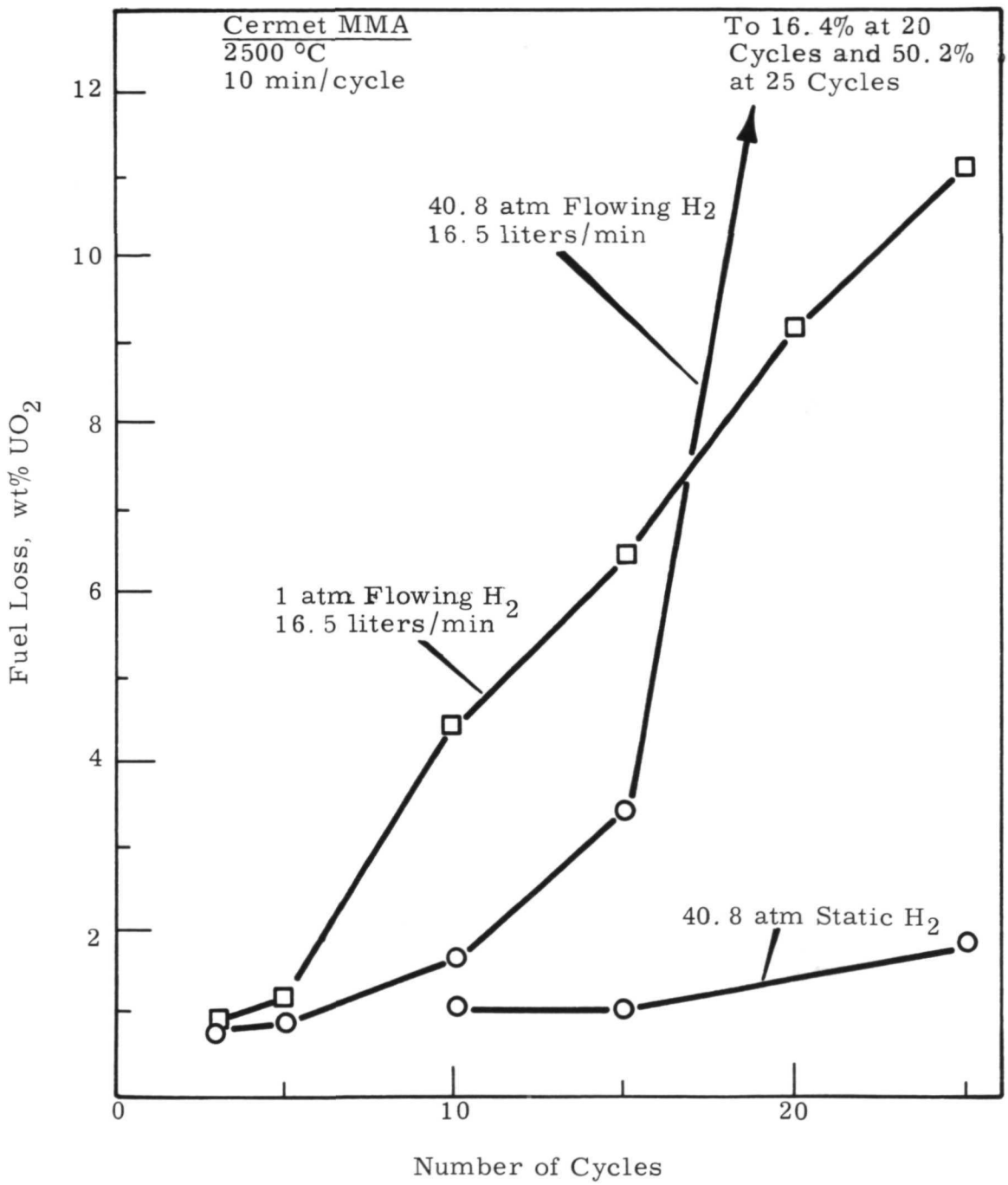
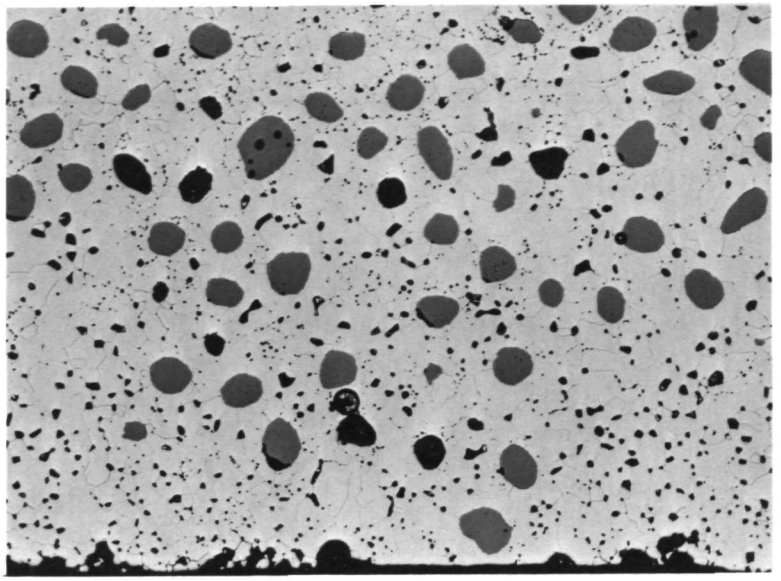
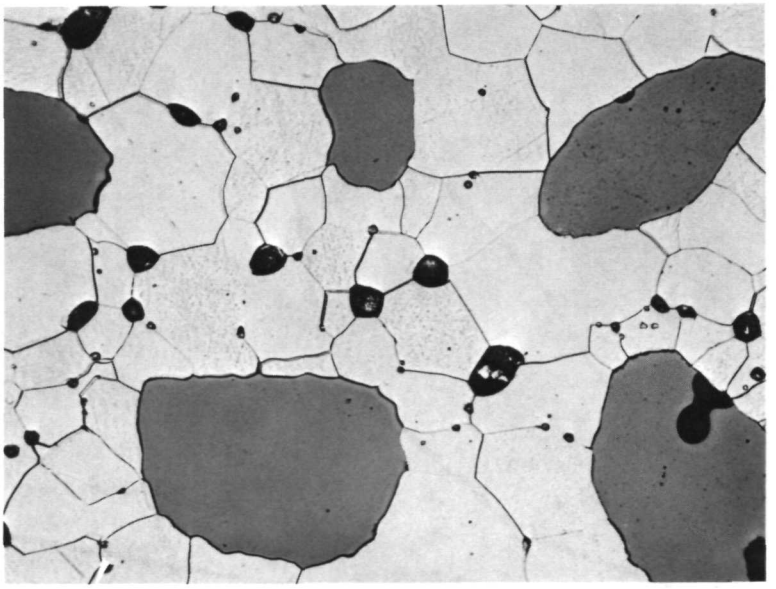


FIGURE 28. Effect of Pressure and Flow Rate on the Thermal Cycling Behavior of a Tungsten-Coated UO_2-W Cermet Containing 13.3 vol% UO_2

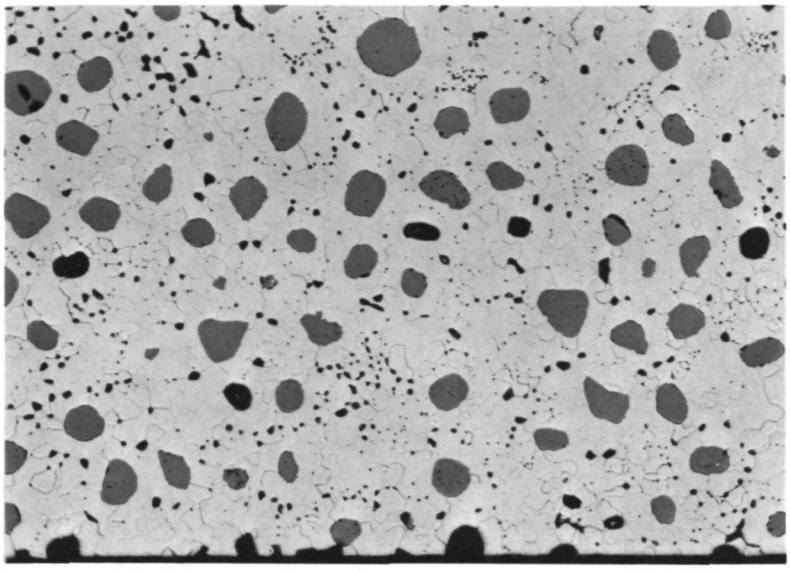


Neg 465222A 100X
Nonetched



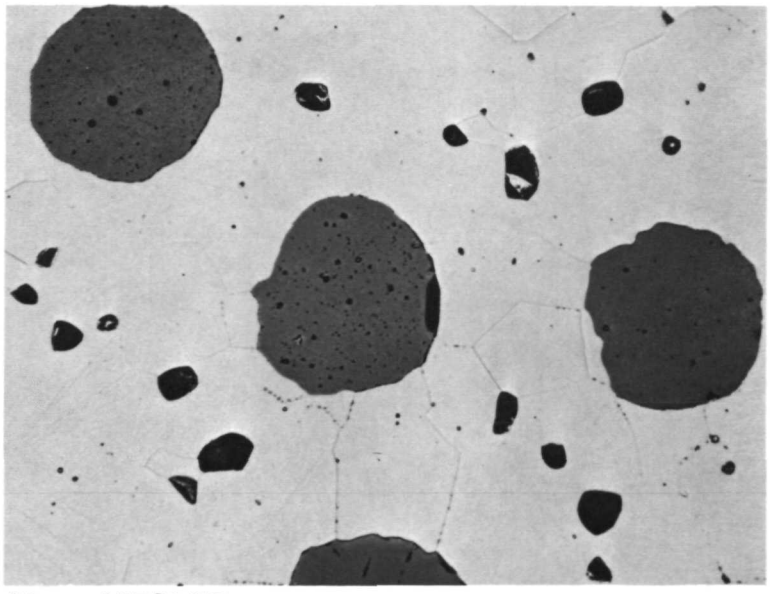
Neg 465222D 500X
Etched-Murakami

FIGURE 29. Microstructure of a Tungsten-Coated 13.3 vol% UO_2–W Cermet After Thermal Cycling to 2500 °C in 40.8 atm Static Hydrogen. (Cermet MMA, 25 Cycles, 1.9 wt% Fuel Loss)



Neg 465218A

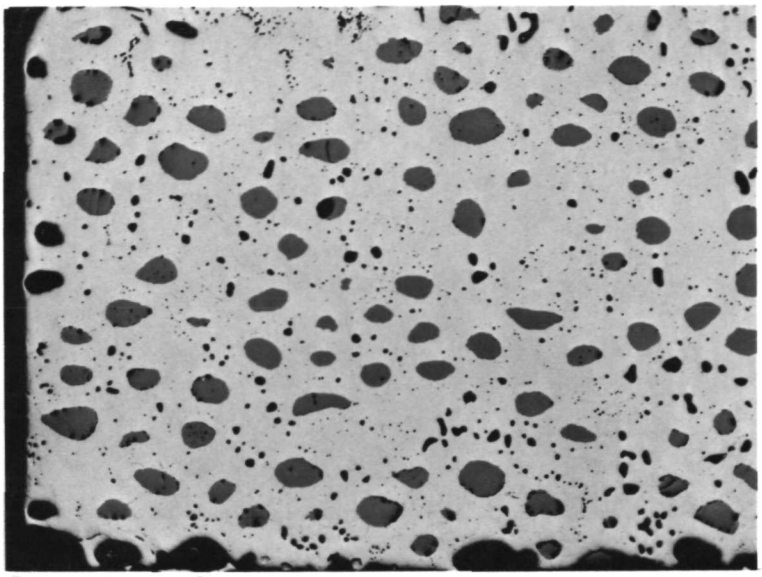
100X
Nonetched



Neg 465218B

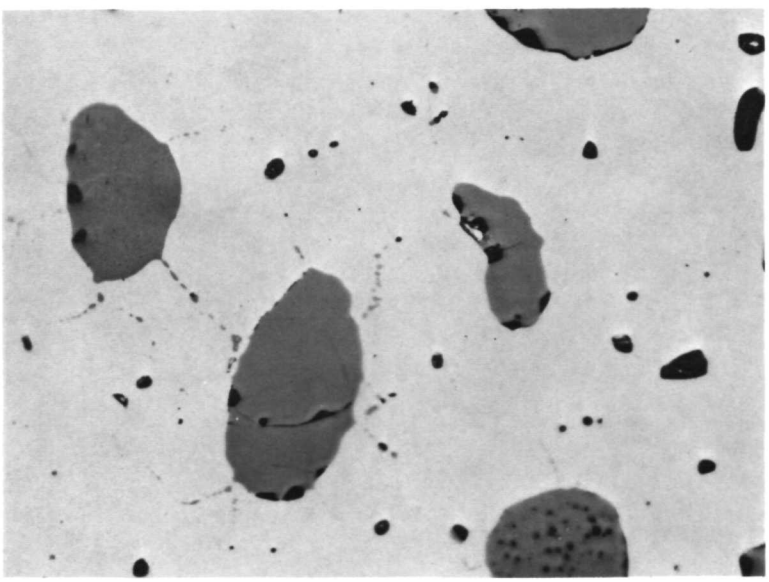
500X
Nonetched

FIGURE 30. Microstructure of a Tungsten-Coated 13.3 vol% UO_2–W Cermet after Thermal Cycling to 2500 °C in 1 atm Flowing Hydrogen (16.5 liters/min). (Cermet MMA, 15 Cycles, 5.8 wt% Fuel Loss)



Neg 46511A

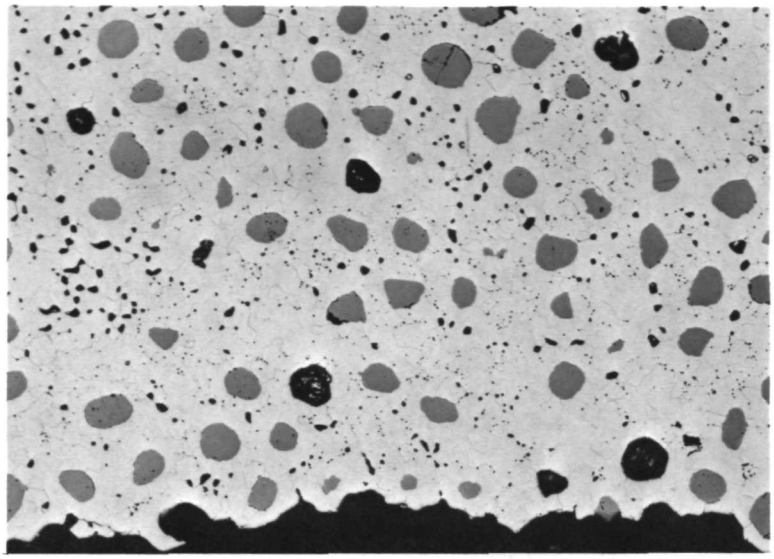
100X
Nonetched



Neg 46511B

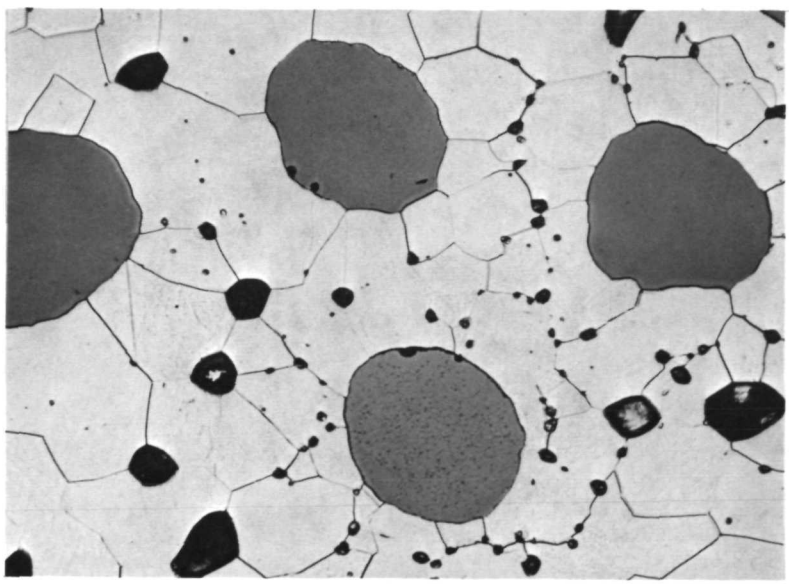
500X
Nonetched

FIGURE 31. Microstructure of a Tungsten-Coated 13.3 vol% UO_2–W Cermet After Thermal Cycling to 2500 °C in 1 atm Flowing Hydrogen (16.5 liters/min) Cermet MMA, 25 Cycles, 11.1 wt% Fuel Loss)



Neg 465219A

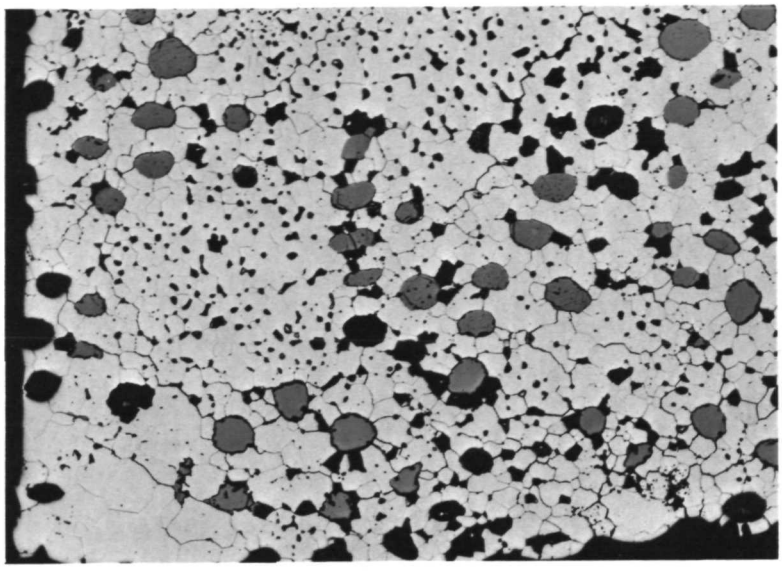
100X
Nonetched



Neg 265219D

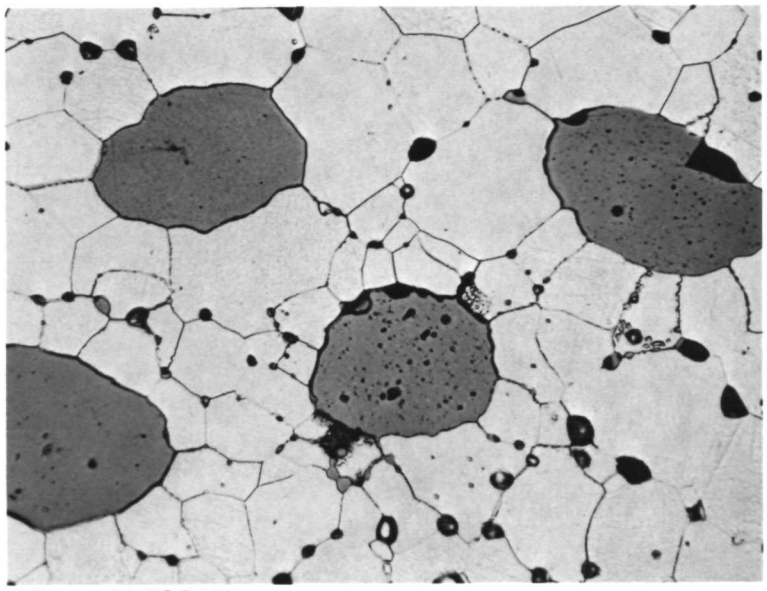
500X
Etched-Murakami

FIGURE 32. Microstructure of a Tungsten-Coated 13.3 vol% UO_2-W Cermet After Thermal Cycling to 2500 °C in 40.8 atm Flowing Hydrogen (16.5 liters/min). Cermet MMA, 15 Cycles, 4.8 wt% Fuel Loss)



Neg 465221A

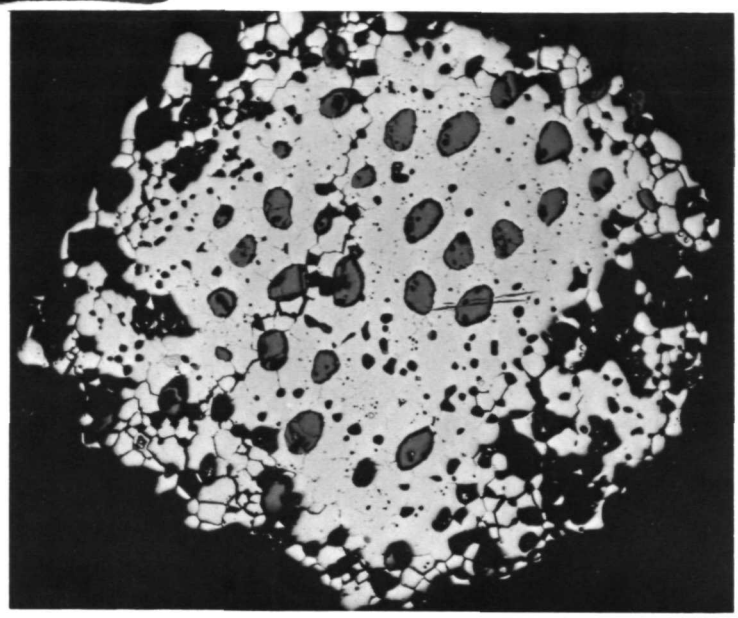
100X
Nonetched



Neg 465221D

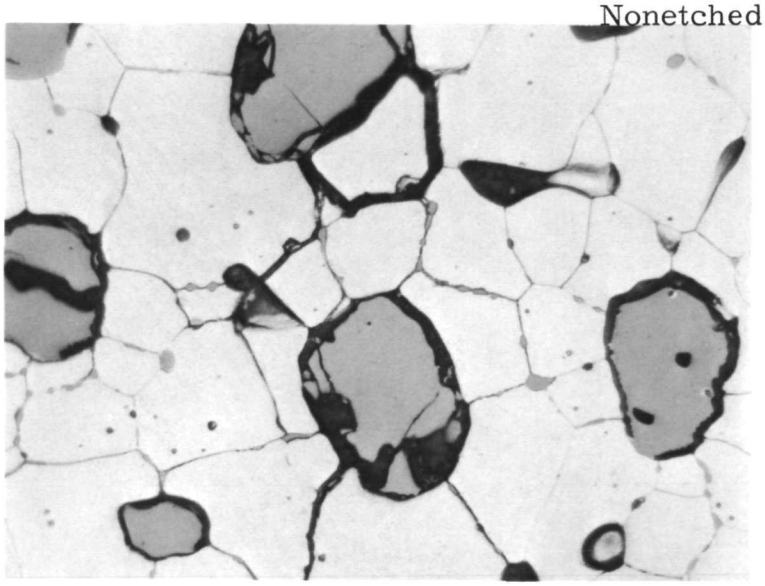
500X
Etched-Murakami

FIGURE 33. Microstructure of a Tungsten-Coated 13.3 vol% UO_2-W Cermet After Thermal Cycling to 2500 °C in 40.8 atm Flowing Hydrogen (16.5 liters/min). Cermet MMA, 20 Cycles, 26.0 wt% Fuel Loss)



Neg 46512A

100X
Nonetched



Neg 46512C

500X
Etched-Murakami

FIGURE 34. Microstructure of a Tungsten-Coated Particle 13.3 vol% UO_2-W Cermet After Thermal Cycling to 2500 °C in 40.8 atm Flowing Hydrogen (16.5 liters/min). Cermet MMA, 25 Cycles, 50.2 wt% Fuel Loss)

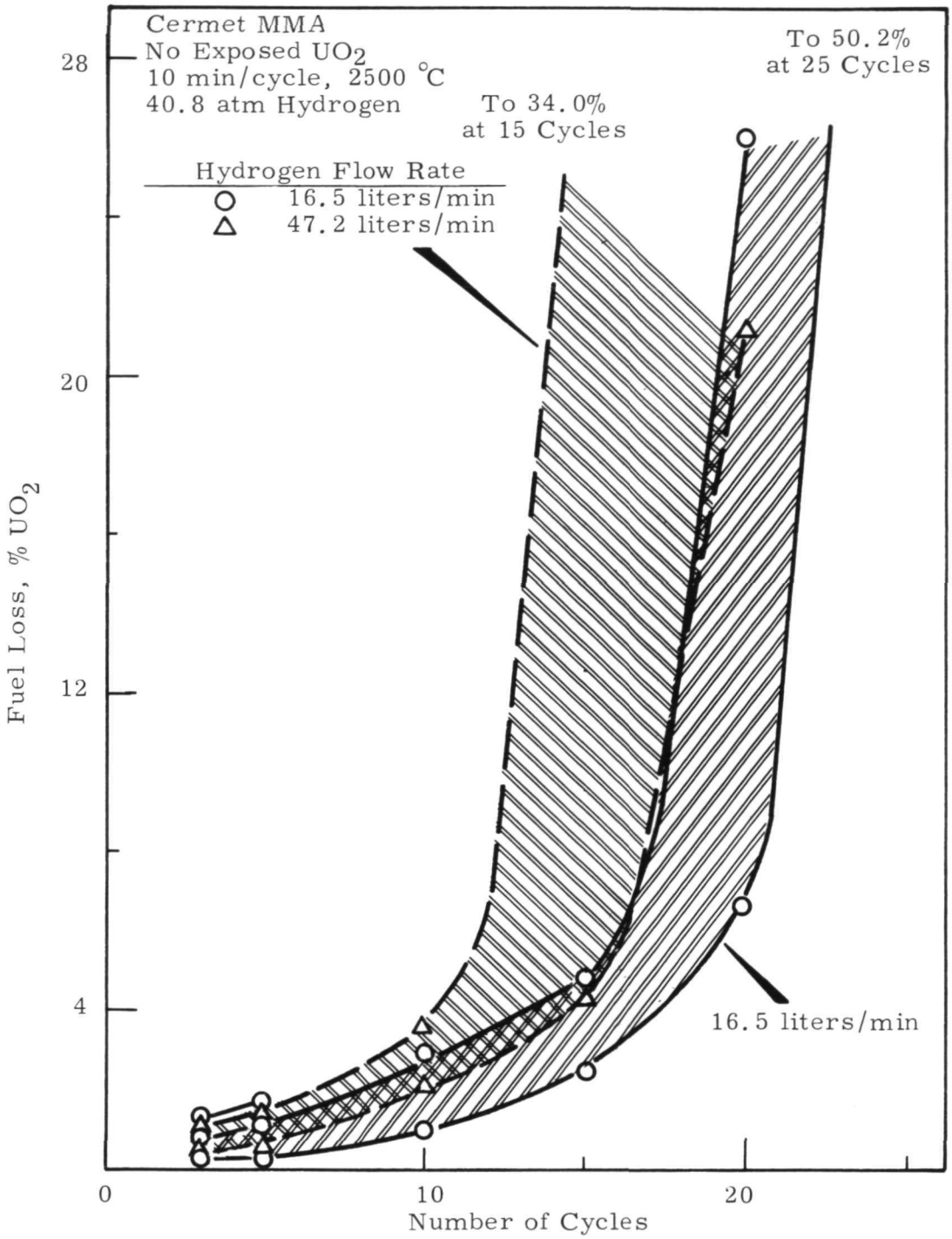


FIGURE 35. Effect of Hydrogen Flow Rate on Fuel Loss During Thermal Cycling of a Tungsten-Coated UO_2-W Cermet Containing 13.3 vol% UO_2

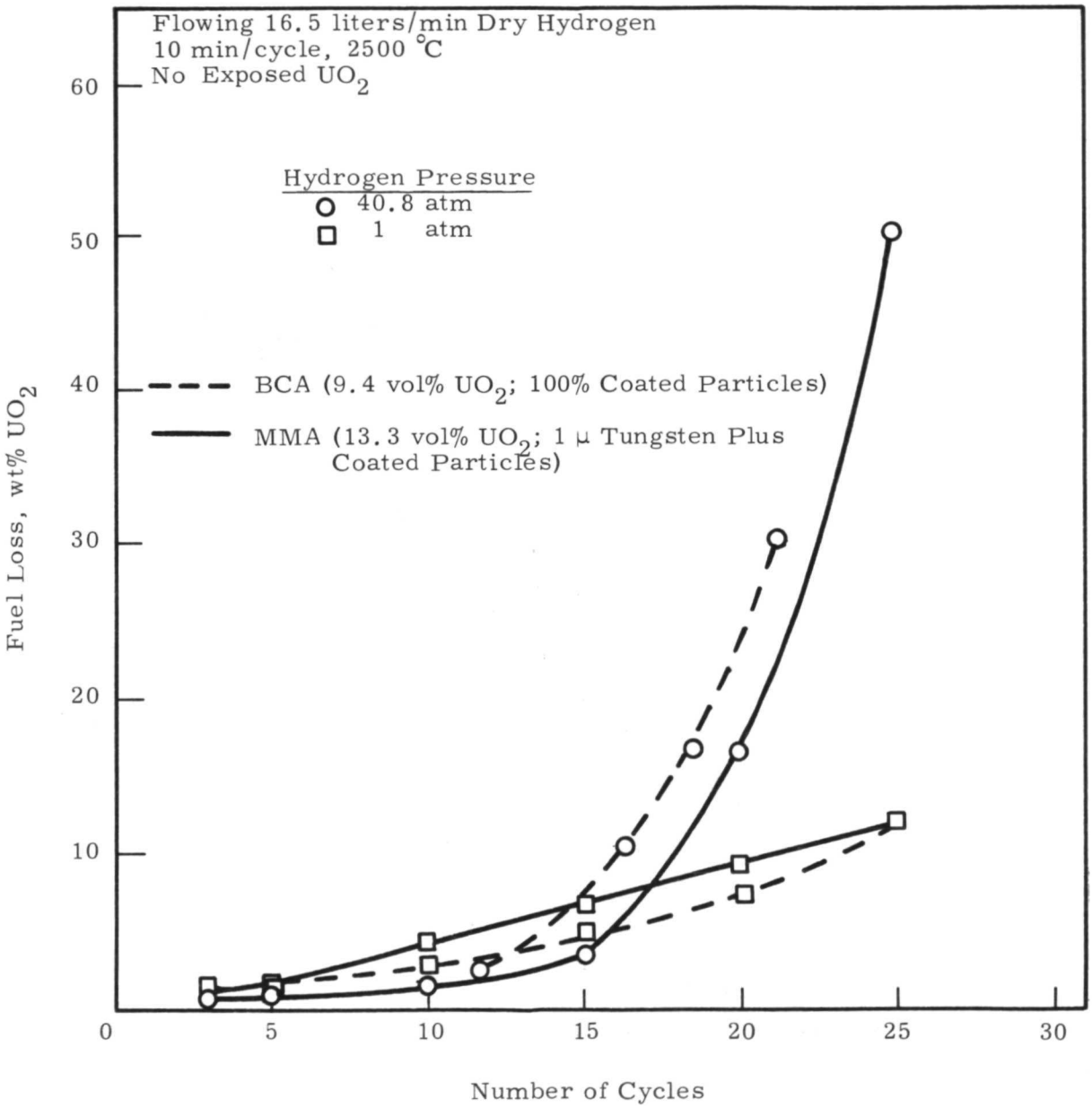


FIGURE 36. Effect of Hydrogen Pressure on Fuel Loss for W-UO_2 Coated Particle Cermets Containing 9.4 and 13.3 vol% UO_2

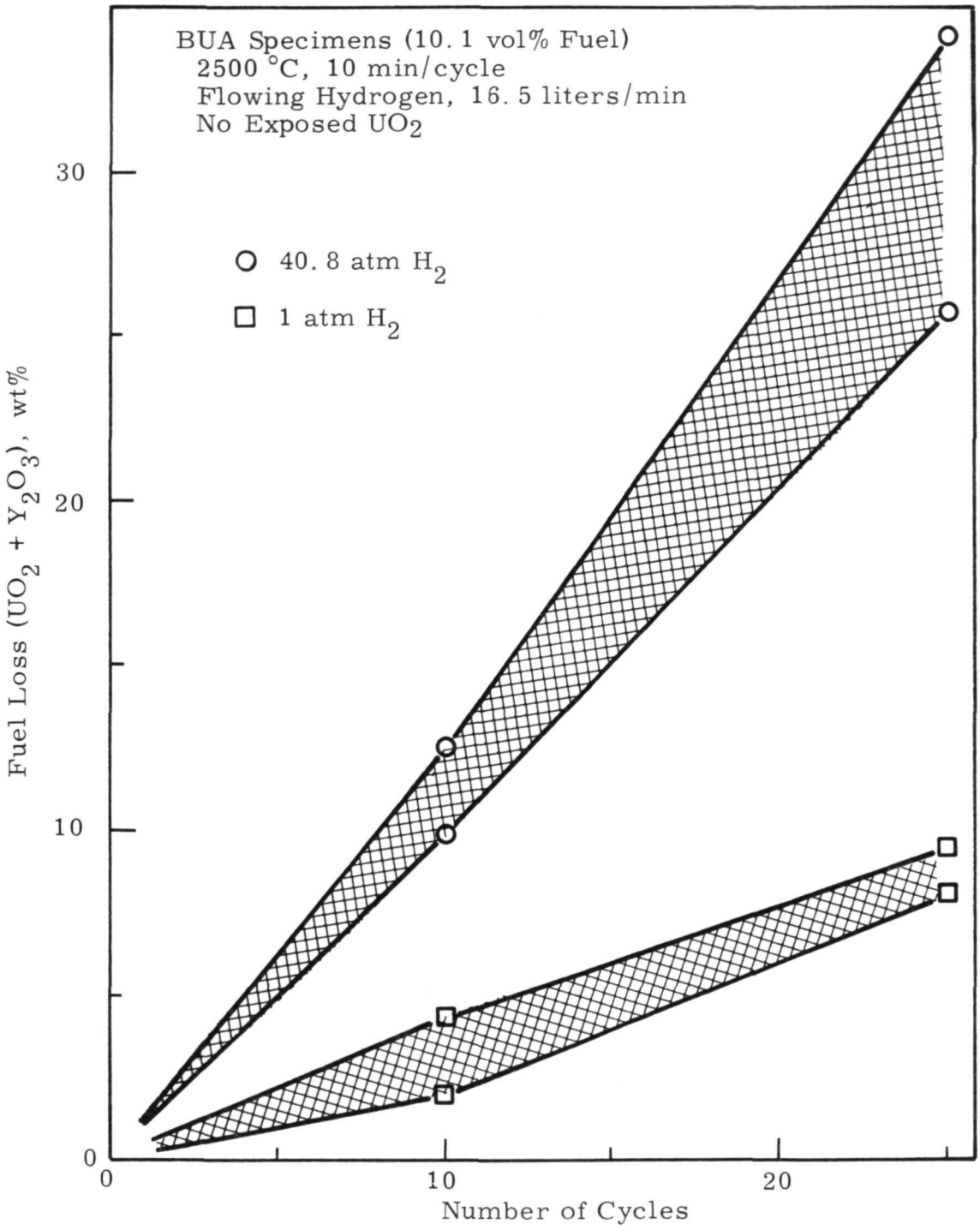


FIGURE 37. Thermal Cycling Behavior of W-UO_2 Coated Particle Cermets Containing 10 Mole% Y_2O_3 in UO_2 Solid Solution

Nominally 35 vol% UO_2–W Cermets. A reverse pressure effect was observed with nonclad, coated particle cermets containing 25 to 45 vol% fuel. Fuel losses occurred in 1 atm flowing dry hydrogen (compare with fuel loss in 40.8 atm flowing hydrogen--cermet BGA, Figure 38). Fuel loss data for a 100% coated particle cermet containing 29.8 vol% fuel (cermet BSA) in which the UO_2 was stabilized with 10 mole% Y_2O_3 in solid solution showed a similar but not so pronounced reversed pressure effect up to 25 thermal cycles (compare with nonstabilized UO_2 coated particle cermets, Figure 39). However, microstructures of cycled BSA specimens show more grain boundary migration of the fuel and wider grain boundaries for cermets cycled in 40.8 atm flowing hydrogen than for specimens cycled in 1 atm flowing hydrogen (Figures 40 and 41). The microstructures also show that the fuel loss at 25 thermal cycles almost completely originates from the layers of coated particles near the surface. The 0.050 cm thick specimens used in these studies consist of 9 to 10 layers of coated particles. The high fuel loss (11 wt% in 40.8 atm and 15.8 wt% in 1 atm flowing hydrogen for 25 thermal cycles) therefore may be dependent only on the integrity of the surface layer of particles and may not be indicative of total cermet performance. The major effect in disturbing the surface layer integrity is the dissolution of the molybdenum assembly used for pneumatic impaction. The acid attacks the tungsten coating which forms the specimen surface. Microstructure of specimens cycled 25 times suggests that the fuel loss curves should crossover upon further cycling. After 50 thermal cycles (Figure 39) the fuel loss curves were found to cross over. The crossover occurs at 15 to 20 wt% fuel loss which corresponds to complete removal of fuel from the surface layer of particles. The effect of pressure on the thermal cycling behavior of coated particle cermets containing 25 to 45 vol% fuel cannot be definitely established because of the possible surface--fabrication effects on the nonclad cermets.

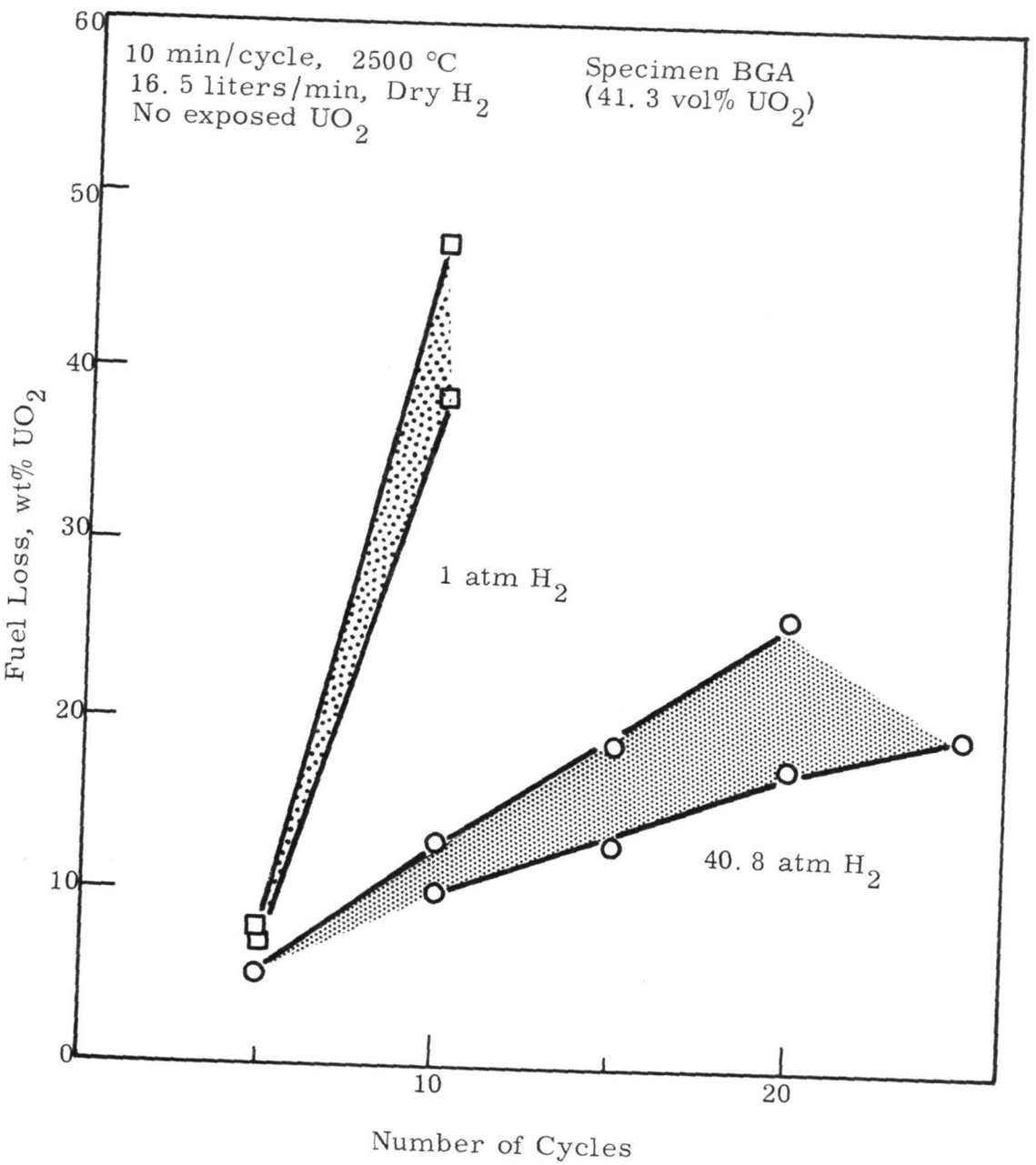


FIGURE 38. Thermal Cycling Behavior of Coated Particle W-UO_2 Cermets

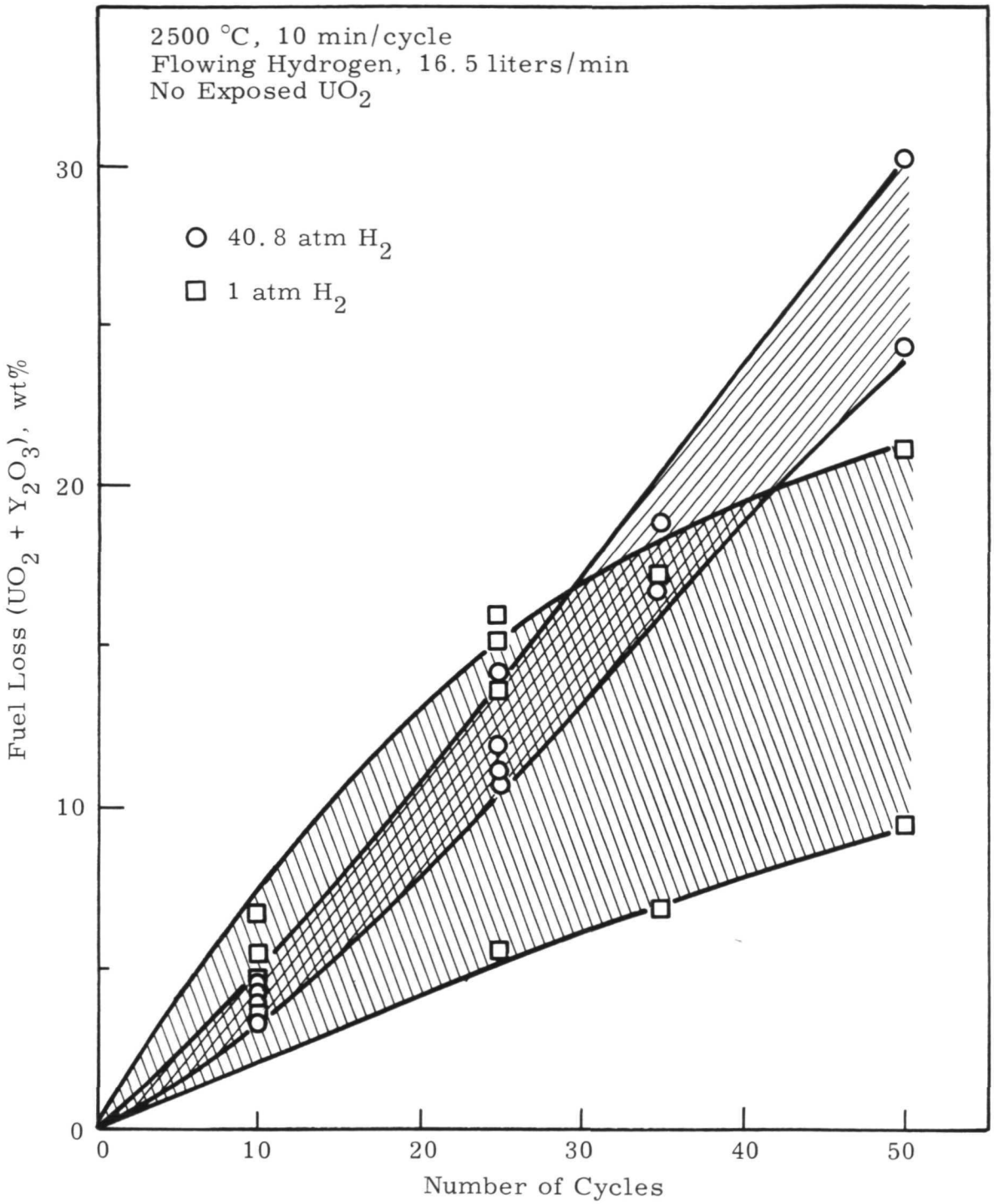
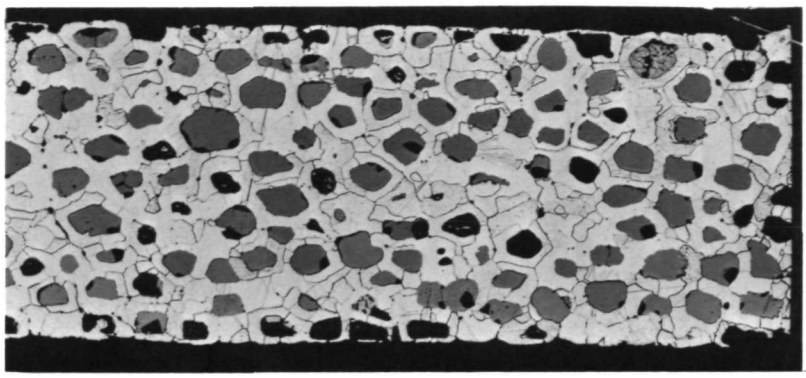
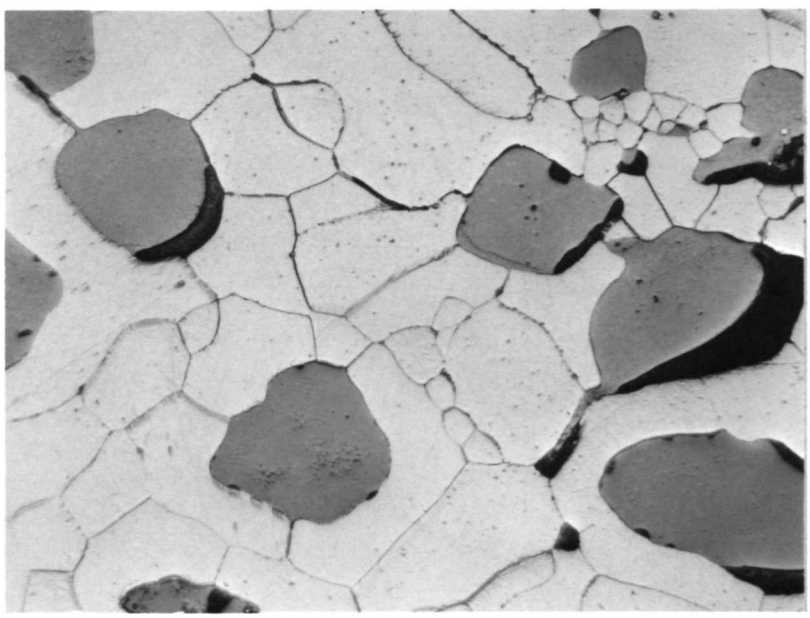


FIGURE 39. Thermal Cycling Behavior of BSA Specimens (29.8 vol% Fuel, 10 Mole% Y_2O_3 in Fuel)



Neg 4651759B

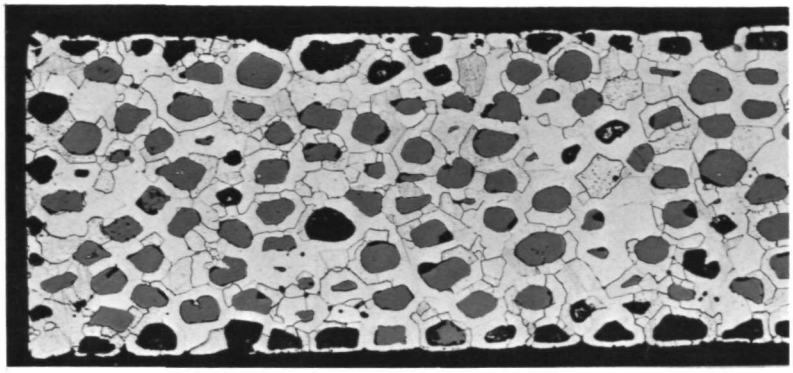
100X
Etchant: Murakami



Neg 4651759D

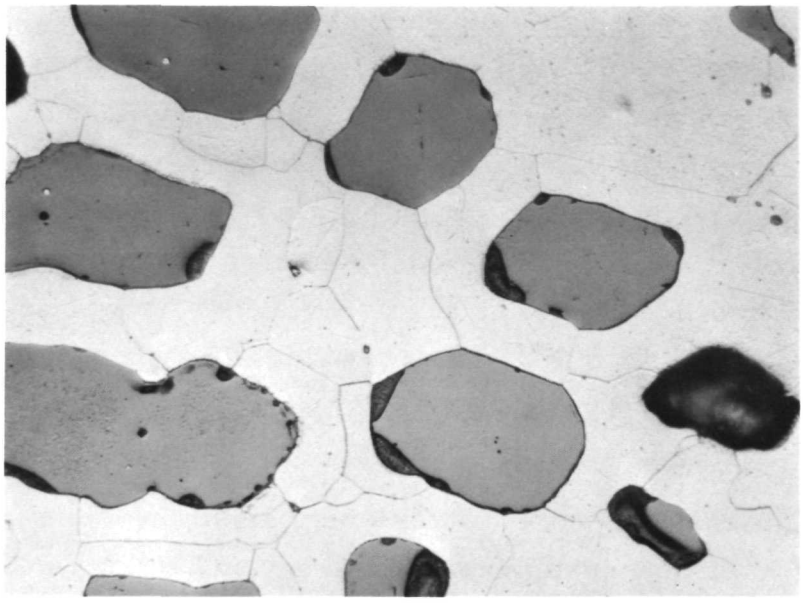
500X
Etchant: Murakami

FIGURE 40. Microstructure of a Thermally Cycled W–29.8 vol% Fuel Coated Particle Cermet Containing 10 Mole % Y_2O_3 in Solid Solution in the UO_2 (Cermet BSA, 25 Cycles in 40.8 atm, 16.5 liters/min Flowing Dry H_2, 11.0 wt% Fuel Loss)



Neg 4651758B

100X
Etchant: Murakami



Neg 4651758D

500X
Etchant: Murakami

FIGURE 41. Microstructure of a Thermally Cycled W–29.8 vol% Fuel Coated Particle Cermet Containing 10 Mole% Y_2O_3 in Solid Solution in the UO_2 (Cermet BSA, 25 Cycles in 1 atm, 16.5 liters/min Flowing Dry H_2, 15.8 wt% Fuel Loss)

Effect of Cermet Composition on Thermal Cycling Behavior

Composition variables studied in order to improve fuel loss behavior under thermal cycling conditions included:

1. Addition of 1μ or 5μ tungsten powders to the coated particles during formulation of the cermet and addition of 0.06μ ThO_2 to the fine grain tungsten,
2. Fuel loading 10 to 40 vol%,
3. Addition of 5 or 10 mole% Y_2O_3 to the UO_2 (in solid solution) as a fuel stabilizer.

Additions of Fine Grain Tungsten. Thermal cycling studies on nominally 10 vol% UO_2–W coated particle cermets (cermet BCA, 100% coated particles, and cermet MMA, 32.1 wt% 1μ W added; Figure 36) show increased fuel loss from cermets with the tungsten powder addition. Thermal cycling studies on nominally 35 vol% UO_2–W coated particle cermets (cermet BGA, 100% coated particles, and cermet ATA, 46.7 wt% 1μ W added; Figure 42) show improved thermal cycling behavior for the 100% coated particle cermet. This difference in thermal cycling behavior may be attributed to the difference in coating thickness on the individual particles.

Additional experiments were performed on coated particle cermets containing 1μ or 5μ tungsten powder additions (Tables V and VII, respectively). These studies showed:

1. Cermets fabricated from a mixture of 1μ W and W-UO_2 coated particles exhibited lower fuel loss than a similar cermet comprising 5μ W and coated particles (compare cermets ATA and AVA; Figure 42),
2. Addition of ThO_2 to a coated particle--5μ W cermet retarded fuel loss and extended specimen integrity to a greater number of cycles (compare cermets AYA and AWA),

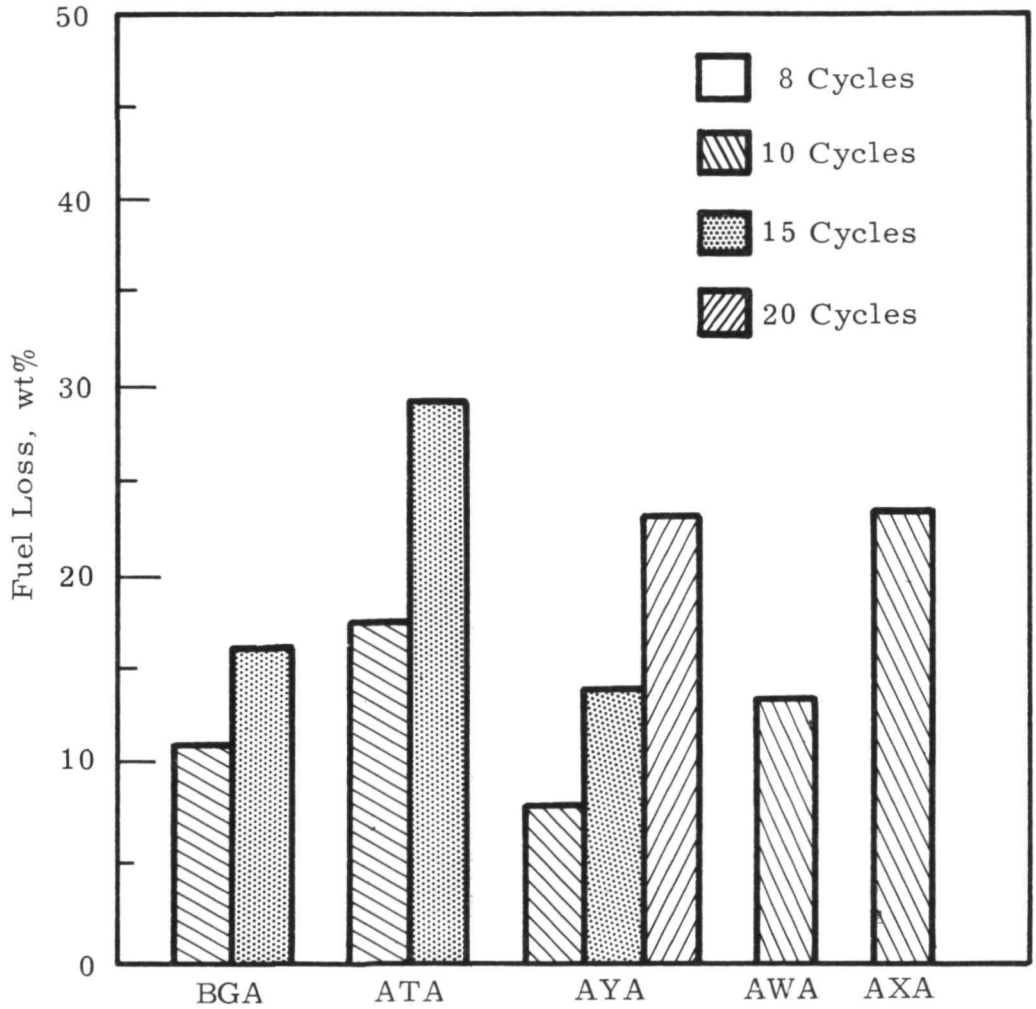


FIGURE 42. Fuel Loss of W-UO_2 Coated Particle Cermets During Thermal Cycling to 2500 °C (10 min/cycle) in 40.8 atm, 16.5 liters/min Flowing Dry Hydrogen

TABLE VII. Composition and Raw Materials for W-UO_2 Coated Particle-W Powder Cermets

Cermets	Composition wt%				Raw Materials		
	UO_2	W	Added W	Matrix Additions	UO_2	Coating Thickness	W Powder
BGA	28.6 (41.3 vol%)	71.4	none	none	44-53μ	10μ	none
ATA	15.3 (24.0 vol%)	84.7	46.7	none	44-53μ	10μ	1μ
AVA	15.3 (24.0 vol%)	84.7	46.7	none	44-53μ	10μ	5μ
AYA	25.7 (37.8 vol%)	74.3	42.8	1.05 ThO_2 (0.06μ)	37-44μ	4.5μ	5μ
AWA	25.7 (37.8 vol%)	74.3	42.8	none	37-44μ	4.5μ	5μ
AXA	13.7 (21.9 vol%)	86.3	69.5	none	37-44μ	4.5μ	5μ

BNWL-394
NASA-CR-54840

3. Increasing the UO_2 content from 20 to 35 vol% reduced the percent fuel loss upon thermal cycling but the mass of UO_2 lost was approximately the same (compare cermets AXA and AWA). This result indicated that the removal of a reaction product (O_2 or H_2O) or a vapor product (a uranium oxide) from the cermet controlled the rate of fuel loss.

Fuel Loading. It was shown in the previous section of this report that nominally 10 vol% UO_2–W coated particle cermets exhibited catastrophic fuel loss in 40.8 atm flowing H_2 as compared to more moderate fuel loss in 1 atm flowing H_2 (Figures 36 and 37). The effect of hydrogen pressure on fuel loss for nominally 35 vol% UO_2–W nonclad coated particle cermets has not been well established. Fabrication variables and perhaps the effects of the W coating thickness on the particles have not allowed a clear definition of the pressure effects on these highly loaded cermets.

Cermet BCA (9.4 vol% UO_2) exhibited little fuel loss after 10 thermal cycles, but failed catastrophically between 15 and 25 thermal cycles (Figure 43). Cermet BEA (32.3 vol% UO_2) exhibited catastrophic fuel loss by 10 thermal cycles. Once both cermets reached catastrophic fuel loss stage, the rates of fuel loss were similar. The delay in catastrophic fuel loss from cermet BCA is thought to be due to the greater coating thickness on the particles used in this cermet. This apparent coating thickness effect may be similar to the anticipated effects of cermet surface cladding on fuel loss.

Y_2O_3 Fuel Stability Effects. The effects of 5 and 10 mole% Y_2O_3 additions to the UO_2 (in solid solution) in coated particle cermets were studied (see Reference 7). Increasing the addition of Y_2O_3 to 10 mole% markedly reduced the fuel loss from nonclad cermets in both 40.8 atm flowing H_2 and in 1 atm flowing H_2 (Figures 44 and 45).

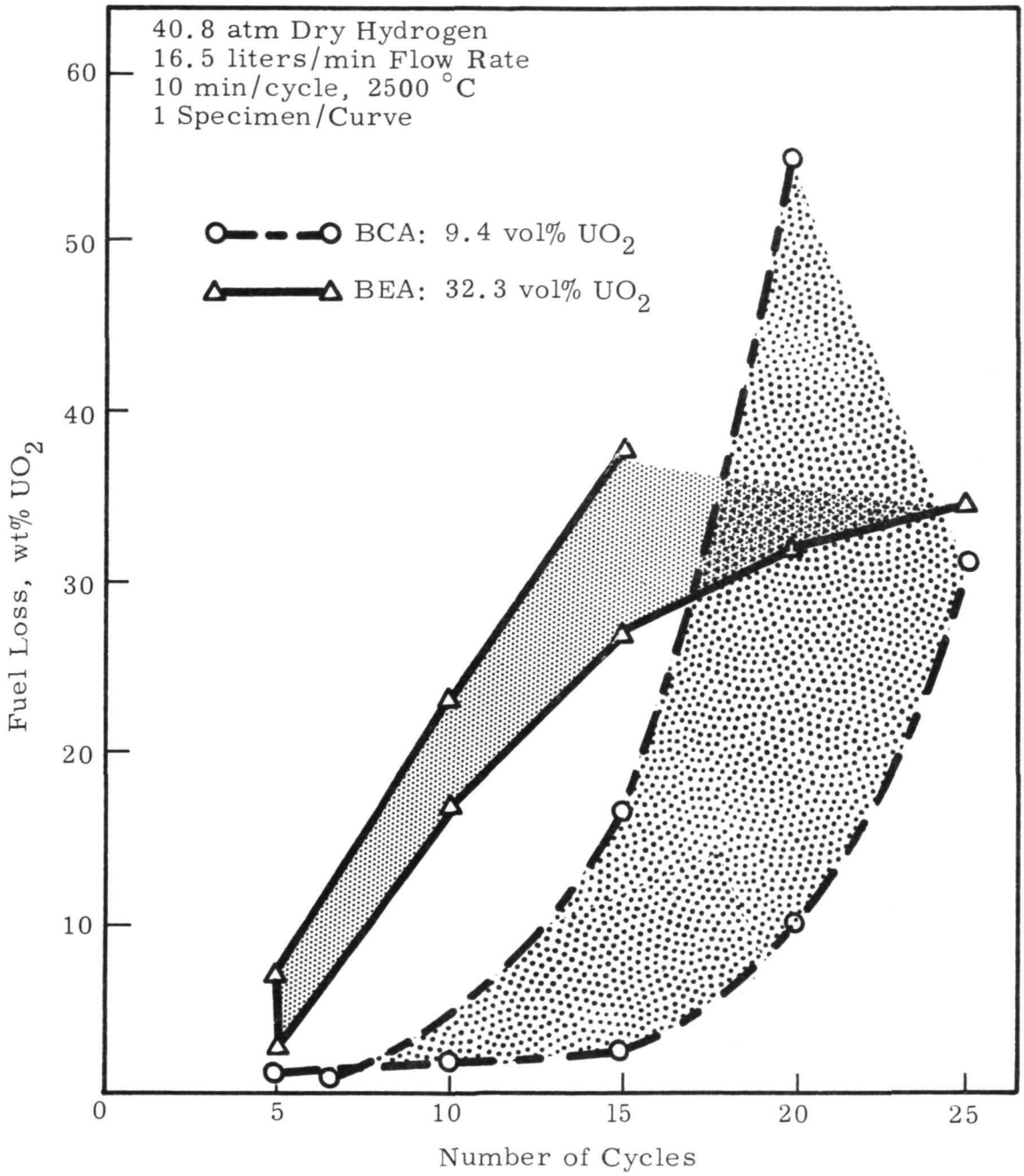


FIGURE 43. Effect of UO_2 Content on Fuel Loss During Thermal Cycling W-UO_2 Cermets

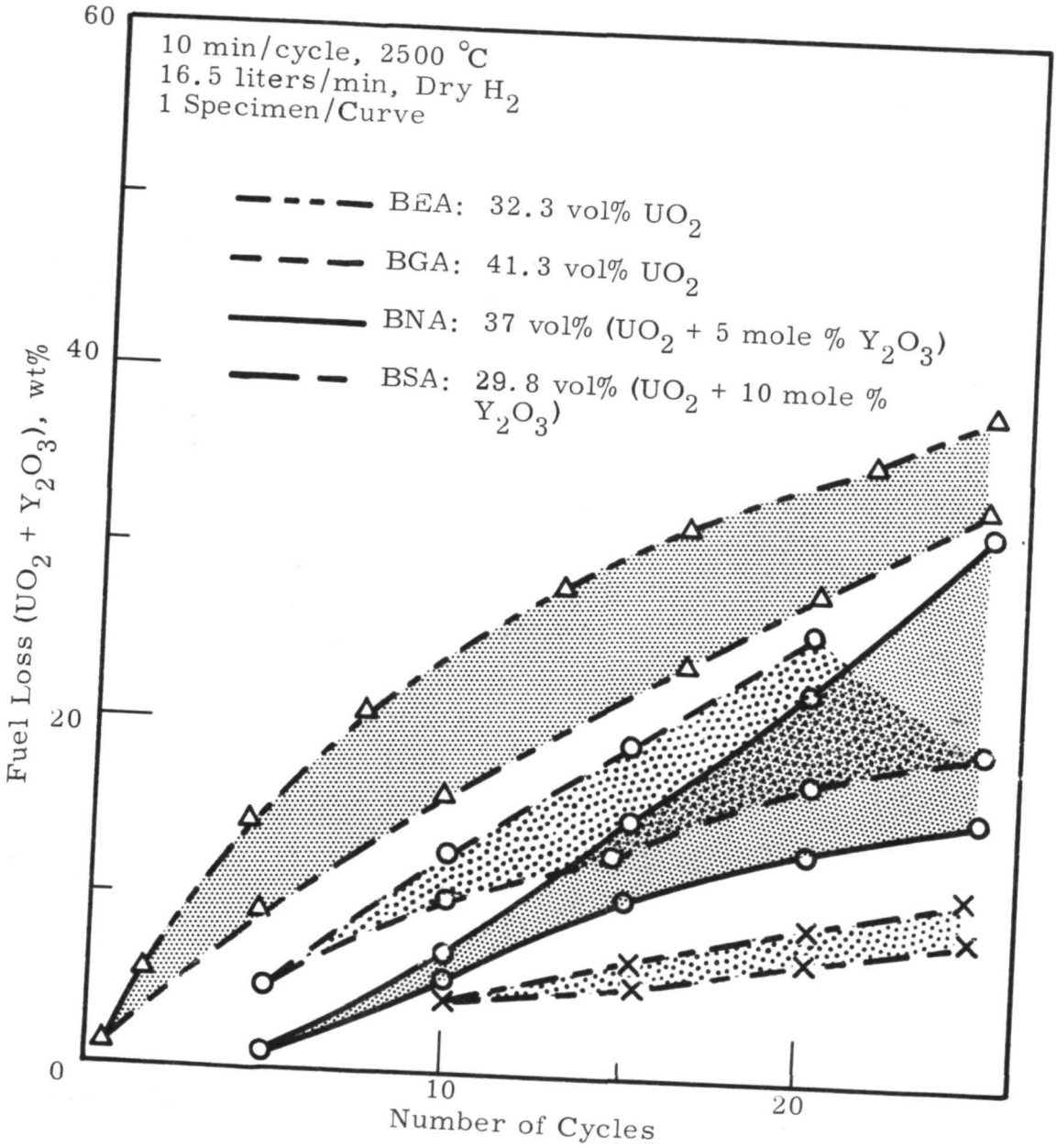


FIGURE 44. Thermal Cycling Behavior of Coated Particle W-UO_2 Cermets under 40.8 atm Flowing Dry Hydrogen

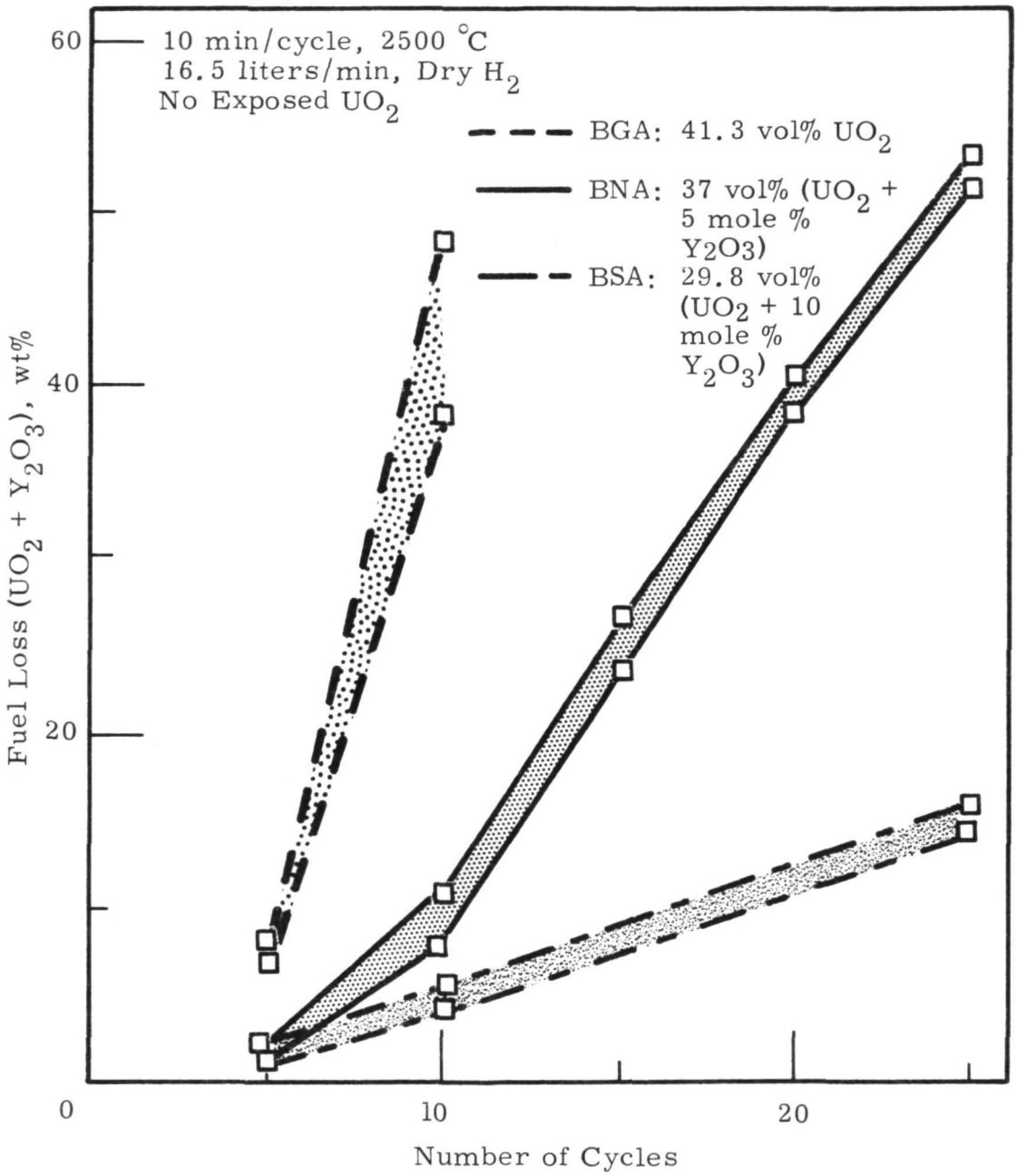


FIGURE 45. Thermal Cycling Behavior of W-UO_2 Coated Particle Cermets Under 1 atm Flowing Dry Hydrogen

CONCLUSIONS

Thermal cycling studies on unclad W-UO_2 coated particle cermets showed:

1. Special H_2 precleaning treatments, inert gas handling, and preimpaction heating in flowing H_2 are not required when the entire cermet composition consists of coated particles. When fine grain W powder is added to the cermet, it is still recommended that the W powder be precleaned and protected from an oxidizing environment through pneumatic impaction.
2. Annealing coated particle cermets (at 1750 °C in hydrogen for 12 hr) prior to testing is beneficial in reducing fuel loss during thermal cycling.
3. Chemical attack on the coated particle cermet surfaces during the dissolution of molybdenum hardware from the impaction assemblies (pneumatically impacted at 1600 °C) resulted in premature fuel loss during thermal cycling.
4. Increased H_2 pressure during thermal cycling had a deleterious effect on the fuel loss behavior from 10 vol% UO_2–W cermets. The effect of hydrogen pressure on the fuel loss behavior for nominally 35 vol% UO_2–W cermets has not been well established perhaps due to the specimen fabrication variables.
5. Cycling under flowing H_2 greatly increased fuel loss when compared to cycling under static H_2.
6. The addition of 10 mole% Y_2O_3 to the UO_2 (in solid solution) was effective in reducing the fuel loss during thermal cycling.

BNWL-394
NASA-CR-54840

PART III

BASIC MECHANISM STUDIES

PART III. BASIC MECHANISM STUDIES

Detailed studies of tungsten-uranium dioxide interactions in thermally cycled cermets, analyses of gas trapped in thermally cycled cermets, and controlled grain boundary experiments led to a hypothesis of the mechanism for the fuel loss and degeneration of tungsten-uranium dioxide cermets thermally cycled in high pressure hydrogen. The results of these studies were applied to the design of cermet systems to improve cermet performance. All the experiments were conducted in a tungsten filament, high pressure, high temperature furnace.

W-UO_2 CERMET INTERACTIONS

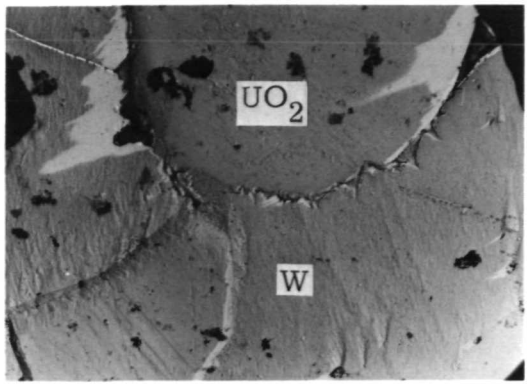
A detailed electron microscopy study of MMA-type cermets (13.3 vol% UO_2; 58.9 vol% W-vapor deposited coating on the UO_2; 27.8 vol% 1 micron tungsten powder matrix addition) which had been thermally cycled to 2500 °C in 1 and 40.8 atm flowing hydrogen revealed:

- Grain boundary phases in the cycled cermets which are more evident in specimens cycled in 40.8 atm, 16.5 liters/min flowing dry hydrogen than in 1 atm flowing hydrogen (Figure 46).
- Reaction layers between the tungsten coating and the uranium dioxide particles which were more evident in specimens cycled in 40.8 atm, 16.5 liters/min flowing dry hydrogen.

The reaction layers and grain boundary phases may be the result of halide impurities at the coating-particle interface, a W-UO_2 eutectic interaction or the formation W-U-O complex ternary compounds. During the time the cermets are at 2500 °C, some W-U-O phases would be molten and thus might contribute to migration of the fuel through the matrix.

ANALYSIS OF GAS CONTENT OF CYCLED CERMET SPECIMENS

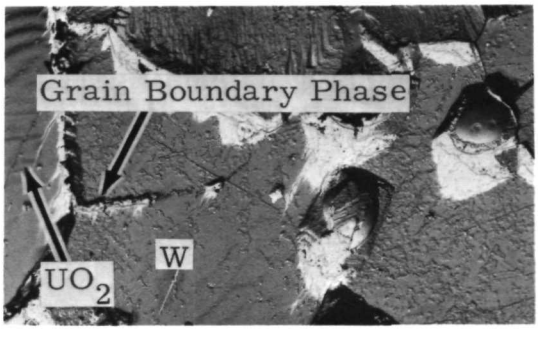
Extensive gas release was observed during the initial heating of cermet specimens in vacuum prior to determination of O/U and O/W ratios. One W-micronized UO_2 cermet (3UA; Table II) and two coated



Neg J2520

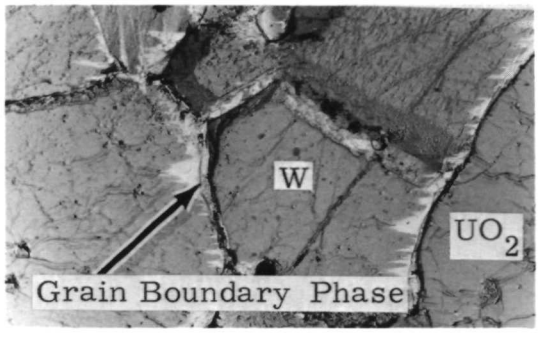
Cermet MMA; As Annealed

H_2 Pressure 1 atm

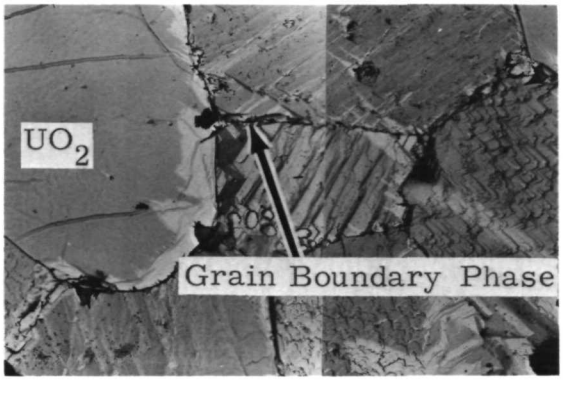


Neg J2831-2
Cermet MMA; 15 Cycles,
5.8 wt% UO_2 Loss

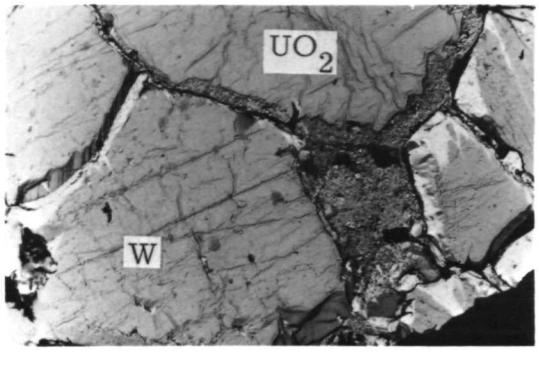
H_2 Pressure 40.8 atm



Neg J2737
Cermet MMA; 15 Cycles,
4.8 wt% UO_2 Loss



Neg J2783-4
Cermet MMA; 25 Cycles
11.1 wt% UO_2 Loss



Neg J2715
Cermet MMA; 20 Cycles
26.0 wt% UO_2 Loss

FIGURE 46. Electron Micrographs of Pneumatically Impacted W-13.3 vol% UO_2 Coated Particle-W Powder Cermets (carbon replicas). Comparison of Effects of 10 min Thermal Cycles to 2500 °C in Flowing Hydrogen at 1 atm and 40.8 atm. (Etched; 1500X)

particle cermets fabricated to contain 19 vol% and 32 vol% UO_2 (BDA and BEA specimens; Table V) were studied to specifically relate volume and composition of released gas to thermal cycling. Data for gas expelled from specimens at 600 °C, after thermal cycling (Figures 47 and 48) show that:

1. Specimens thermally cycled in 40.8 atm flowing hydrogen release as much as 4 to 5 cc of gas per gram of cermet; mass spectrographic analyses showed at least 75% of the gas to be hydrogen. Considering only the solubility of hydrogen in tungsten and its subsequent entrapment in the cermet, the released gas is three orders of magnitude greater than predicted according to Aitken et al.[8] and about one order of magnitude less than predicted according to Moore and Unterwald.[9]
2. Releasable gas content appears to reach a plateau (or a maximum for BEA) after about 15 thermal cycles. This maximum corresponds approximately to the number of cycles at which the cermets begins to break up, and occurs within the stage of accelerated UO_2 loss.
3. The highest hydrogen sorption and entrapment occurs during the highest rate of fuel loss per cycle during thermal cycling.

GRAIN BOUNDARY PHENOMENA IN W-UO_2 CERMETS

Experiments were conducted to investigate the effect of tungsten grain boundary parameters and environmental conditions on UO_2 migration. Variables of particular interest included:

- Intergranular mismatch (low and high angle grain boundaries),
- Environment (H_2 and He),
- Pressure (1 atm and 40.8 atm),
- Thermal cycling,
- Solid diffusion, and
- Vapor diffusion.

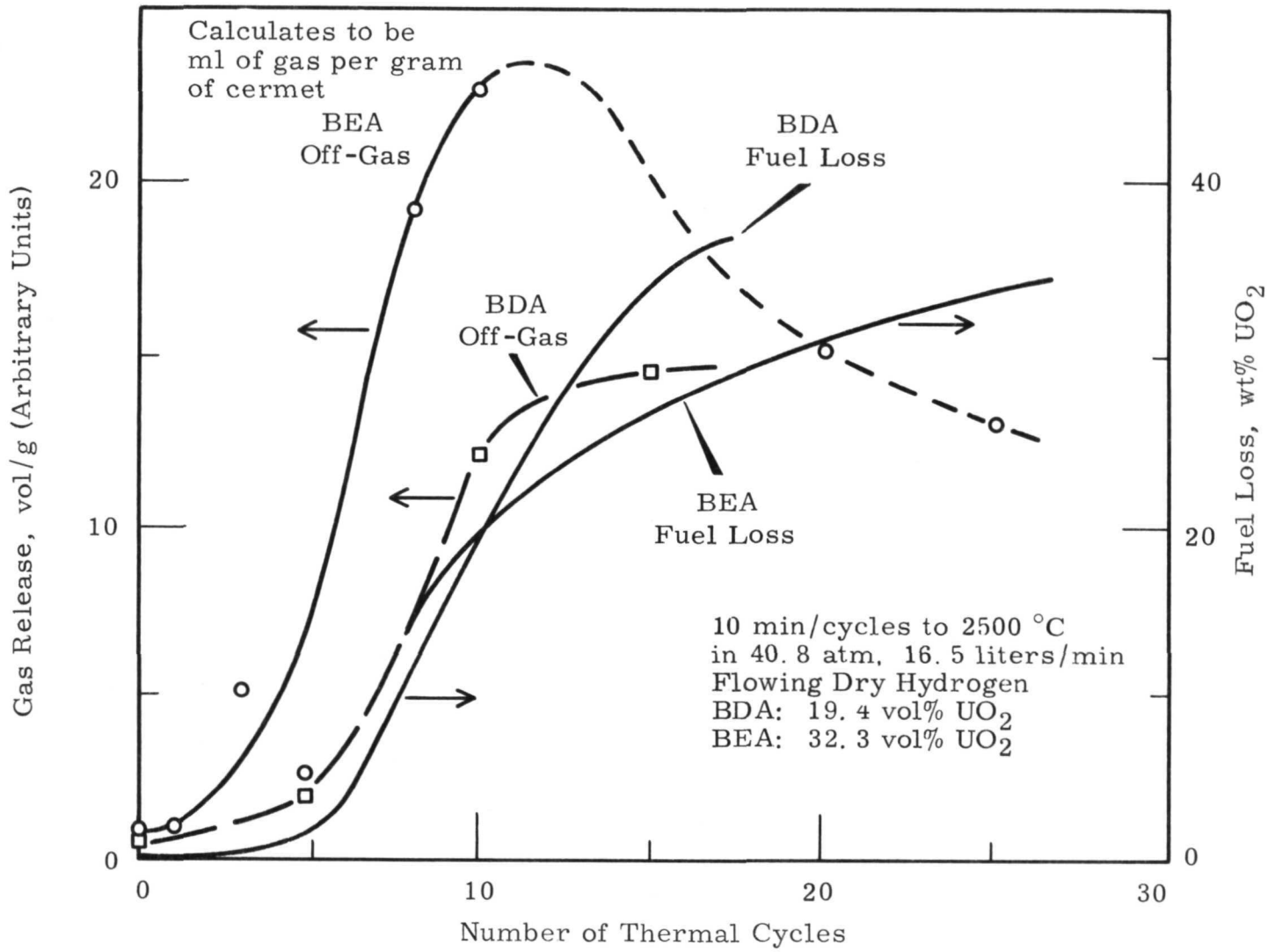


FIGURE 47. Outgassing Characteristics of Cycled Cermets

BNWL-394
NASA-CR-54840

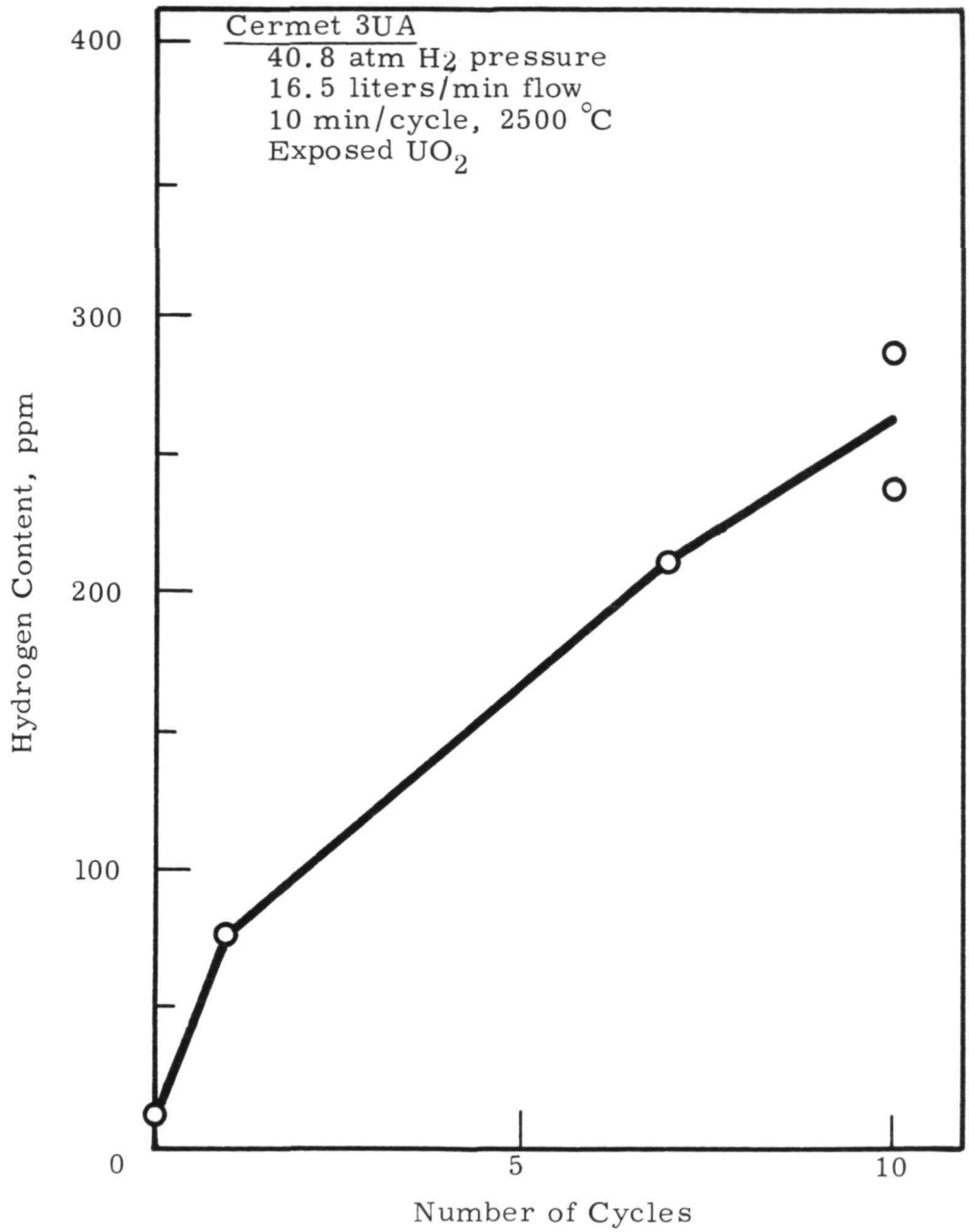


FIGURE 48. Effect of Thermal Cycling on the Hydrogen Content of a W–20 vol% Micronized UO_2 Cermet

All experiments were performed using electron beam refined tungsten and the same tungsten filament high pressure furnace used for the thermal cycling studies. The experimental approach was to isolate the tungsten-tungsten grain boundary from the complexity of the total cermet system. The specific experimental configurations consisted of:

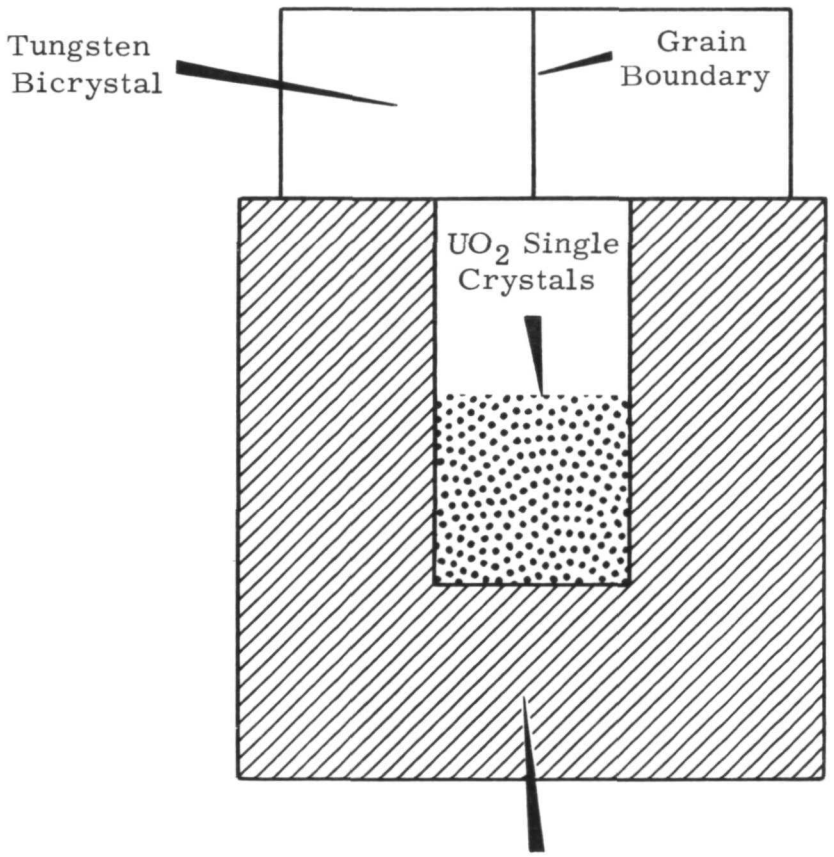
1. GB-type experiments in which a tungsten bicrystal of measured mismatch was placed over a cavity in a 3/16 in. single crystal tungsten cube containing UO_2 single crystal fragments (Figure 49). The purpose of this configuration was to determine W grain boundary--fuel vapor specie effects and to study the effects of thermal cycling variables on the W-W grain boundaries themselves. The assembly was heated on the tungsten filament for the experiment. Variations included leaving the cavity empty and heating the tungsten bicrystal specimens directly on the filament.
2. BC-type experiments in which the tungsten cube comprised the bicrystal specimen containing a cylindrical UO_2 single crystal within the cavity. The cavity was closed with a thoriated tungsten plug (Figure 50). The purpose of this configuration was to study W grain boundary--fuel or fuel product contact effects and the effects of thermal cycling conditions on W-W grain boundaries themselves. A variation was to replace the UO_2 pin with a uranium metal pin.

Electron microscopy observations showed the electron beam refined tungsten to contain very few grain boundary inclusions. Grain boundary mismatch measurements were made by conventional Laue back reflection techniques. The UO_2 single crystals used in these experiments were produced by arc melting. They had an O/U ratio of 2.006.

[redacted]

[redacted]

Scale 1 in. = 1/16 in.



Electron Beam Refined Tungsten Crucible
(Single Crystal)

FIGURE 49. GB-Type Experiments

Scale 1 in. = 1/16 in.

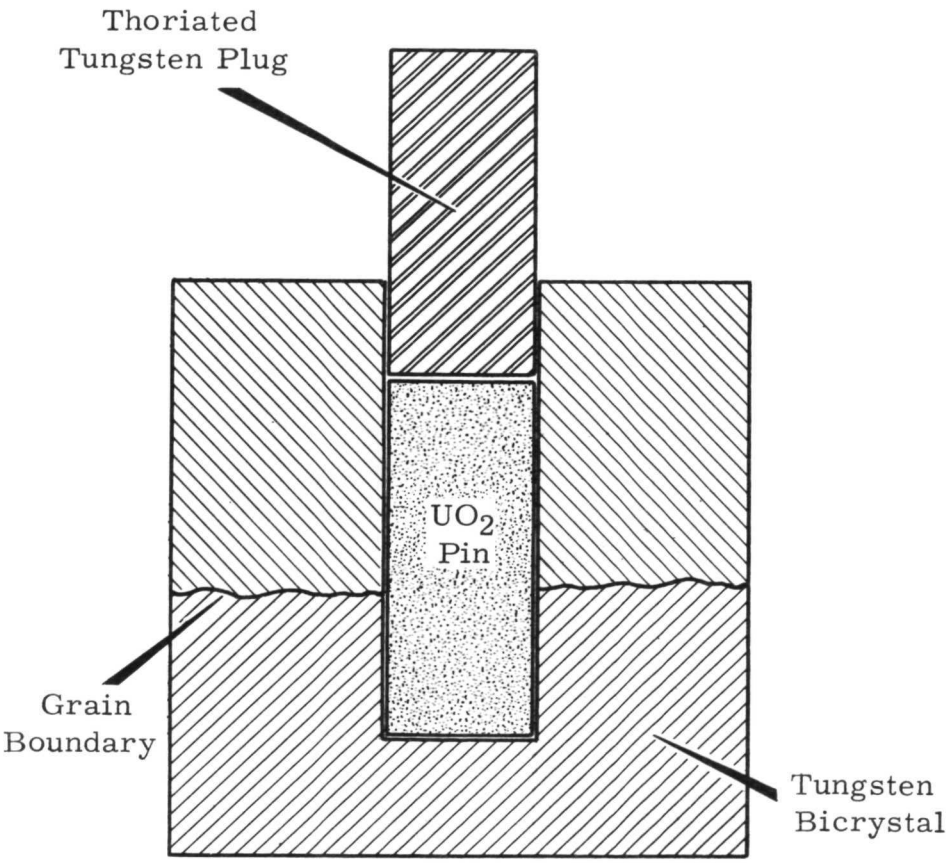


FIGURE 50. BC-Type Experiments

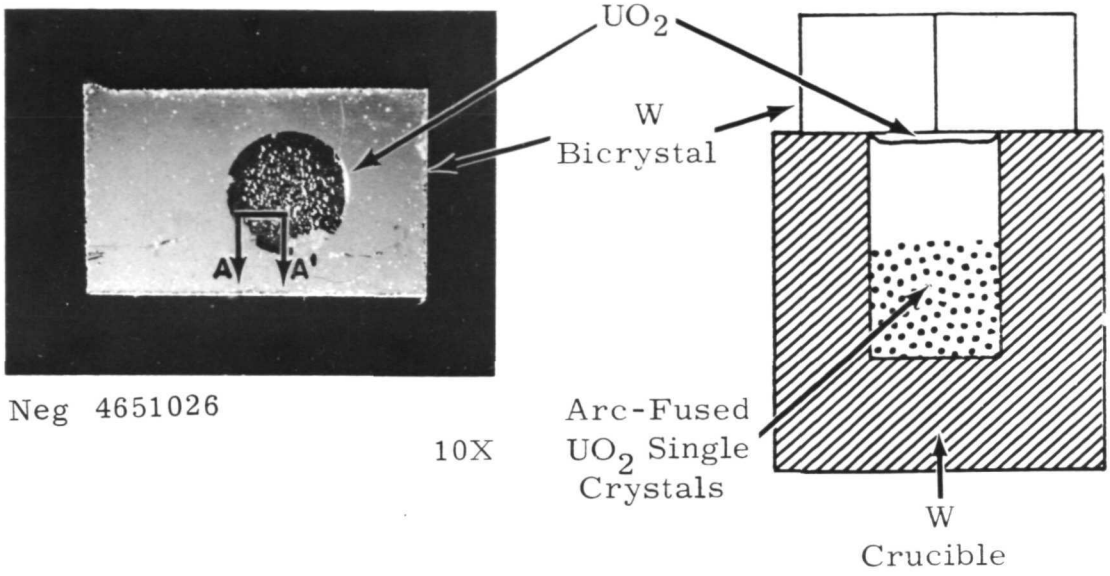
Grain Boundary Experiments

The results of these experiments are summarized as follows (Figure 49; Table VIII):

1. Effect of UO_2. UO_{2-x} was vapor deposited on the tungsten bicrystal specimens during thermal cycling and long-time heat treatments. The uranium metal formed at the W-deposit interface reacted, upon cooling, with hydrogen to form UH_3 (identified metallographically; Figure 51).
2. Hydrogen pressure effects. A bicrystal specimen placed directly on the filament (specimen GB-18) and cycled in 40.8 atm hydrogen fractured violently at the grain boundary on the third heating cycle while another specimen (GB-22) successfully withstood 25 thermal cycles in 1 atm hydrogen. However, large grain boundary bubbles (Figure 52a) developed in specimen GB-22.
3. Environmental effects. Specimens (GB-19 and 23) cycled in 40.8 atm, 16 liters/min grade A helium and ultrapure helium, respectively, exhibited far less grain boundary void formation than specimens cycled in 1 atm hydrogen (Figure 52a, b, c). The difference in the amount of void formation between the specimens cycled in the grade A (< 50 ppm impurity) and ultrapure helium (<10 ppm impurity) is probably due to the difference in the water contents of the grades of gas. The bubbles in these specimens possibly resulted from hydrogen produced in a $W-H_2O$ reaction.
4. Effect of tungsten grain boundary mismatch. Specimens having very small mismatch could be subjected to 25 thermal cycles to 2500 °C in 40.8 atm, 16.5 liters/min flowing dry hydrogen without formation of any grain boundary voids (BG-16). Bicrystals of large mismatch break apart after a very few cycles in 40.8 atm hydrogen (specimen BG-18) and develop large grain boundary voids when cycled in 1 atm of hydrogen.

TABLE VIII. Tungsten Grain Boundary Experiments (GB-Type Experiments)

Specimen	Grain Boundary Mismatch Tilt	Grain Boundary Mismatch Rotation		
GB-9	52°	38°	1 short thermal cycle (< 5 sec. heating to 2500 °C; cooled immediately upon attaining 2500 °C) in 40.8 atm, 16.5 liters/min flowing dry H_2.	UO_2 single crystal fragments in crucible; faint ring of UO_2 (brown) on the W specimen; voids present in grain boundary.
GB-10	52°	38°	25 ten min thermal cycles (1 min heating to 2500 °C, 10 min hold, 1 min cooling) in 40.8 atm, 16.5 liters/ min flowing dry H_2.	UO_2 single crystal fragments in crucible; some grain boundary voids in region not over the crucible mouth; extensive voids in boundary over the crucible cavity; UH_3 in UO_2 on specimen.
GB-11	23°	15°	3 hr at 2700 °C in 40.8 atm/ 16.5 liters/min flowing dry H_2.	UO_2 single crystal fragments in crucible; W specimen fell apart at grain boundary after experiment.
GB-15	2°	2°	3 hr at 2500 °C in 40.8 atm, 16.5 liters/min flowing dry H_2.	UO_2 single crystal fragments in crucible; no grain boundary voids seen in optical microscope; UH_3 in UO_2 on specimen.
GB-16	2°	2°	25 ten min thermal times to 2500 °C in 40.8 atm, 16.5 liters/ min flowing dry H_2.	UO_2 single crystal fragments in crucible; no bubbles, no alteration of the grain boundary.
GB-17	42°	38°	25 ten min thermal cycles to 2500 °C in 40.8 atm, 16.5 liters/ min flowing H_2; W spacer between specimen and W filament.	No UO_2 in crucible; large bubbles in grain boundary; small bubbles within the grains.
GB-18	42°	38°	25 ten min thermal cycles to 2500 °C in 40.8 atm, 16.5 liters/ min flowing dry H_2; specimen heated directly on the W filament.	No crucible; specimen fractured on heating during the third cycle
GB-19	42°	38°	25 ten min thermal cycles to 2500 °C in 40.8 atm, 16.5 liters/ min, flowing dry He (Grade A); specimen heated directly on filament.	No crucible; a few gas bubbles in the grain boundary.
GB-22	42°	38°	25 ten min thermal cycles to 2500 °C in 1 atm, 16.5 liters/ min flowing dry H_2; specimen heated directly on W filament.	No crucible; large bubbles in the grain boundary.
GB-23	42°	38°	25 ten min thermal cycles to 2500 °C in 40.8 atm, 16.5 liters/min flowing dry He; specimen heated directly on W filament.	No crucible; only very few small bubbles.



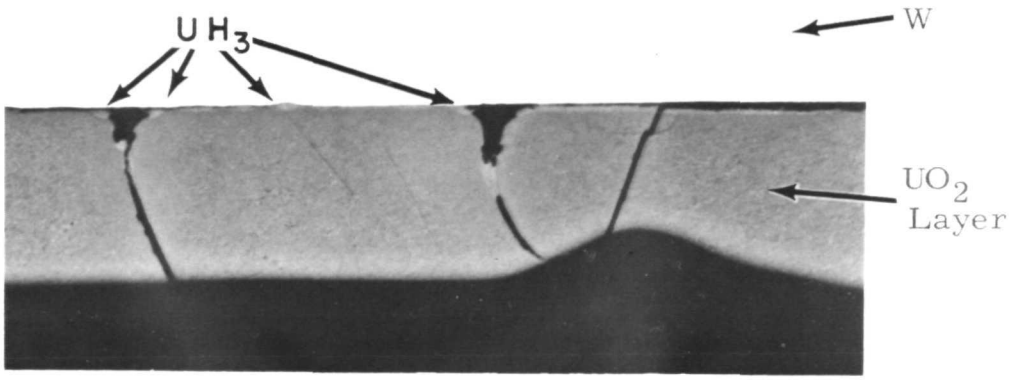
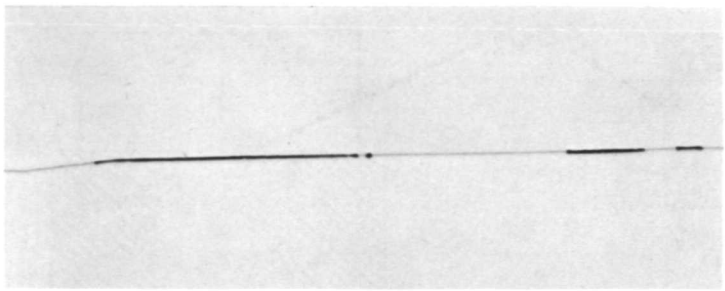
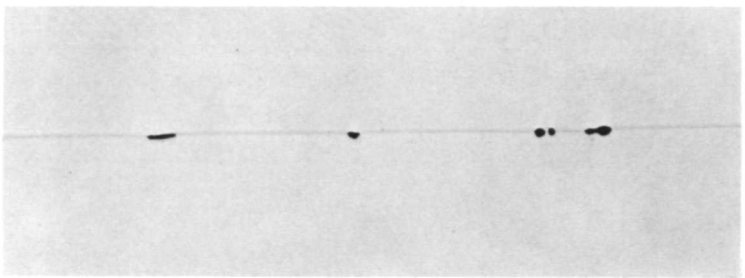


FIGURE 51. Results of Tungsten-UO_2 Vapor Diffusion Experiment (Heated at 2500 °C for 3 hr Under 408 atm, 16.5 liters/ [illegible] Flowing, Dry Hydrogen



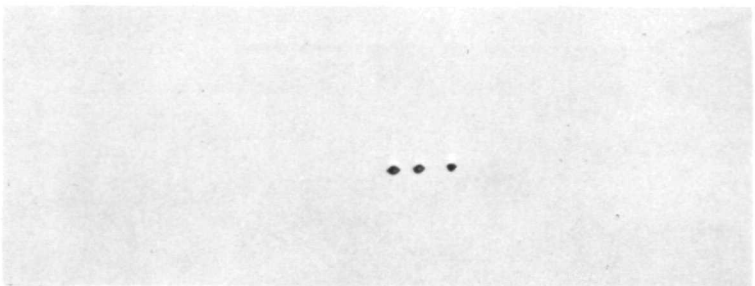
a. Hydrogen
1 atm

Neg 4652031A 250X
No Etchant
Misorientation 42°. Tilt 38° Rotation



b. Grade A Helium
40.8 atm

Neg 1798C 250X
No Etchant
Misorientation 42° Tilt 38° Rotation



c. Ultrapure Helium
40.8 atm

Neg 2032B 500X
No Etchant
Misorientation 42° Tilt 38° Rotation

Specimens Heated Directly on the Filament

FIGURE 52. Hydrogen and Helium Penetration of Electron Beam Refined Tungsten Bicrystals; Specimens GB-22, GB-19, and GB-23; 25 Thermal Cycles to 2500 °C in 16.5 liters/min Flowing Dry H_2, Grade A He and Ultrapure He Respectively

5. Heating rate effects. The difference in the tungsten bicrystal specimen heating rate resulting from heating the specimen directly on the filament or atop the crucible is sufficient to allow a high mismatch bicrystal to be cycled 25 times to 2500 °C in 40.8 atm, 16.5 liters/min flowing dry hydrogen without fracturing (Table VIII; GB-17 and 18). However, many large grain boundary voids result even with the slower heating rate.

Bicrystal Cube Experiments

Further experiments on the effects of environmental parameters and grain boundary mismatch were performed on bicrystal crucibles (the crucible comprised the specimen). The results of these experiments are summarized as follows (Figure 50; Table IX):

1. Fuel effects. The effect of thermal cycling conditions on the integrity of the W bicrystals themselves overshadowed any effect of the presence of fuel.
2. Hydrogen pressure effects. Thermal cycling to 2500 °C in 40.8 atm, 16.5 liters/min flowing dry hydrogen led to catastrophic failure of highly mismatched tungsten bicrystal grain boundaries (grain boundary "explosion"). Thermal cycling to 2500 °C in 1 atm, 16.5 liters/min flowing, dry hydrogen resulted in hydrogen penetration of the tungsten grain boundaries, but was grossly less effective in disrupting the grain boundaries than cycling in 40.8 atm hydrogen (Table IX; compare BC-1 and BC-4 with BC-5).
3. Tungsten grain boundary mismatch. Low angle grain boundary tungsten bicrystals were relatively unaffected by cycling in 40.8 atm, 16.5 liters/min flowing dry hydrogen. After 25 thermal cycles, there was no evidence of grain boundary voids in the low angle mismatch specimen. High angle specimens "explode" during the third or fourth cycle (Table IX, compare specimen BC-3 with BC-1 and BC-4).

[redacted] [redacted]

TABLE IX. Tungsten Bicrystal Cube Experiments
(BC-Type Experiments)

Specimen	Grain Boundary Mismatch Tilt	Grain Boundary Mismatch Rotation	Experimental Conditions	Descriptions and Results
BC-1	23°	15°	3 ten min thermal cycles to 2500 °C in 40.8 atm, 16.5 liters/min flowing, dry H_2.	UO_2 pin in crucible; grain boundary "exploded" during heating for fourth cycle.
BC-4	39°	30°	2 ten min thermal cycles to 2500 °C in 40.8 atm, 16.5 liters/min flowing, dry H_2.	No UO_2 in crucible; grain boundary "exploded" during heating for third cycle.
BC-2	23°	15°	3 hr at 2500 °C in 40.8 atm, 16.5 liters/min flowing, dry H_2.	UO_2 pin in crucible; grain boundary badly parted.
BC-5	50°	40°	25 ten min thermal cycles to 2500 °C in 1 atm, 16.5 liters/min flowing, dry H_2.	UO_2 pin in crucible; W grain boundary did not intersect the cavity; many bubbles in the grain boundary.
BC-3	3°	2°	25 ten min thermal cycles to 2500 °C in 1 atm, 16.5 liters/min flowing, dry H_2.	UO_2 pin in crucible; no apparent grain boundary penetration by either hydrogen or UO_2.
XS-2	42°	38°	Heated to 2500 °C in ~2 sec, held at 2500 °C for 15 sec, and cooled to less than red heat in 2 sec in 40.8 atm, 16.5 liters/min flowing, dry H_2.	U metal pin in crucible; UH_3 formation in the U metal-W grain boundary region.
XS-3	42°	38°	Heated to 2500 °C in ~2 sec, held at 2500 °C for 15 sec and cooled to less than red heat in 2 sec in 40.8 atm, 16.5 liters/min flowing, dry H_2.	U metal pin in crucible; UH_3 formation in the U metal-W grain boundary region.

CONFIDENTIAL

BNWL-394
NASA-CR-54840

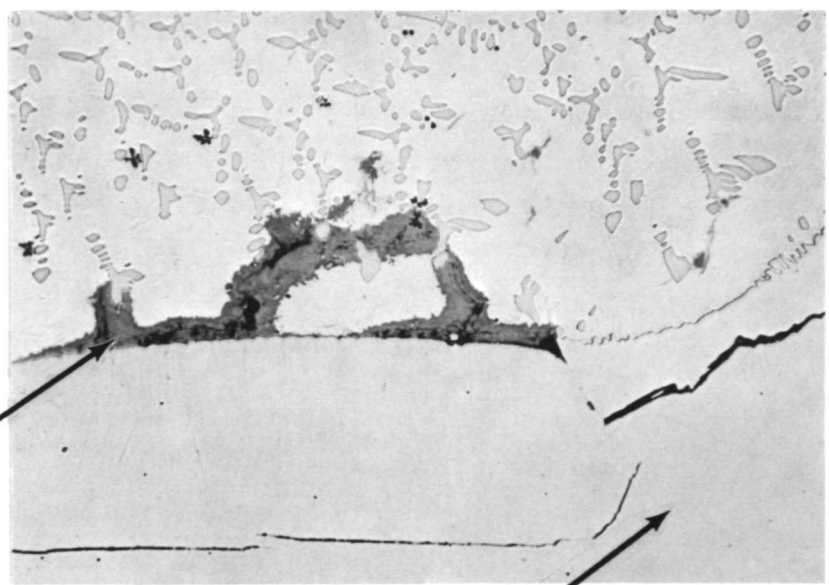
4. Time at temperature. Single cycle, long time heating of highly mismatched tungsten grain boundaries had a disruptive effect on these grain boundaries (BC-2) but did not cause the explosive fracture of the grain boundary.
5. W-U-H_2 experiments. Further evidence of the preferential grain boundary diffusion of hydrogen in tungsten was obtained from experiments in which a uranium metal pin was substituted for the UO_2. The test specimens were pressurized to 40.8 atm, 16.5 liters/min flowing dry hydrogen, heated to 2500 °C in ~2 sec, maintained at 2500 °C for 15 sec and cooled to less than red heat in 2 sec. After cooling, the specimens were sectioned perpendicular to the plane of the tungsten grain boundary and examined metallographically. Essentially identical results were obtained with both specimens. A large number of tungsten dendrites having preferred orientations were found in the uranium core (Figure 53). In each specimen a yellow-brown phase (UH_3) was observed metallographically on the top of the uranium core and at the grain boundary-core interface after each of four successive polishings. The latter observation indicates that a belt of UH_3 was formed around the periphery of the core at its intersection with the tungsten grain boundary.

The combined grain boundary experiments show:

1. Significant deleterious effects of 40.8 atm hydrogen W bicrystals thermally cycled to 2500 °C.
2. Deleterious effects of long time exposure at 2500 °C in 40.8 atm hydrogen, though not as dramatic as those of thermal cycling in 40.8 atm hydrogen.
3. Hydrogen to be responsible for the effects shown (see negative confirmation in helium experiments).



Neg 465565A 75X
Unetched



Neg 465565B 500X
Unetched

FIGURE 53. Tungsten Bicrystal with Uranium in Cavity.
(After Heating to 2500 °C for 15 sec in 40.8 atm,
16.5 liters/min Hydrogen, Specimen XS-2)

PROPOSED MECHANISM OF FUEL LOSS AND DEGENERATION OF W-UO_2 CERMETS DURING THERMAL CYCLING

The hypothesized mechanism comprises the three stages depicted sequentially* in Figure 54. The first stage consists of hydrogen penetration into the cladding and/or cermet via the bulk and grain boundary diffusion in the tungsten. Hydrogen collecting in the grain bounding upon cooling results in void formation and W-W bond degradation during subsequent heatings. Point A is the breakover point between stages 1 and 2. Stage 2 comprises migration of fuel and oxygen (as water vapor) through the cermet which is enhanced by stage 1 and eventual free vaporization of the fuel at the surfaces of the cermet. Point B is the breakover point between stages 2 and 3 in this proposed mechanism. Stage 3 represents the final gross disintegration of the cermet brought on by the hydriding of free uranium in the fuel particle in W-UO_2 cermets (non-stabilized) and uranium hydride formation, gross migration and/or ratcheting of the fuel in W-stabilized UO_2 fueled cermets. These stages are not distinctly separable except, perhaps in a single grain boundary or coated particle. For example, to observe the first stage directly, clad specimens may be required, in which case the observed first stage would most likely represent penetration of hydrogen through the cladding. The second stage may characteristically appear only in clad cermets containing stabilized fuel particles where it represents the progressive reduction of U^{VI} to produce a defect lattice in the stabilized fuel. The third stage is more readily observed in cermets having neither a fuel stabilized additive nor cladding in which UH_3 has been observed metallographically. In these cermets the first and second stages occur during the first one or two cycles and are thus not observable.

---

* Sequential, although the three stages may be found concurrent among various locations throughout the cermet body.

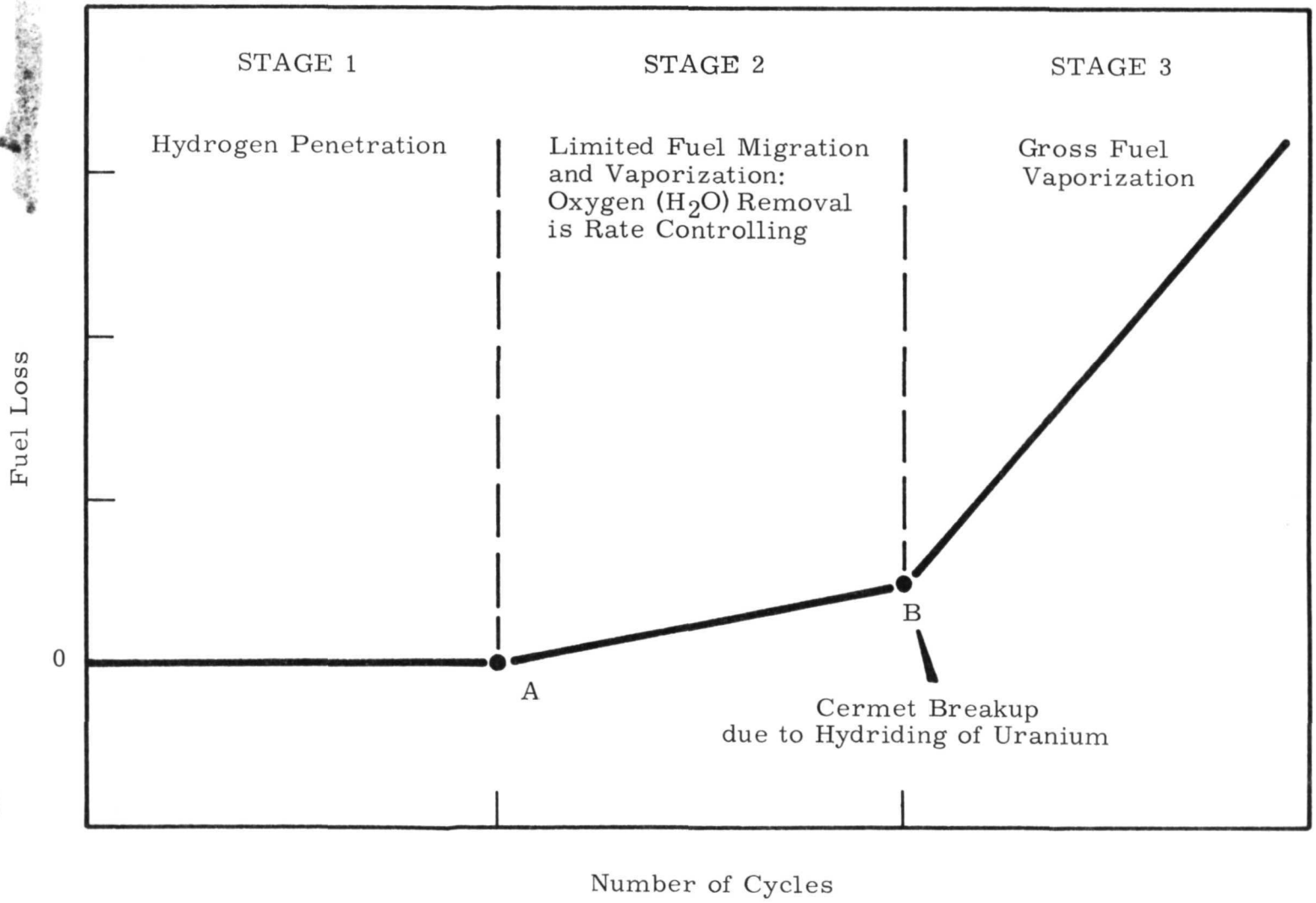


FIGURE 54. Proposed Mechanism of the Thermal Cycling Behavior of W-UO_2 Cermets

BNWL-394
NASA-CR-54840

Stage 1 - Hydrogen Penetration

As is depicted in Figure 54, this stage in the fuel loss mechanism is not measurable under normal thermal cycling testing. This stage establishes the conditions required for stages 2 and 3 to occur and may actually take place in as few as 1 or 2 cycles depending on the nature of the matrix material. Three variables thought to affect the role of hydrogen in degrading the cermets are the degree of mismatch in the tungsten grain boundaries; the pressure and temperature of the hydrogen; and the heating and cooling rate under which the cermets are tested. The entrance of hydrogen into the cermet is principally via bulk and grain boundary diffusion. The rate controlling reaction affecting permeation of the cermet with hydrogen is probably the dissolution rate of monatomic hydrogen after catalytic dissociation of hydrogen molecules on the tungsten surface.[8] Tungsten bicrystal grain boundary studies demonstrated that highly mismatched grain boundaries can explode, with failure occurring during heating in the third or fourth thermal cycles to 2500 °C in 40.8 atm hydrogen and with no involvement of fuel in the process. Low angle grain boundaries, on the other hand, successfully withstood 25 standard thermal cycles without accumulation of either hydrogen or fuel in the grain boundaries. Increasing tungsten grain boundary mismatch to 45° tilt, 45° rotation (cubic system) should increase the available sites for the accumulation of hydrogen. The expansion of the gas collected at the tungsten grain boundaries during subsequent rapid heating stresses the highly mismatched grain boundary before the gas can be dissolved and diffused throughout the tungsten grains. This results in grain boundary explosions in the idealized bicrystal experiments. Grain boundary voids in cycled coated particle cermets may contain accumulated hydrogen gas or may result from tungsten vapor deposition impurity (halide) reaction products produced during thermal cycling.

These data suggest that:

a. It is desirable that the cermet consist of UO_2 particles encapsulated in low angle grain boundary tungsten. This configuration can be approached in two ways–by producing a low angle grain boundary tungsten matrix, or by covering the cermet with a low angle grain boundary cladding. The role of tungsten cladding, shown by NASA Lewis Research Center to inhibit fuel loss, is interpreted by us as limiting the sites of hydrogen accumulation, and/or limiting the removal of oxygen rich decomposition products of UO_2 at high temperature from the cermet core. The tungsten vapor deposition process can be controlled to produce a very low angle grain boundary tungsten coating. The achievable uniformity of such coatings is expected to be of significant importance in the performance of a clad cermet fuel grid in the nuclear reactor. Plasma spray coating has also been shown to produce effective cladding. However, it is believed that the vapor deposition process, being more uniform, and producing low angel grain boundaries over the entire cermet surface, is potentially the better of the two processes. The plasma-sprayed coating process will produce grain boundaries of random mismatch. In a cermet grid several grossly mismatched grain boundaries in a small area would lead to early and rapid catastrophic failure of the entire grid once a path for fuel loss is established.

b. The grain boundary experiments also indicated the role of external gas pressure on the penetration of hydrogen into the tungsten grain boundaries. Whereas well characterized grain boundaries tested in 40. 8 atm, 16. 5 liters/min hydrogen have failed in as few as three or four thermal cycles, one similar grain boundary specimen was cycled 25 times without failure in 1 atm, 16. 5 liters/min hydrogen. Examination

of the latter specimen revealed gas bubbles throughout the grain boundary. Thus, the effect of pressure may simply be to increase the hydrogen concentration gradient and therefore the driving force for hydrogen diffusion into the cermet and also the absolute content of hydrogen in the cermet. The bombardment rate of molecular hydrogen on the tungsten surface should increase and therefore the equilibrium concentration of monatomic hydrogen available for penetration of tungsten grain boundaries and for solution in the tungsten should increase. The storage of hydrogen in the cermets in some form as a result of thermal cycling has been verified by the analyses of cycled cermets.

c. Both heating rate and cooling rate will affect the extent of W grain boundary damage. This effect can be best illustrated by considering the action during one or two thermal cycles. During the first thermal cycle, the specimen is heated to 2500 °C. While being held at the peak temperature, monatomic hydrogen is formed on the tungsten surface and subsequently penetrates the cermet. This monatomic hydrogen is located on the grain boundary surfaces and in the tungsten grains. (The solubility of hydrogen in tungsten at 1700 ° C is ~0.25 at. %[9] and may be substantially greater at 2500 °C. Tungsten catalyzed hydrogen dissociation is established at temperatures below 2500 °C, but is probably most significant above 2000 °C.) During cooling, monatomic hydrogen is exsolved from the tungsten and recombines at the tungsten grain boundaries and other surfaces. If the cooling rate is sufficiently rapid, molecular hydrogen will be trapped at the tungsten grain boundaries. Thermal pressurization of the molecular hydrogen during the second thermal cycle tends to rupture the tungsten grain boundaries. Since the catalytic effect of the tungsten

becomes significant only at high temperatures, (probably above 2000 °C) molecular hydrogen has a relatively broad temperature range in which to stress the grain boundaries. In experiments in which large mismatch tungsten grain boundaries have been ruptured, grain boundary failure has always occurred during heating, and explosively.

d. The effect of dispersed phases in cermet matrixes is related to the first stage of degeneration. For example, several oxides, including thorium dioxide, inhibit grain growth of tungsten, thereby maintaining a maximum available tungsten grain boundary surface for storage of hydrogen and also increasing the path length for the penetration of hydrogen to the fuel as well as the path for vapor product removal. The two properties that make such oxides useful are their highly refractory nature and their stiochiometric stability. In a uranium dioxide fuel system ThO_2, or perhaps Y_2O_3, fulfill these requirements. The presence of nitrides, carbides, borides, etc. probably would have a deleterious effect on the performance of the oxide fuel because of possible high temperature reaction with the oxide fuel.

Stage 2 - Limited Fuel Migration and Vaporization

The onset of stage 2 of this proposed mechanism is the straining of grain boundaries to form channels for the transport of vapors through the cermet. The stage begins with the first measurable fuel loss from within the specimens. Depending on the cermet system--stabilized or nonstabilized, clad or nonclad-- stage 2 may be established during the second or third thermal cycle depending on the resistance of the tungsten grain boundaries to hydrogen penetration.

Fuel migrates through the cermet in two manners; by vapor diffusion through a strained tungsten grain boundary, or by formation of a ternary composition, free Uranium, or a W-UO_2 eutectic liquid that

can migrate through grain boundaries to the surface and eventually vaporize. In a typical cermet it is believed that the latter may be controlling. A W-UO_2 eutectic below 2000 °C has been observed.[10] A ternary W-U-O composition would probably be achieved in two ways: by the presence of tramp oxygen in the tungsten matrix, effectively making WO_3 available to react with UO_2; or, the presence of impurities at the UO_2-W interface that would catalyze or otherwise increase the reaction rate between the fuel and the tungsten matrix (for example, fluorine left on the surface of coated UO_2 particles after the vapor deposition process.)

The principal second stage reaction leading to the third stage of the loss mechanism is the reduction of U^{VI} by molecular or monatomic hydrogen, and removal of excess oxygen in the fuel which may require that water be removed from the system via the strained tungsten grain boundaries. This is probably the rate controlling step. From these considerations, both the effect of hydrogen flow rate and the desirable behavior of the stabilized fuel particles are clarified.

Cermets tested at PNL have suffered significantly greater weight loss in 16.5 liters/min flowing hydrogen than in static hydrogen. Flowing hydrogen reduces the thickness of the diffusion layer at the cermet surface and probably sweeps away decomposition products.

It has been established at Argonne National Laboratories[11] and elsewhere[12] that rare earth oxide stabilized UO_2 fuels in equilibrium with low partial pressures of oxygen maintained an oxygen-to-metal atom ratio of 2.0 to 2.1 even with the addition of as much as 40 mole% $RO_{1.5}$, (where R is a rare earth atom) depending upon preparation conditions. The defect lattice established by solid solution of the stabilizing R_2O_3 in UO_2 is easily filled with oxygen atoms and some U atoms must be in the hexavalent state to retain electronic neutrality.[7] U^{IV} cannot be reduced to metal in the presence of U^{VI}; therefore, initial loss of water vapor from the cermet is accompanied by creation of anion

vacancies in the lattice rather than by formation uranium metal. The fuel remains intact until all hexavalent uranium atoms are reduced. Then formation of free uranium metal will then no longer be inhibited and the third stage of fuel loss will begin. Also, solid solutions of R_2O_3 in UO_2 are more stable to reduction reaction than UO_2 because of lower oxygen partial molar free energy. The effect of the stabilizing agent is to delay point B (Figure 54) to a greater number of cycles.

Stage 3 - Mechanical Failure and Gross Fuel Migration

Stage 3, the final mechanical failure of the cermet, is brought on when the fuel is depleted of excess oxygen. Under these conditions nonstabilized UO_2 undergoes thermal dissociation at high temperatures to product a single phase UO_{2-x}. Oxygen may be removed as H_2O or by diffusion loss of free oxygen to the surface. The free uranium metal precipitated from the substoichiometric high temperature phase during cooling will then be converted to a hydride, and catastrophic expansion of the cermet will occur when cycled through the hydriding range. This leads to the final failure of the cermet by effectively making the entire cermet a free surface accessible for massive fuel vaporization.

For W-stabilized UO_2 cermets, gross degeneration of the cermet to allow free vaporization of the fuel may be caused by either one or a combination of (1) excessive channeling due to internal gas pressures built up in the cermets during cycling, and (2) fuel migration and fuel ratcheting.

Other observations which support this three-stage mechanism of fuel loss include improved behavior of cermets made from tungsten coated particles over that of cermets made from blended fuel and tungsten powders, and the effectiveness of the hydrogen precleaning treatments previously used. The latter removes tramp oxygen from the tungsten matrix and thereby inhibits formation of a ternary W-U-O phase in the tungsten grain boundaries. Coated particles produce a microstructure

of matrix tungsten of greater grain boundary strength than does fine grain tungsten powder in the cermets fabricated to date, reflecting the difficulty of achieving and maintaining the purity of the fine tungsten powder during processing. The coating of the particles, however, does not completely eliminate fuel loss from them because the tungsten is either hot worked, as in pneumatic impaction or gas pressure bonding, or is processed in such a manner that the coating is recrystallized by the time it is ready to be thermally cycled (or irradiated). The ultimate solution will probably require both the use of coated particles and tungsten vapor deposited tungsten cladding after cermet fuel body is fabricated.

CONCLUDING REMARKS AND RECOMMENDATIONS

It is evident from these studies that additional fuel containment will be required in order to meet operation goal of less than 1 wt% fuel loss after 25 thermal cycles to 2500 °C in 40.8 atm for the tungsten, water-moderated nuclear rocket reactor. These studies point to the desirability of using a cladding on the cermet which has a minimum number and/or a minimum mismatch of grain boundaries. The addition of Y_2O_3 to the UO_2 (in solid solution) significantly increased fuel stability, and this effect should be further investigated to evaluate its potential to further increase cerment stability. Additional development studies on the effects of impurities, such as halide contaminants, and on the effects of hydrogen pressure on fuel loss are recommended.

Further research studies suggested to further elucidate the fuel loss mechanism include:

1. Determination of the R_2O_3-UO_2 solid solution decomposition equilibrium and kinetics (loss of oxygen) and the R_2O_3-UO_2 solid solution vaporization stability.
2. Evaluation of other potential stabilizers.
3. Further experiments and analysis of the gas buildup in cermets, particularly as related to accelerated fuel loss and hydrogen pressure.

4. Identification of the species migrating during thermal cycling and the role of free uranium metal and/or hydrides in the catastrophic failure of cermets containing stabilized fuel.

BNWL-394
NASA-CR-54840

APPENDIX A

HIGH CAPACITY, HIGH TEMPERATURE, HIGH PRESSURE HYDROGEN FURNACE

APPENDIX A

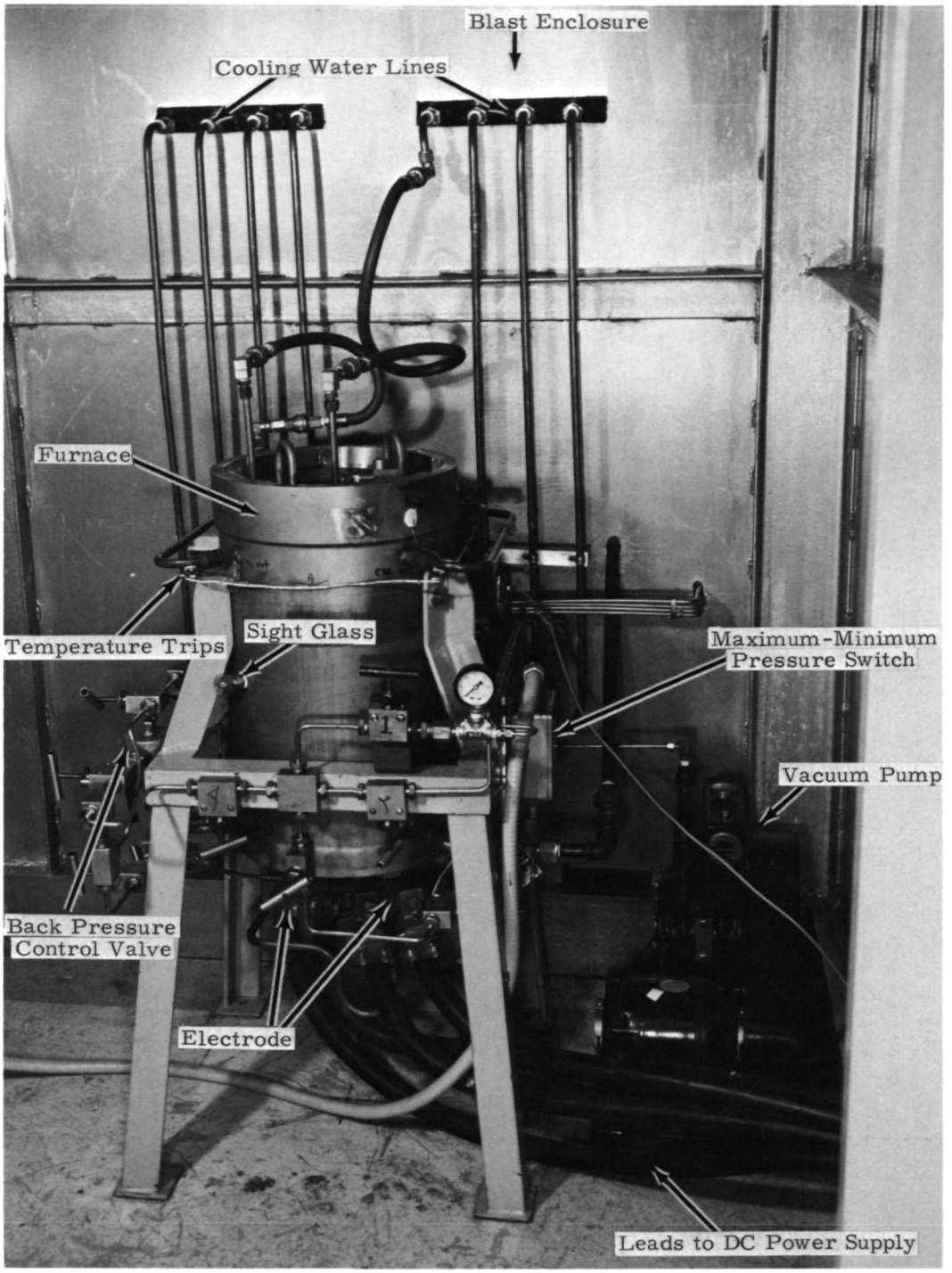
HIGH CAPACITY, HIGH TEMPERATURE, HIGH PRESSURE HYDROGEN FURNACE

I. Description

The scope of the FY-1965 program included the construction and testing of a high pressure, high temperature furnace to test 2.5 cm x 2.5 cm x 0.05 cm test specimens in flowing hydrogen. The furnace herein described was built in accordance with Section VIII of the ASME Boiler and Pressure Vessel Code. The furnace system consists of the furnace vessel (Figures 55 and 56), a DC power supply, appropriate gas, water and electrical connections (Figures 56, 57, and 58) and control and safety instrumentation.

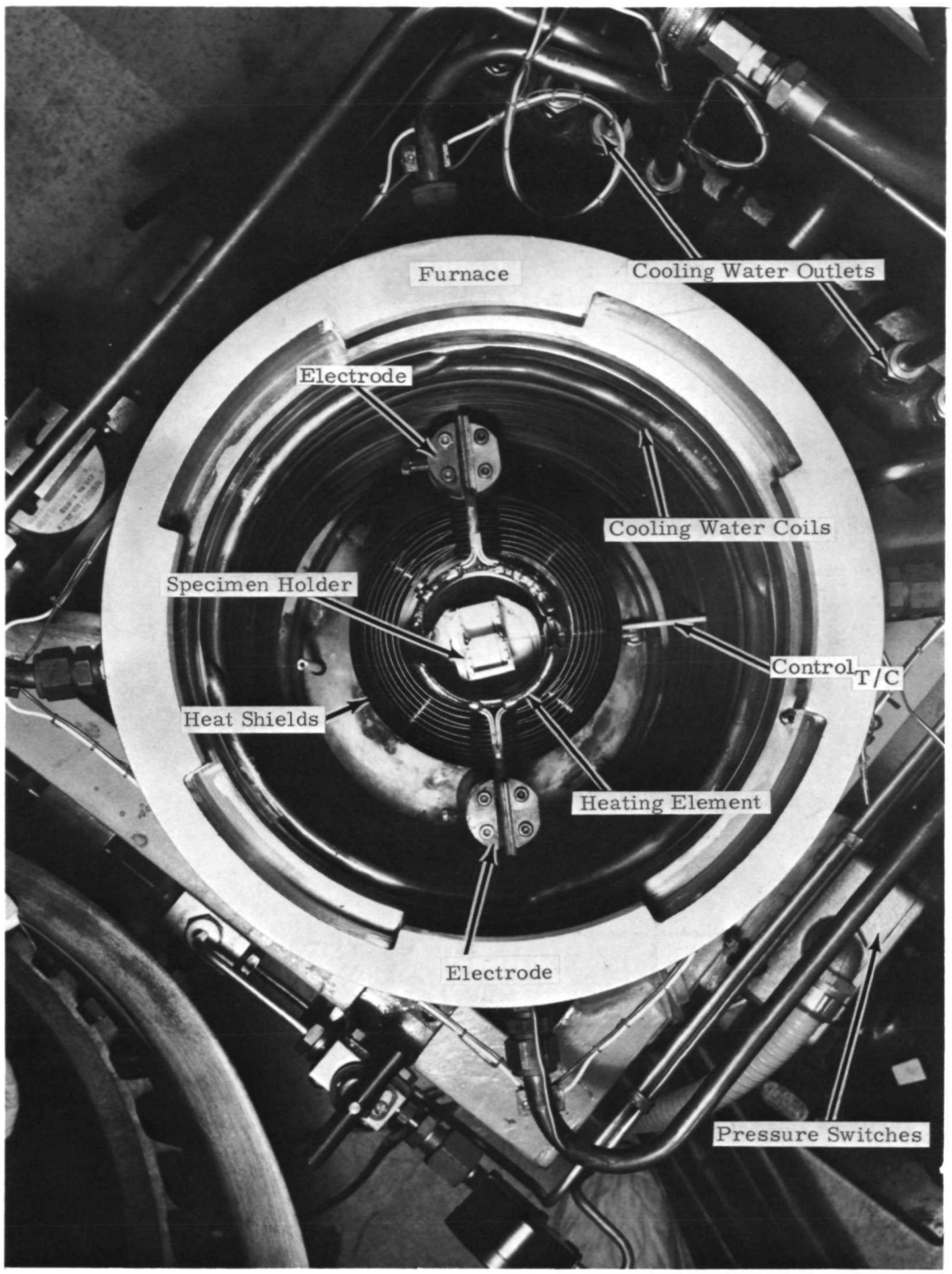
The furnace vessel contains: Water cooled copper electrodes inserted into the pressure vessel to conduct high amperage direct current to a tungsten heating element, cooling coils silver-soldered to the vessel walls and heads, and the appropriate heat shields and supporting fixtures (Figure 55). The breech-type top closure with an O-ring seal permits relatively rapid loading and unloading of specimens. A safety valve mounted on the top head insures depressurization before the head can be removed. Design specifications for the furnace (Figure 59) include:

A.	Design Pressure	100 atm
B.	Vessel Design Temperature	94 °C (maximum wall temperature
C.	Heating Capacity	75 kW
D.	Heater Temperature	2800 °C
E.	Inside Diameter	27.3 cm



Neg 0661824-2

FIGURE 55. High Capacity, High Temperature, High Pressure Hydrogen Furnace - Front View



Neg 40849-1

FIGURE 56. High Capacity, High Temperature, High Pressure Hydrogen Furnace - Top View

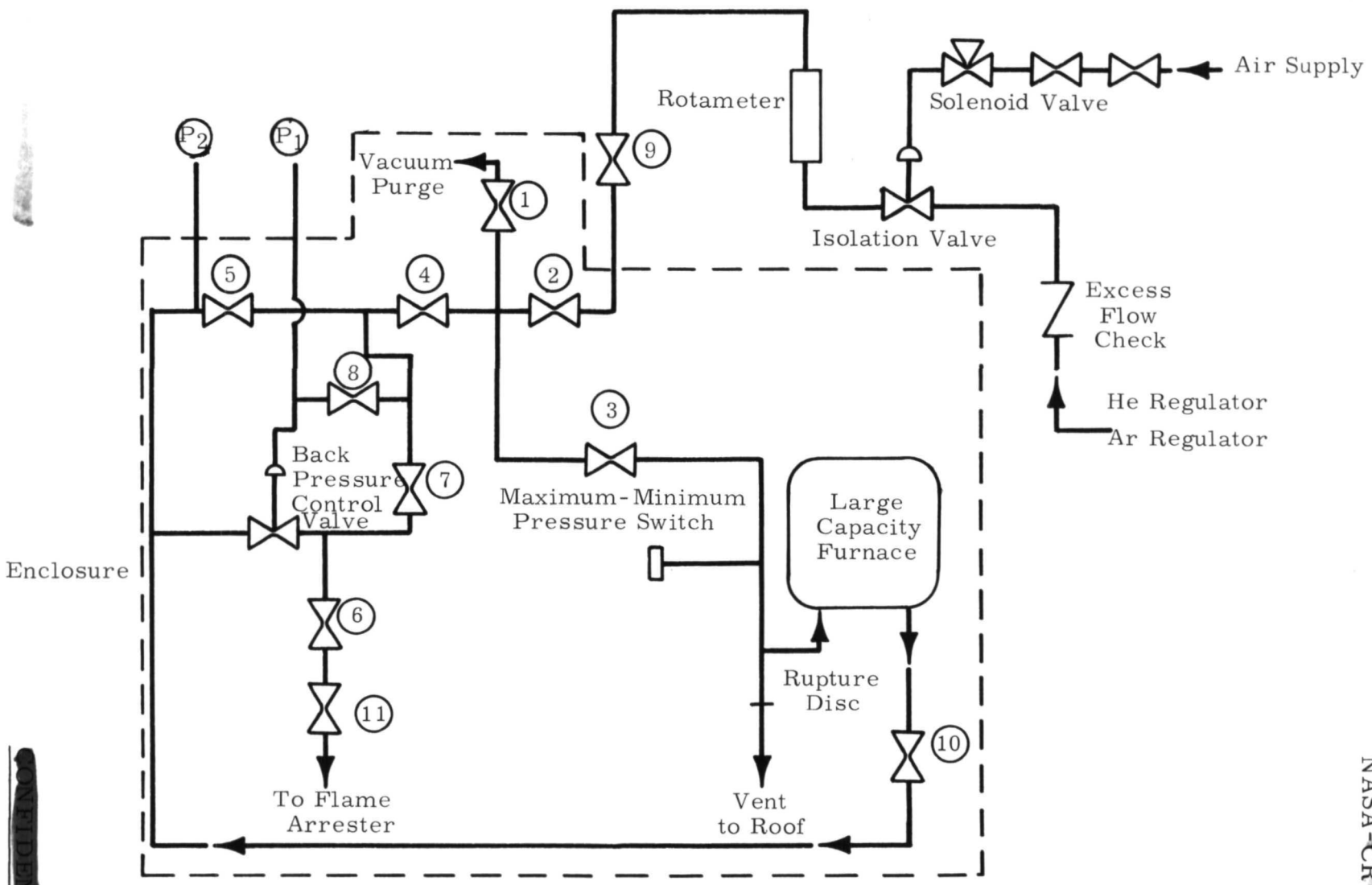
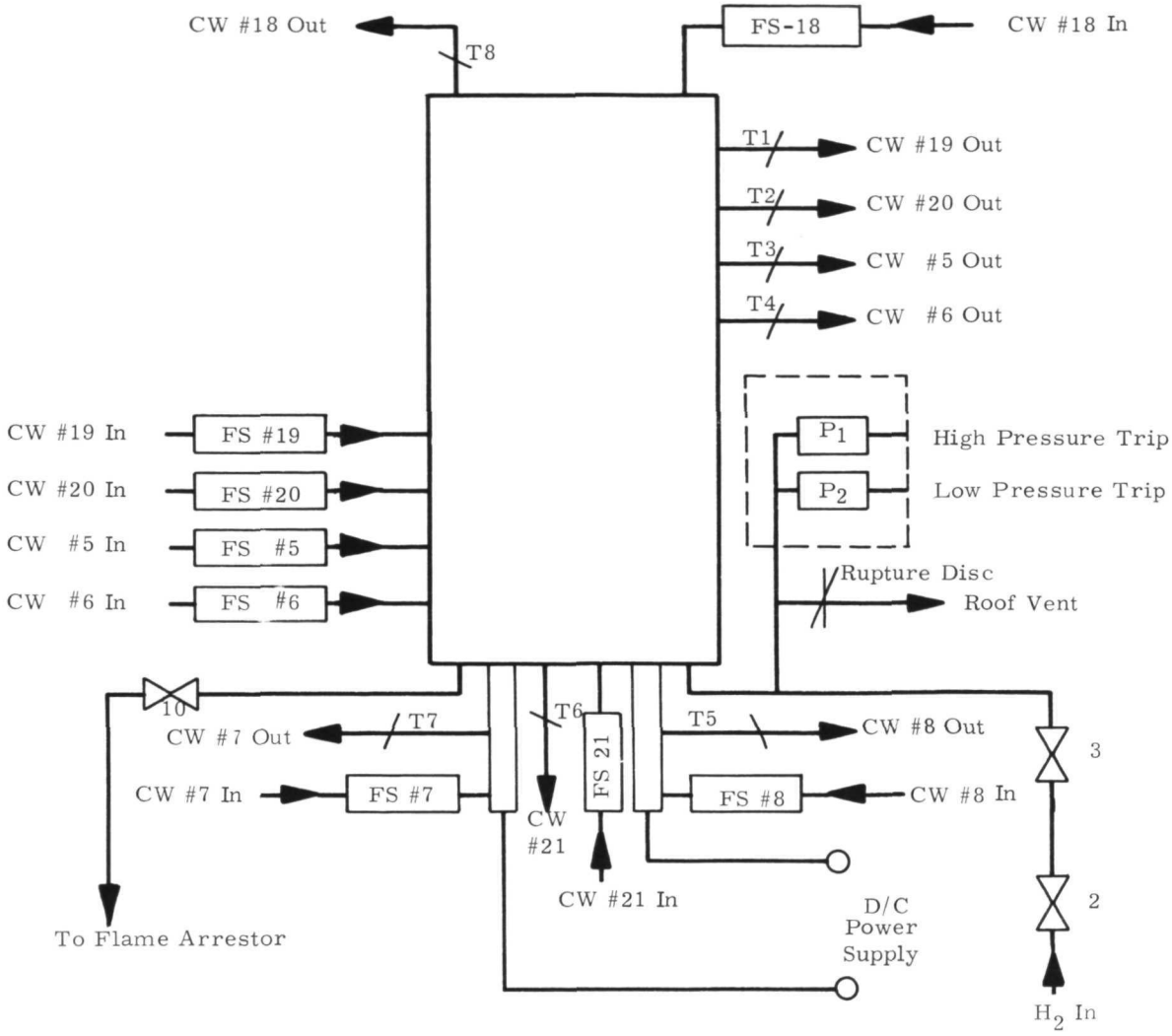


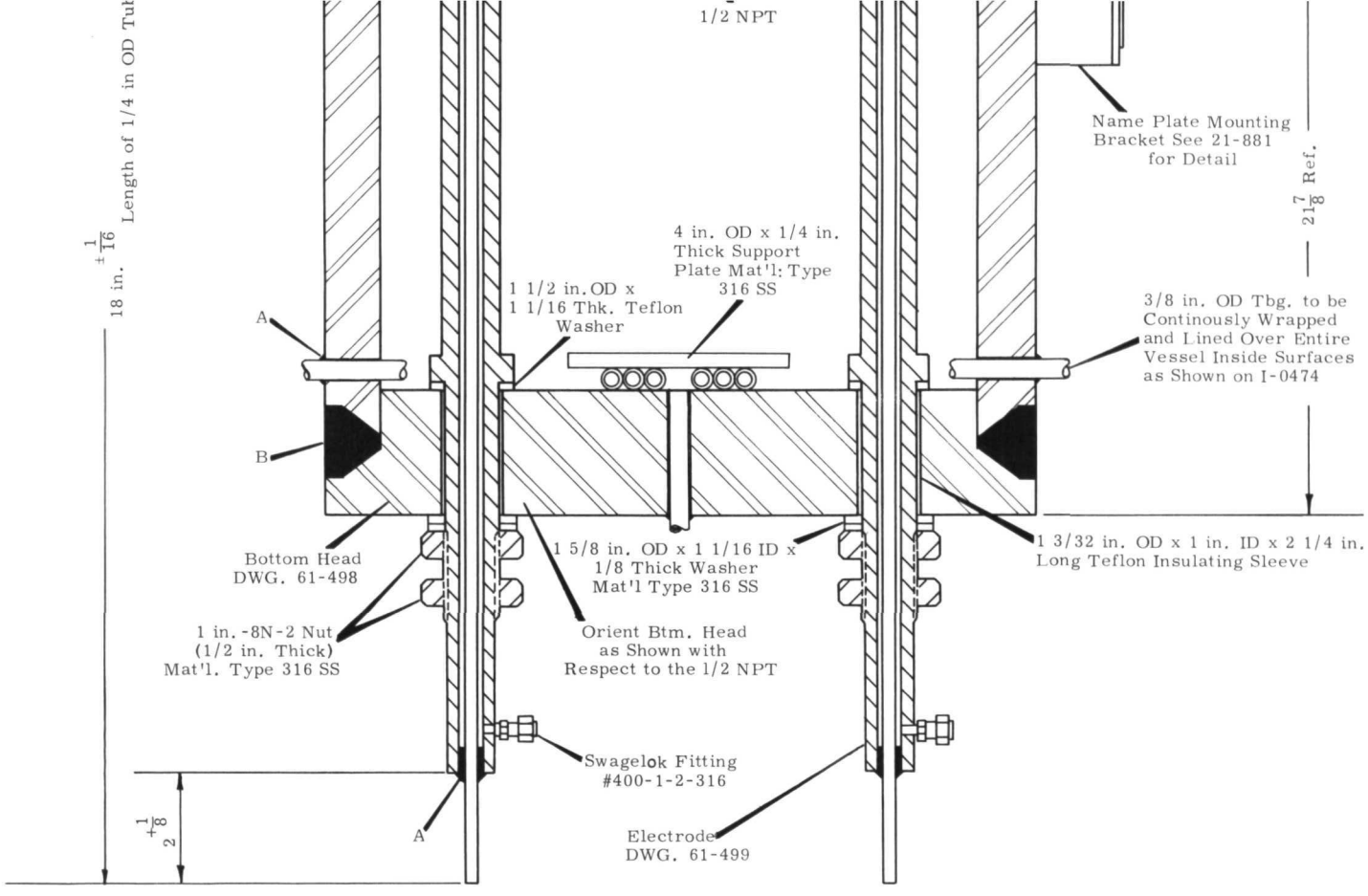
FIGURE 57. Gas Flow and Regulation System Schematic

CONFIDENTIAL



FS	Magnetrol F504 Flow Switch
P_1&P_2	Meletron Pressure Switch B2TA32 S/S Barksdale
T/	Fenwall Thermostat
CW	Cooling Water Circuit
X	Rupture Disc Black Sivalls and Bryson Inc. #189064F Size 0.718in

FIGURE 58 Cooling Water Flow System Schematic Large Capacity, High Temperature, High Pressure, Hydrogen Furnace



WELDING PROCEDURE:

A Material: Tubing, AISI Type 316 SS
Silver Solder Using Eutecrod 1801
and Eutectic "T" Flux

B Material: Body - A-182-F316
Head - A182-F316

1. Heliarc Root Pass with ER 316SS Heliarc Rod
2. Complete Welding with E-316SS Electrodes using Multipass Method
3. Prepare Weld for Radiographing by Grinding

Test Pressure Hydrostatically to 2250 PSI @ 70 °F

Pneumatic W/Nitrogen to 1500 PSIG @ 70 °F

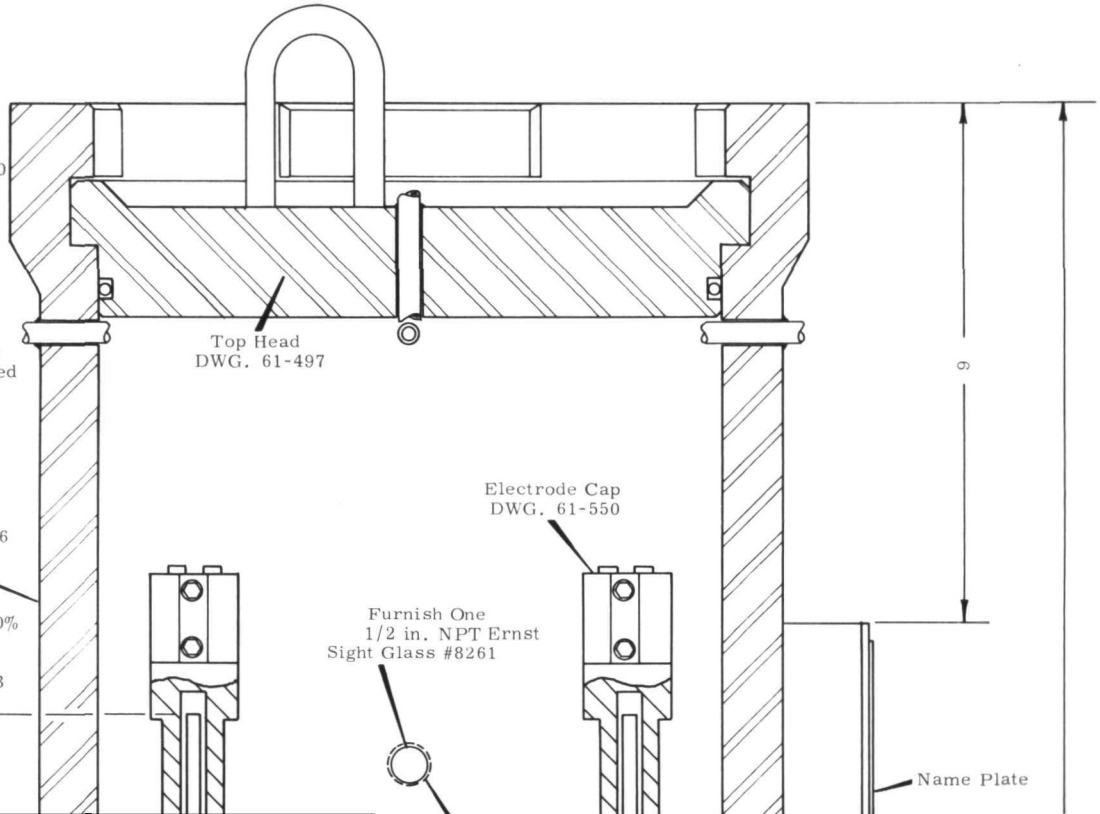
FIGURE 59. Design Details of the High Capacity, High Temperature, High Pressure Furnace

CONFIDENTIAL

BNWL-394
NASA-CR-54840

Loc: MARKING DATA
Work Press. 1500 PSI
Design Temp. 200 F.
Serial No. 61-A-496B
Year Built 1965
12 in. High Pressure Test
Furnace
Dia. 10.750 Length 16
Thk. Head 2.250 Shell 1.000
Air 1500 @ AMB Thk.
Removable Head
Hydro 2250 @ AMB 1.875

INSPECTION:
All Cooling System
(Tubing). Welds to be
Dye Penetrant Inspected



CONFIDENTIAL

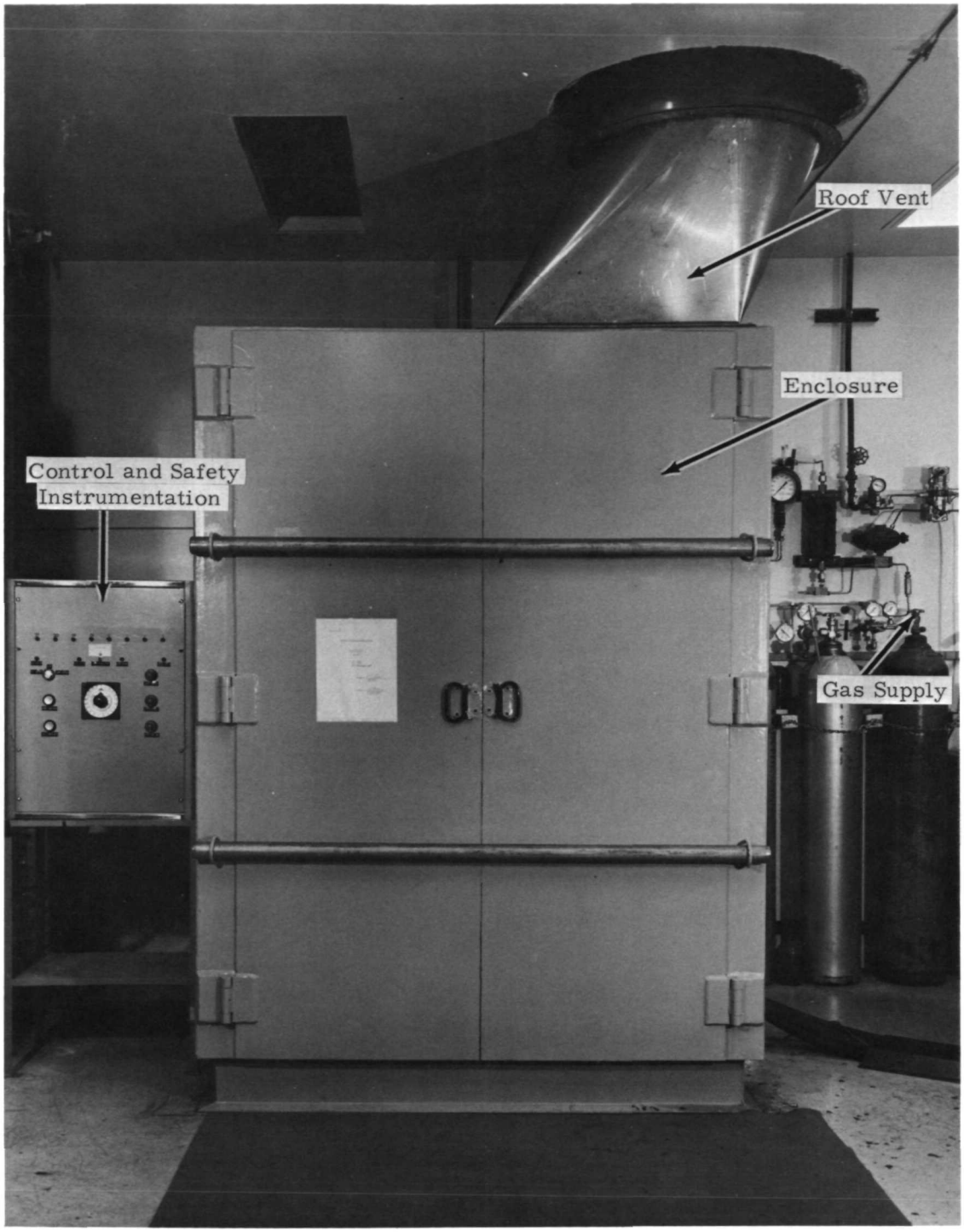
To insure safe operation, extensive precautions were taken to provide for the automatic shutdown of the system in the event of any malfunction. The power to the heater and the hydrogen flow are shut off if:

1. The cooling water flow to any of eight cooling coils is interrupted
2. The cooling water exit temperature exceeds 82 °C
3. The furnace gas pressure falls below a minimum or rises above a maximum set on a pressure switch
4. The heater control thermocouple fails
5. The instrument power is shut off
6. The air supply to air-operated devices is interrupted
7. The exhaust ventilation system is not operating.

In addition, the furnace vessel is protected with a rupture disc to prevent a large overpressure excursion.

A blast enclosure consisting of 0.64 cm steel plate supported on 15 cm channel iron was fabricated to enclose the high pressure furnace (Figure 60). The enclosure was designed to withstand an overpressure of 0.07 atm. An exhaust vent was connected to the containment system to provide for both a means of continuous ventilation and a relief port to prevent overpressurization of the enclosure in the event of a pressure excursion (Figure 61). At overpressures of 0.007 atm or greater, a normally closed cover opens and discharges gases outside the building. To prevent accumulation of hydrogen, an exhaust fan with an explosion-proof motor provides ventilation of the cubicle; failure of the fan will automatically shut down the power supply and hydrogen flow.

The specimen holder and pedestal (Figure 62) were designed to provide maximum exposure of the specimens to the hydrogen flow and to distribute the hydrogen flow as evenly as possible throughout the holder. The holder is rotated 180° after each weighing to further assure that all specimens are cycled under the same average conditons.



Neg 0661824-4

FIGURE 60. Safety and Control Systems for the High Capacity, High Temperature, High Pressure Furnace

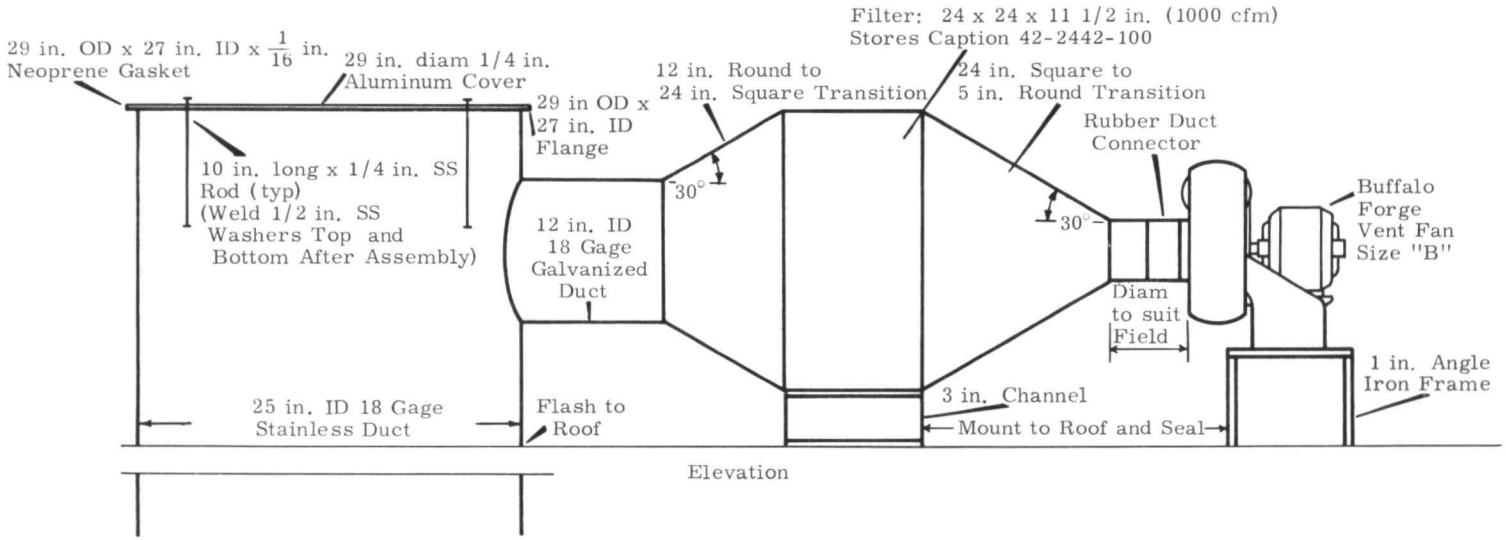
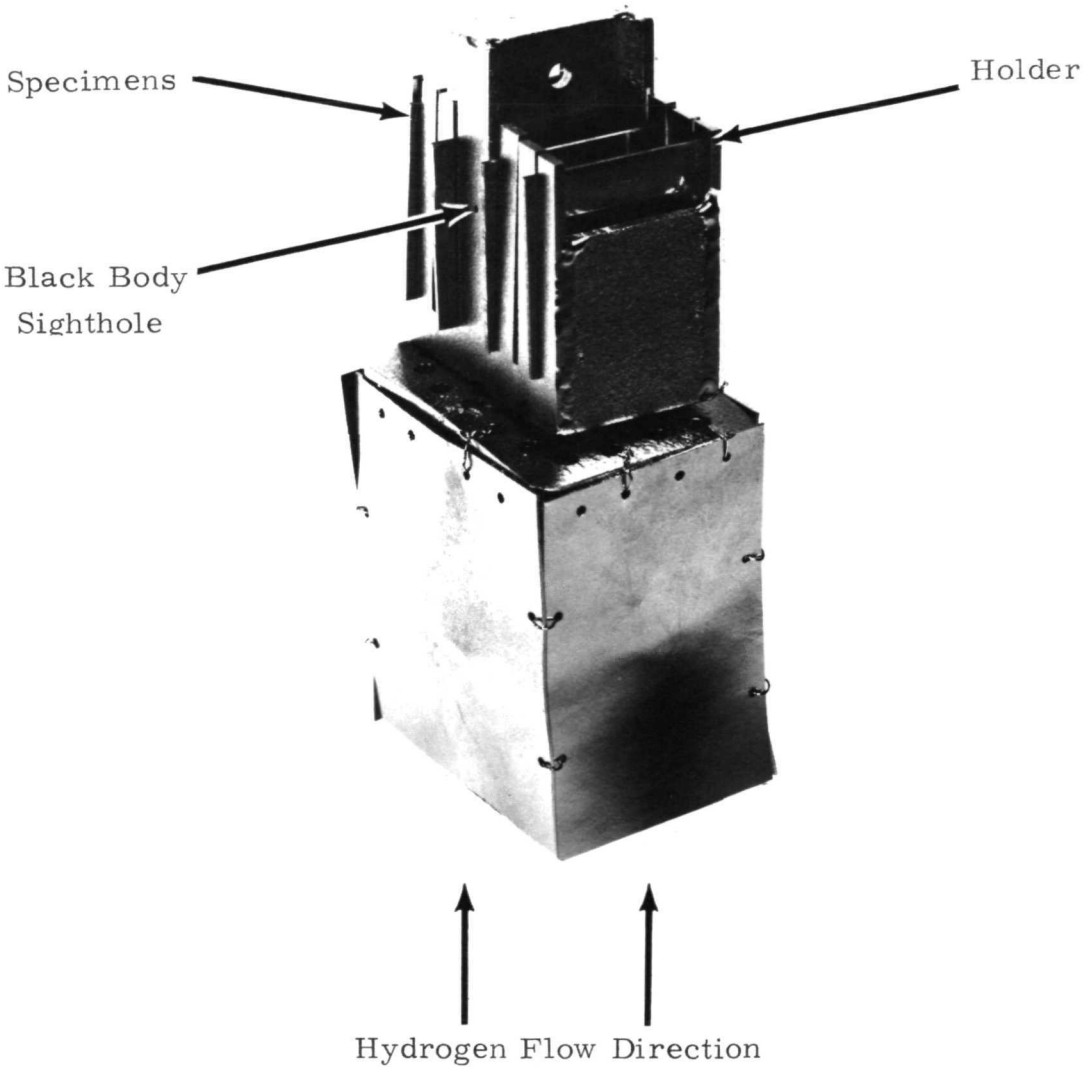


FIGURE 61. Details of Building Exhaust

BNWL-394
NASA-CR-54840



Neg 0662458-2

FIGURE 62. Specimen Holder and Perforated Pedestal

II. Operation

Prior to operation of the furnace, procedures call for verifying the functioning of the safety circuit trips and establishing those conditions which allow power to be supplied to the heating element (cooling water on, operating pressure established, cooling water temperature normal, and exhaust fan on). Before introduction of hydrogen, the entire system is pressurized to 13.6 atm with argon and vented three times to purge the furnace vessel.

During operation, hydrogen pressure is established on the diaphram of the backpressure control valve at a pressure slightly below that desired in the furnace. Then hydrogen is introduced into the furnace, increasing the supply pressure until it exceeds the pressure control valve setting and the required flow is registered on the rotameter. Hydrogen exiting from the furnace is routed through the pressure control valve to a burner mounted outside the building. The heating element is turned on and power adjusted to bring the temperature up to operating conditions (determined by both an optical pyrometer and thermocouple) at the required heating rate. After the desired time at temperature is achieved, the power is shut off and the hydrogen flow adjusted to cool the specimens at the required rate. The system is then depressurized and purged with argon for five minutes prior to opening the top closure.

BNWL-394
NASA-CR-54840

APPENDIX B

THERMAL EXPANSION CHARACTERISTICS OF PNEUMATICALLY IMPACTED W-UO_2 CERMETS

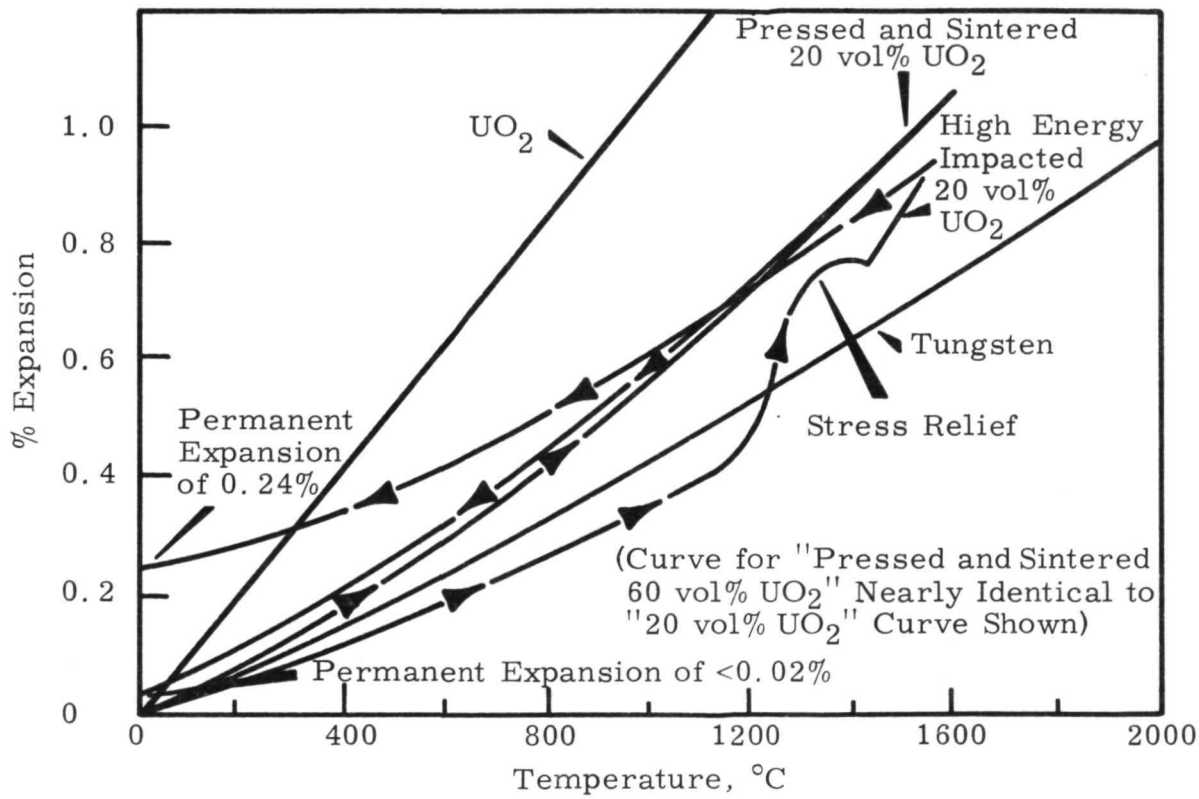
APPENDIX B

THERMAL EXPANSION CHARACTERISTICS OF PNEUMATICALLY IMPACTED W-UO_2 CERMETS

Thermal behavior of the UO_2-W cermets, and the associated metallography, indicate that chemical stability and UO_2 retention are closely related to intergranular bond characteristics. Physical property studies such as tensile strength,[13] thermal expansion, and crystal growth measurements provide valuable information about the bonding. Thermal expansion characteristics have been found by other workers[14] to be directly related to the number of thermal cycles in a manner similar to that of fuel loss.

Measurements were made of the thermal expansion characteristics of three tungsten-UO_2 cermets: a pressed and sintered W–20 vol% UO_2 cermet, a pressed and sintered W–60 vol% UO_2 cermet. The measurements were made in air at a pressure of less than 2 by 10^{-5} torr, and the results were compared with those of earlier measurements on W[15] and UO_2 single crystal.[16] (Figure 63)

The 20% and 60% UO_2 pressed and sintered specimens exhibited a uniform thermal expansion to the maximum test temperature of about 1575 °C. The thermal expansions of these two cermets were nearly identical to about 1400 °C, beyond which 60% UO_2 expanded at a slightly greater rate with increasing temperature. Upon cooling, the curves for the two cermets again were nearly superimposable below 1400 °C. The 20% UO_2 specimen exhibited a 0.014% ± 0.01% permanent elongation after the thermal cycle and the 60% UO_2 had a 0.012% ± 0.01% contraction. Weight loss for the 20% UO_2 sample was 0.08% and for the 60% UO_2 sample it was 0.42%.



Neg 0642631-6

FIGURE 63. Thermal Expansion of Sintered and Unannealed Impacted 80 vol% W–20 vol% UO_2 Cermets (One thermal cycle)

The high energy-rate impacted 20 vol% UO_2 cermet exhibited a very low thermal expansion up to about 1150 °C. Between 1150 °C and 1400 °C, a sudden increase in expansion rate indicated probable stress relief of the tungsten matrix. At temperatures above 1400 °C to the maximum of 1530 °C, there was a continued increase in the rate of thermal expansion. Upon cooling, the thermal expansion was equal to that of pure tungsten; permanent elongation of 0.24% remained and a weight loss of 0.26% was measured.

BNWL-394
NASA-CR-54840

APPENDIX C

PROGRESS TOWARD CONSTITUENT ANALYSIS OF W-UO_2 CERMETS

APPENDIX C

PROGRESS TOWARD CONSTITUENT ANALYSIS OF W-UO_2 CERMETS

Many methods have been published for the determination of the stoichiometry of uranium dioxide. The more widely accepted of these include:

1. Dissolution in a non-oxidizing medium followed by redox or electrochemical titration of the U(VI) present [17, 18, 19]
2. High temperature thermogalvanic measurements [20, 21]
3. Thermogravimetric measurements coupled with oxidation [22, 23]
4. X-ray diffraction techniques [24]
5. Gaseous reduction techniques. [25, 26]

The presence of the large amount of tungsten metal in the cermets markedly restricts the use of most of the above methods. In both the redox titration and thermogalvanic methods the reducing properties of the tungsten will mask the measurement completely. In the thermogravimetric and X-ray diffraction methods the large mass and high atomic number of the tungsten reduces the precision of the method so drastically that prohibitively exacting techniques are required to obtain adequate determinations. The gaseous reduction approach on the other hand, measures the quantity of interest, namely the oxygen which is in excess of that necessary to form stoichiometric uranium dioxide. The method has been proven to be quantitative and to have sufficient sensitivity in the case of oxide samples. This section describes the progress to date on the development of a procedure which also makes it selective and therefore permits the determination of both quantity and location of the excess oxygen in tungsten-uranium dioxide cermets.

As a first step in defining the conditions under which specificity could be achieved, thermobalance reductions were made on uranium dioxide of known stiochiometry and on tungsten of known oxygen content using both carbon monoxide and hydrogen as reductants. Thermobalance reductions were restricted, by nature of the available apparatus, to flowing streams of explosion-proof gas at atmospheric

pressure. Therefore the conditions to be used later in the gas handling system could not be exactly defined. Under the conditions available, carbon monoxide and hydrogen reductions of uranium dioxide with an O/U ratio of 2.025 and of tungsten dioxide* were carried out. Carbon monoxide reduction of the uranium dioxide commenced at about 510 °C and was complete at 670 °C. Carbon monoxide did not significantly alter the weight of tungsten dioxide below 1000 °C. Hydrogen reduction of the uranium dioxide started at about 600 °C and was complete at about 730 °C while the hydrogen reduction of tungsten dioxide started at about 750 °C and was complete at about 900 °C. Thus it can be seen that a wide range of conditions exists under which carbon monoxide will quantitatively reduce hyperstoichiometric uranium dioxide without altering the oxygen content of the tungsten significantly. A similar but narrower range exists for hydrogen reduction. Based on these results and the results of a large number of reductions carried out under fixed conditions in the gas handling system, the following procedure was developed to determine the oxygen-to-uranium ratio of the uranium dioxide contained in a cermet.

1. The sample is weighed in a platinum boat and placed in the furnace tube of the gas handling system. If sufficient sample is available, about 2 grams is usually taken.
2. The sample is dried under vacuum by heating to 600 °C for 15 min.
3. The sample is cooled and carbon monoxide is admitted to the system until the pressure reaches about 180 mm.
4. The reduction is carried out by heating the sample to 600 °C for 15 min in this atmosphere of circulating carbon monoxide. (The carbon dioxide formed should not be removed from the carbon monoxide stream as long as the unknown is hot because it suppresses the carbon monoxide disproportionation reaction.)
5. The unknown is cooled and the carbon dioxide removed from the circulating gas with a liquid nitrogen trap.

*Prepared from WO_3 by reduction

6. The carbon monoxide is pumped off.
7. The trap is warmed and the carbon dioxide measured manometrically.

The hyperstoichiometric oxygen content of the sample can be calculated from the measured quantity of CO_2. This number coupled with the uranium content of the sample (its determination will be discussed later) can be used to calculate the O/U ratio of the cermet.

After carbon monoxide reduction the oxygen remaining in the cermet is either present as stoichiometric uranium dioxide or an oxide of tungsten. Under the proper conditions, hydrogen will quantitatively remove the oxygen from tungsten oxides without affecting stoichiometric uranium dioxide. Therefore, the tungsten oxide content of a cermet may be determined on the carbon monoxide-reduced sample by the following procedure:

1. After the removal of the carbon dioxide from the system, hydrogen is admitted to a pressure of about 180 mm.
2. Reduction is carried out by heating the sample in a circulating stream of hydrogen for 90 min at 800 °C. The stream is circulated through the liquid nitrogen trap to continuously remove any water formed.
3. The sample is cooled and the hydrogen removed from the system.
4. Helium is admitted to a pressure of 180 mm and circulated between the cold trap and electrolytic P_2O_5 cell.
5. The cold trap is warmed and the water titrated coulometrically as it is carried into the electrolytic cell.
6. The oxygen content of the tungsten can be calculated directly from the measured water value.

To relate the hyperstoichiometric oxygen numbers to an oxygen-to-uranium ratio one must also know the uranium content of the sample. The most difficult task in performing a total uranium determination on a tungsten-uranium dioxide cermet is to achieve complete dissolution of the sample. A procedure was developed for this analysis based on placing

the sample in solution by pyrosulfate fusion followed by the x-ray fluorescence determination of the uranium directly on the melt. It may be outlined as follows:

1. Approximately 0.2 g of powdered sample is accurately weighed into a porcelain boat and approximately 2 g of potassium pyrosulfate added.
2. Approximately 2 ml of concentrated sulfuric acid and a precise amount of internal standard are added and the sample heated slowly on the hot plate until the majority of the particles are dissolved. The sulfuric acid addition may have to be repeated.
3. The mixture is fused over a Meeker burner until a clear yellow melt is obtained.
4. The melt is cooled, ground, and a portion mounted for X-ray fluorescence measurements.
5. The intensity ratios of the following lines: U Kα, Sr Kα, Y Kα are measured, making the proper background corrections.
6. The uranium and additive (yttrium or cerium) concentrations are calculated.

The function and even the desirability of the drying step in the O/U ratio determination is open to some debate, particularly considering the fact that a high vacuum is not maintained within the system. It should be studied more completely. However, this operation has provided some valuable information in the case of thermally cycled cermets. Significant quantities of gas were released from these specimens during this operation and correlation was found to exist between the quantity of gas released and the number of thermal cycles which the fuel had undergone. The interpretation of this correlation has contributed to the development of a theory as to the fuel loss mechanism as discussed in Part III.

The particular temperature and duration of the carbon monoxide reduction were selected to insure a complete reduction, to insure selectivi ty, and to maintain the blanks at acceptable levels. Blanks arise from the disproportionation of carbon monoxide to carbon and carbon dioxide on the hot surface of the cermet. Short reduction times, low reduction temperatures and small sample surface areas all help to minimize the blank.

The quantities of water involved in the tungsten oxide determination by reduction with hydrogen are small (50 to 500 μg), and unusual techniques are required for their accurate measurement. A complete description of the technique would constitute a report in itself and can only be summarized here. A conventional P_2O_5 eletrolytic hygrometer cell is black-waxed directly into the glass system and electrically connected to a dc power supply and current integrator. The current integrator used in these studies was a conventional operational amplifier capacitor-circuit[27] using a Dymec Model 2460A operational amplifier. The readout can be either a digital voltmeter or a recorder.

The gas handling system used in this work is shown in line diagram form in Figure 64. One of the major problems associated with the quantitative measurement of small quantities of water in a gas handling system is adsorption of the water on the walls of the system. In the titrations described in this report a dynamic equilibrium exists which should be studied more completely. In fact, more complete understanding or control will be absolutely necessary if it is ever desired to go below the 50 microgram level. However, all the data collected to date indicate that the equilibrium is sufficiently reproducible to permit satisfactory operations in the range of present interest, namely, from 50 to 1000 micrograms of water per titration and therefore an extended study of the equilibrium has not been made.

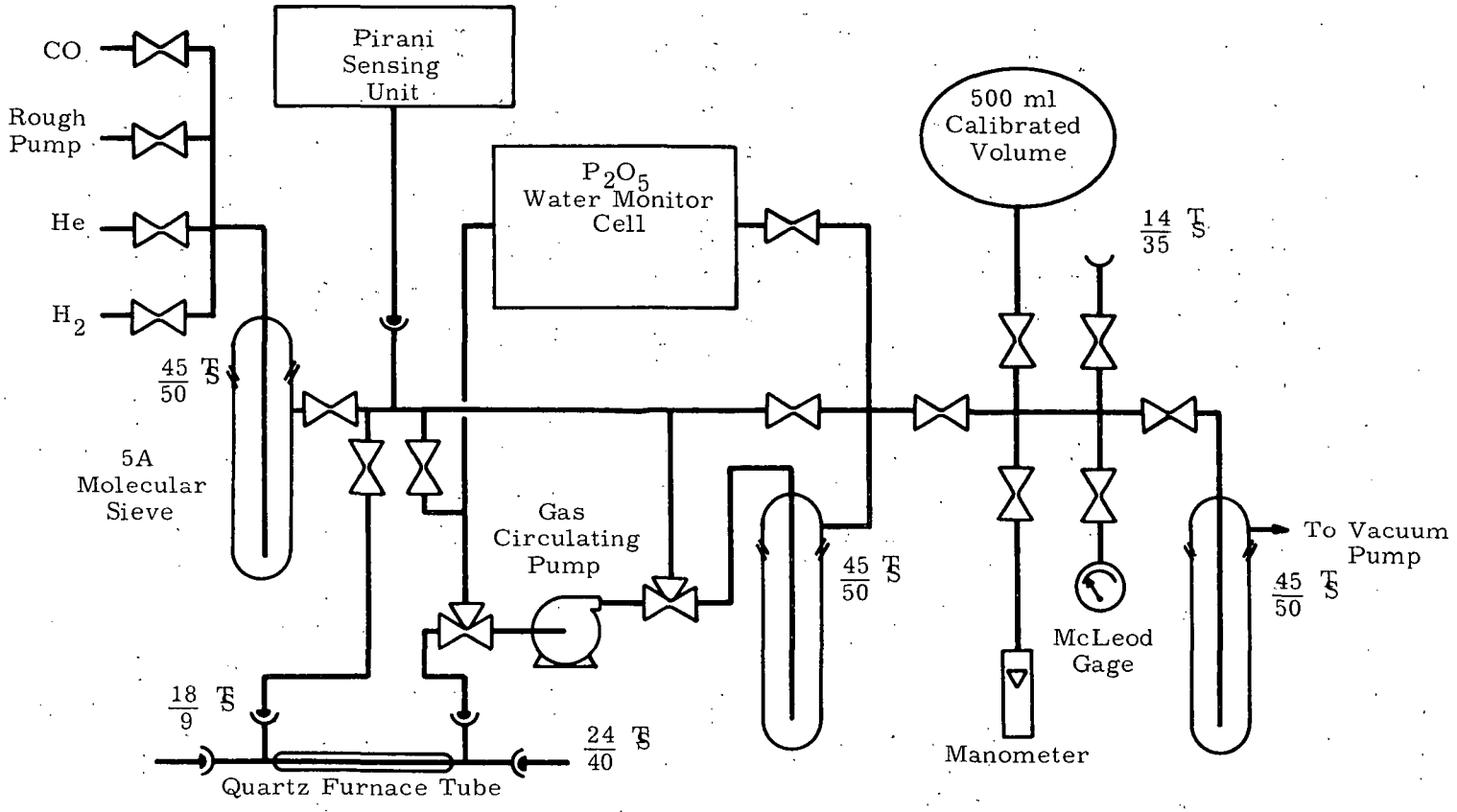


FIGURE 64. Gas Handling System

NASA-CR-54840

The limiting factor in both the carbon monoxide and hydrogen reductions is the blank size. Assuming a 2 gram sample of 10 to 20 wt% uranium dioxide is used, with the present operating procedure and blanks variations from stoichiometry of about ± 0.002 O/U ratio units can be detected with a precision of about ± 0.002 units. Oxygen in tungsten can be detected at about 10 ppm level with a precision of about ± 5 ppm.

In work such as this, one always questions the completeness of the gas-solid reaction. To insure completeness and speed, the original work was done on powdered and screened samples. (The entire sample was powdered to pass through a 100 mesh screen.) Most of the samples were powdered in air. This, of course, raises the question of reaction of the sample with air during the sample preparation step. Several pieces of evidence exist which indicate that such exposure does not significantly increase the oxygen content of the samples. These are:

1. Samples of low-oxygen heli-arc tungsten which were powdered in this manner do not exhibit a detectable oxygen content.
2. Two portions of a given cermet sample, powdered to different mesh sizes, exhibit the same apparent oxygen content.
3. The oxygen pickup of a powdered sample has been measured as a function of time over a period of several days and is shown in Figure 65. The rate of pickup is too slow to add a significant amount of oxygen to the sample if it is analyzed within the first few hours. This does not exclude the possibility that a significant pickup occurred as the new surface was formed during powdering.

In spite of this evidence, it was felt that significant hazards were involved in powdering samples in air. They can be eliminated by either performing the entire sample handling operation in an inert atmosphere or by performing the reductions on massive cermet peices.

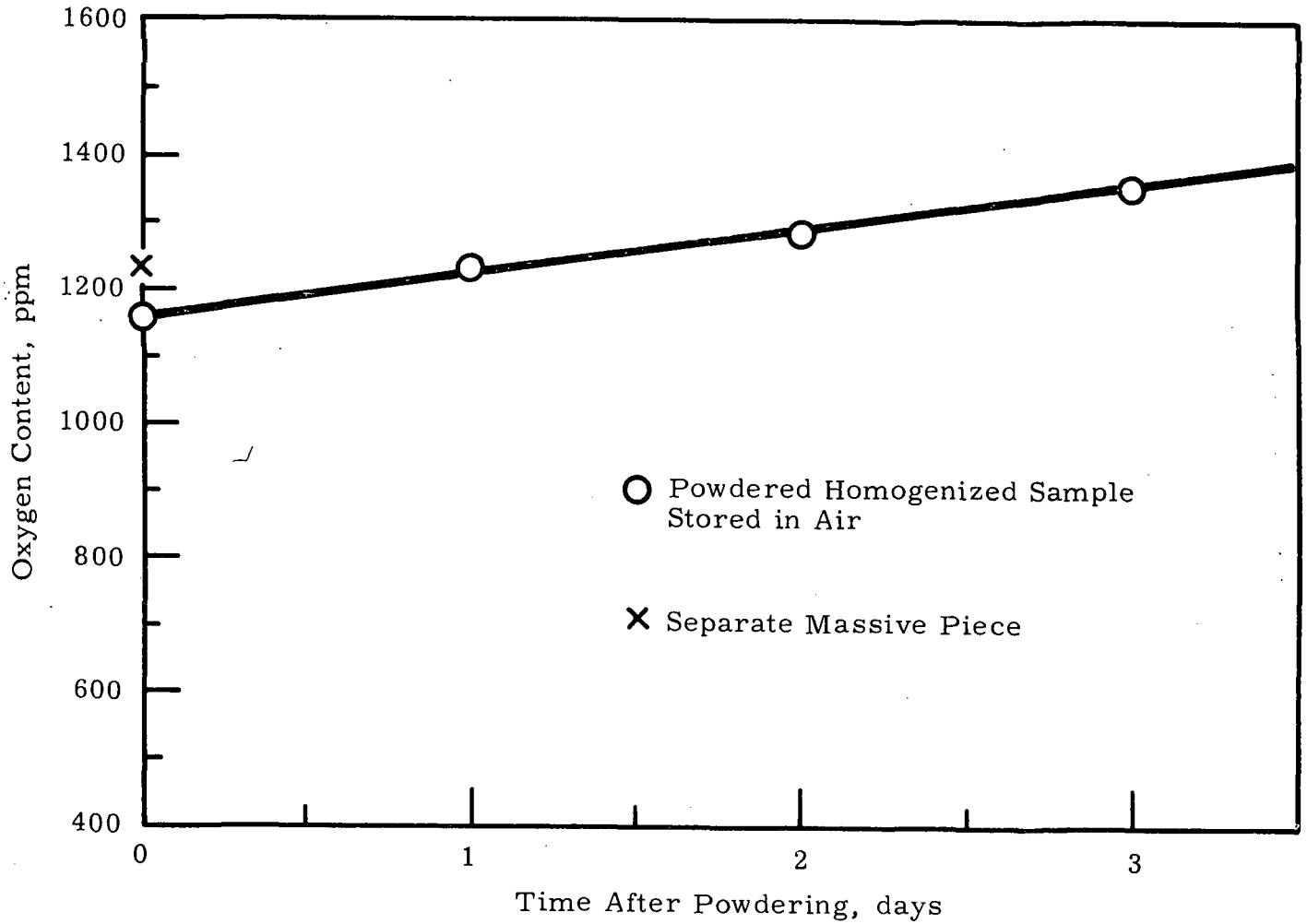


FIGURE 65. Uptake of Oxygen by Powdered Cermet

BNWL-1000
NASA-CR-54840

After reviewing the work of J. O. Hibbits[28] on the measurement of uranium metal in cermets by hydriding techniques it was decided to attempt reductions on massive cermet samples. After running many such pieces, the author feels that realistic values for oxygen-to-uranium ratios and tungsten oxide content are obtained. This has not been proven completely to the author's satisfaction, however, because all of the pieces analyzed to date except one have shown excellent oxygen-to-uranium ratios. Either the fabrication procedures used always produce cermets with stoichiometric uranium dioxide (which is probable) or the carbon monoxide is not reaching the oxide in the massive pieces. A massive cermet piece containing uranium dioxide of known excess oxygen to uranium ratio should be run if such a piece can be obtained.

In the area of tungsten-uranium dioxide cermets containing additives, only some very preliminary experiments have been performed but they show that the approach holds promise of providing useful information. If a sample of mixed oxide is "analyzed" or put through the procedure described above, the following facts are soon evident:

1. The carbon monoxide reduction does not remove a significant amount of the oxygen.
2. The hydrogen reduction does remove a significant and reproducible amount of the oxygen from these mixed oxides.
3. This removal is not instantaneous (Figure 66). Note that there appear to be two distinct slopes to the curve suggesting the possibility of the reduction of two distinct species.
4. R. J. Beals[29] has shown the O/M ratio of gadolinium containing uranium dioxide in the range of 0 to 40 mole per cent gadolinium to be 2.00. The uncertainties in the meager hydrogen reduction data obtained in the present investigation on yttrium containing uranium dioxide are too large to permit firm conclusions regarding the

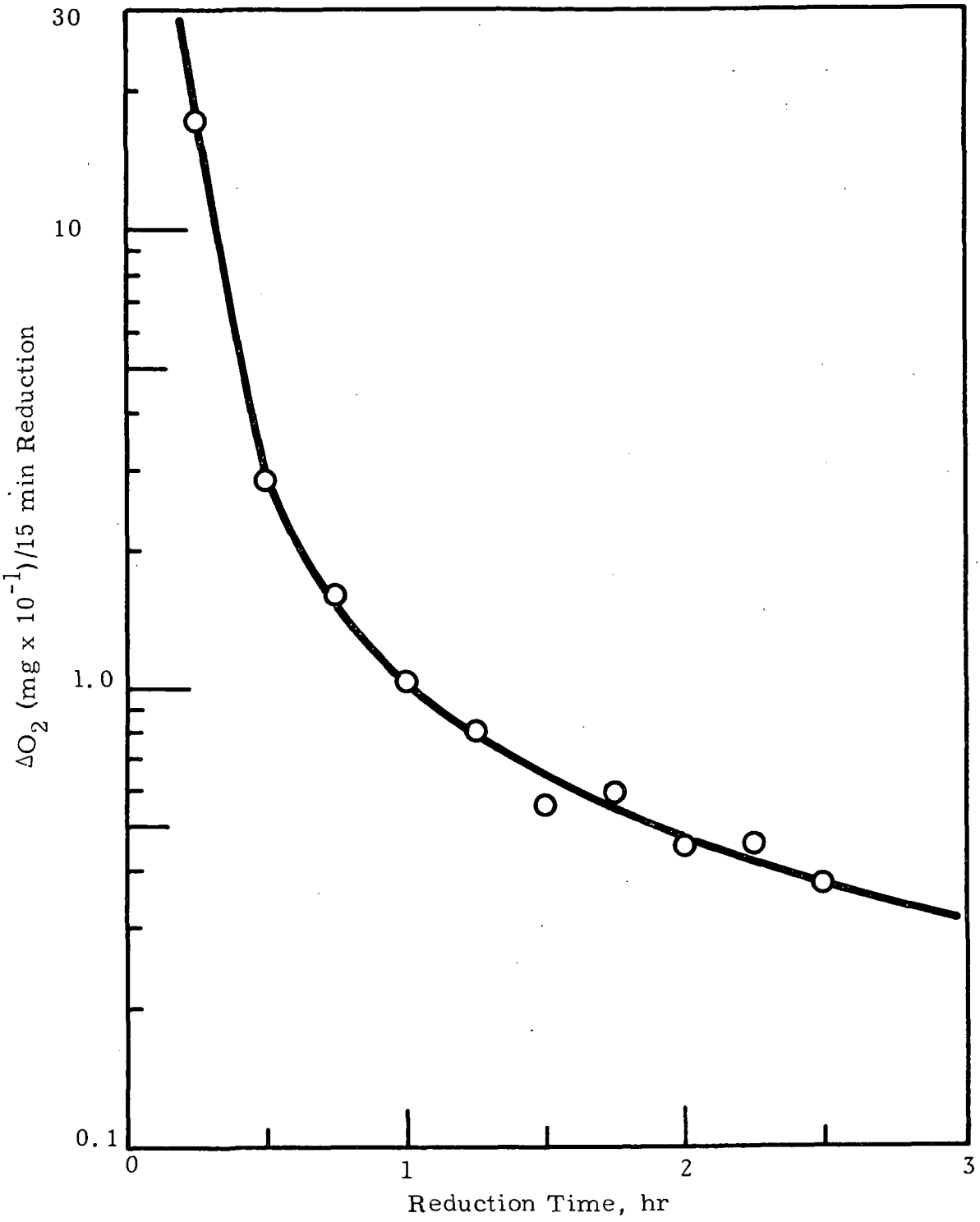


FIGURE 66 Rate of Oxygen Removal from Mixed Oxide Ceramics

stoichiometry of the mixed oxide but show some evidence that only about 80% of the oxygen necessary for the completion of the reaction

$$H_2 + 2RO_2 \rightarrow R_2O_3 + H_2O$$

is being released.

The work to date on the analysis of mixed oxides and cermets containing them, by gaseous reduction, has created more questions than it has answered. Some of these areas which are believed to be worthy of further investigation are:

1. An attempt should be made to define what we call "available oxygen"--the reproducible quantity of oxygen which the hydrogen removes.
2. A search for some correlation of the quantity of available oxygen, the rate of its release, or the temperature of its release with fuel retention ability should be made.
3. Attempts should be made to develop an analytical method which is specific for the various forms of oxygen in a cermet containing mixed oxides. Scouting experiments using reductions on a thermobalance similar to those described earlier in this document could be used as the initial step.
4. Attempts should be made to interpret the reduction rate curves to identify the two species present and aid in the understanding of the mechanism of additive action.

REFERENCES

1. P. D. Takkunen and R. J. Baker. Thermal Cyclic Stability of Fully Clad Cermets Prepared from Tungsten Coated UO_2, NASA-TM-X (to be published).
2. P. D. Takkunen, R. E. Gluyas, and M. A. Gedwill. Thermal Cyclic Behavior of Stabilized Tungsten-Uranium Dioxide Cermets, NASA-TM-X (to be published).
3. "Tungsten Water-Moderated Nuclear Rocket" Nuclear Rocket Technology Conference. NASA-SP-123. Lewis Research Center. 1966.
4. R. G. Nelson, F. B. Quinlan, D. W. Brite, and K. R. Sump. Development of Tungsten-Uranium Dioxide Cermet Fuel Plates: Fabrication by Rolling or by Pneumatic Impaction. NASA-CR-54850, BNWL-309. Pacific Northwest Laboratory, Richland, Washington, 1966.
5. M. Garfinkle. Effect of Additives on Thermal Stability of Tungsten-Uranium Dioxide Composites, NASA-TM-X-1118. 1965.
6. M. A. Gedwill. An Investigation of Some Variables Affecting and Methods of Inhibiting Thermal Cyclic Fuel Losses From Tungsten-Uranium Dioxide Composites. NASA-TM-X-1296. 1966.
7. R. E. Gluyas, and M. A. Gedwill. Stabilization of Tungsten-Uranium Dioxide Composites Under Thermal Cycling Conditions. NASA-TM-X-1295. 1966.
8. E. A. Aitken, P. K. Conn, E. C. Duderstadt, and R. E. Fryxell. Measurement of the Permeability of Tungsten to Hydrogen and to Oxygen. NASA-CR-54918. General Electric Company, NMPO. 1966.
9. G. E. Moore and F. E. Unterwald. "Thermal Dissociation of Hydrogen." J. Chem. Phys., vol. 40, no. 9, pp. 2639-2652. 1964.
10. L. N. Grossman. "High Temperature Thermal Analysis of Ceramic Systems," paper no. 34-B-66, Presented at the 68th Annual Meeting of the American Ceramic Society, May 9 through 12, 1966.
11. Private communications with R. J. Beals; also, J. American Ceram. Soc. 48, no. 5, pp. 271-274. 1965.
12. W. Precht, and L. Sundquist. Investigation of Fuel Loss from Tungsten-Uranium Dioxide Bodies, MND-3178, pp. 22 to 24. November 30. 1964.

13. E. A. Snajdr. Fracture Stresses of UO_2-Tungsten Cermets Evaluated by the Diametral Tensile Test, HW-79676. General Electric Company, Richland, Washington. January, 1964.

14. J. McGurdy, NMPO, General Electric Co., Private Communication.

15. S. J. Worthington. Physical Review, vol., 10, no. 6, pp. 638-641. 1917.

16. E. A. Evans (Ed.). Ceramics Research and Development Operation, Quarterly Report, HW-81602. General Electric Company, Richland, Washington. July to September, 1964.

17. H. I. Shalgosky, R. C. Smart, and J. Watting. The Precise Determination of O/U Ratios in Uranium Dioxide by Comparative Polarography. AERE-R-4270. Atomic Energy Research Establishment, Harwell, Great Britain, June, 1964.

18. R. M. Burd and G. W. Goward. The Polarographic Determination of Hexavalent Uranium in Uranium Oxides (The Determination of Oxygen/Uranium Ratios), WAPD-205, Bettis, Atomic Power Laboratory. April, 1959.

19. R. W. Stromatt and R. E. Connally. "Determination of the Stoichiometry of Uranium Dioxide by Controlled Potential Coulometry," Analytical Chemistry, vol. 33, p. 354. March, 1961.

20. T. L. Markin and R. J. Bones. The Determination of Changes in Free Energy for Uranium Oxides Using a High Temperature Galvanic Cell, Part 1, AERE-4042. Atomic Energy Research Establishment, Harwell, Great Britain, 1962.

21. T. L. Markin and R. J. Bones. The Determination of Some Thermo-Dynamic Properties of Uranium Oxides with O/U Ratios Between 2.00 and 2.03 Using High Temperature Galvanic Cell, Part 2, AERE-R-4178. Atomic Energy Research Establishment, Harwell, Great Britain.

22. L. G. Stonhill. "The Determination of Atomic Ratios in the Uranium-Oxygen System by a Thermogravimetric Method." Canadian Journal of Chemistry. vol. 37, pp. 454-459. 1959.

23. W. L. Lyon. The Measurement of Oxygen to Metal Ratio in Solid Solutions of Uranium and Plutonium Dioxides, GEAP-4271. General Electric Company, Atomic Products Division, 1963.

24. W. A. Young, L. Lynds, J. S. Mohl, and G. G. Lebowitz. An X-Ray and Density Study of Non-stoichiometry in Uranium Oxides, NAA-SR-6765. North American Aviation Inc., 1962.

25. L. E. J. Roberts and E. A. Harper. The Determination of Oxygen in Uranium Oxides, AERE-C/C-885. Atomic Energy Research Establishment, Harwell, Great Britain, 1952.

26. T. L. Markin, A. J. Walter and R. J. Bones. The Determination of Oxygen/Metal Ratios for Uranium, Plutonium, and (R, Pu) Oxides, AERE-R-4608. Atomic Energy Research Establishment, Harwell, Great Britain. 1964.

27. G. L. Booman. "Instrument for Controlled Potential Electrolysis and Precision Coulometric Integration," Analytical Chemistry, vol., 29, p. 213. 1957.

28. J. O. Hibbits. Private communication.

29. R. J. Beals, and J. H. Handwerk. "Solid Solutions in the System Urania - Rate Earth Oxides: I." UO_2-GdO_2, Journal of the American Ceramic Society, vol., 48, no. 5, pp. 271-274. May, 1965.

DISTRIBUTION

Number of Copies	
1	ACF Industries, Inc.
1	AEC Patent Office
2	Aerojet-General Corporation (NASA)
1	Aerojet-General Corporation, Sacramento
2	Aeronautical Systems Division
1	Aerospace Corporation
1	Air Force Foreign Technology Division
1	Air Force Headquarters
1	Air Force Rocket Propulsion Laboratory
1	Air Force Strategic Air Command
2	Air Force Weapons Laboratory
1	Air University Library
2	Albuquerque Operations Office
1	Allison Division-GMC
1	Argonne National Laboratory
3	Argonne National Laboratory J. Marchaterre R. A. Noland J. Schumar
1	Army Chief of Research and Development
1	Army Materials Research Agency
1	Army Missile Command
1	Army Picatinny Arsenal
1	Aro, Inc.
1	AEC-NASA Space Nuclear Propulsion Office, Nevada
10	Atomic Energy Commission, Washington
4	Atomic Energy Commission, Washington AEC/NASA Space Nuclear Propulsion Office Division of Reactor Development H. G. Finger J. M. Morrissey F. C. Schwenk W. Yingling
2	Atomic Energy Commission, Washington AEC/NASA Space Nuclear Systems W. Kern J. Powers
2	Atomic Energy Commission, Washington Division of Isotope Development W. K. Eister G. Y. Jordy

Number of Copies	
1	Atomics International
1	Battelle Memorial Institute, Columbus Laboratories
1	Brookhaven National Laboratory
1	Central Intelligence Agency
1	Chicago Patent Group
1	Defense Atomic Support Agency, Sandia
1	Director of Defense Research and Engineering
1	du Pont Company, Aiken
1	EG&G, Inc., Goleta
1	EG&G, Inc., Las Vegas
1	General Atomic Division
1	General Dynamics/Fort Worth
1	General Electric Company, Cincinnati
1	General Electric Company (FPD)
1	Institute for Defense Analyses
1	Jet Propulsion Laboratory
1	Johns Hopkins University (APL)
1	Lockheed-Georgia Company
2	Los Alamos Scientific Laboratory
1	NASA Goddard Space Flight Center
1	NASA Langley Research Center
6	NASA Lewis Research Center
9	NASA Lewis Research Center Report Control Office Patent Council Office Office of Reliability and Control Assurance S. J. Kaufmann A. F. Lietzke S. Weiss R. E. Gluyas N. T. Saunders P. D. Takkunen
1	NASA Manned Spacecraft Center
5	NASA Marshall Space Flight Center
3	NASA Scientific and Technical Information Facility
6	NASA Scientific and Technical Information Facility NASA Representatives
4	National Reactor Testing Station, Inc.
1	Naval Air Systems Command
1	Naval Missile Center
2	Naval Ordnance Systems Command
1	Naval Radiological Defense Laboratory

Number of Copies	
1	Naval Ship Systems Command Headquarters
1	Nevada Operations Office
1	Oak Ridge Operations Office
1	Office of the Chief of Naval Operations
1	Pratt and Whitney Aircraft Division (NASA)
1	Rand Corporation
1	Rocketdyne
2	Sandia Corporation
1	Sandia Corporation R. P. Stromberg Division 9333
1	TRW Systems
1	Union Carbide Corporation
5	Union Carbide Corporation (ORNL)
1	Union Carbide Corporation (Paducah Plant)
2	University of California, Livermore
1	Westinghouse Electric Corporation (NASA)
2	White Sands Missile Range
10	Division of Technical Information Extension
3	Division of Technical Information Extension for retransmittal to NASA Flight Research Center P.O. Box 273 Edwards, California 93523 Library (1) NASA Western Operations (1) 150 Pico Boulevard Santa Monica, California 90406 National Aeronautics and Space Administration, Washington Library (1)
42	Battelle-Northwest D. T. Aase F. W. Albaugh R. J. Baker, Jr. (5) J. L. Bates D. W. Brite J. J. Cadwell/O. J Wick J. L. Daniel

Battelle-Northwest (contd)

D. R. de Halas
R. F. Dickerson
K. Drumheller
P. L. Farnsworth
J. C. Fox
W. L. Hampson, Jr.
K. M. Harmon
H. Harty
G. A. Last
S. J. Mayhan
J. E. Minor
R. E. Nightingale
W. E. Roake
R. K Robinson
F. A. Scott
E. A. Snajdr
J. C. Spanner
K. R. Sump
E. E. Voiland
Technical Information Files (10)
Technical Publications